FACULTY OF INFORMATION TECHNOLOGY AND ELECTRICAL ENGINEERING
DEGREE PROGRAMME IN ELECTRONICS AND COMMUNICATIONS ENGINEERING

MASTER'S THESIS

SNR-BASED EVALUATION OF COEXISTENCE IN WIRELESS SYSTEM OF HOSPITAL

Author	Martti Savolainen
Supervisor	Adj.Prof. Matti Hämäläinen
Second Examiner	Dr. Heikki Karvonen
Technical Advisor	Prof. Jari Iinatti

February 2021

Savolainen M. (2021) SNR-based evaluation of coexistence in wireless system of hospital. University of Oulu, Faculty of Information Technology and Electrical Engineering, Degree Programme in Electronics and Communications Engineering. Master's Thesis, 108 p.

ABSTRACT

The wireless system (IEEE Std. 802.11) of North Karelian Central Hospital (NKCH) has been studied in the newly opened J2 building of the hospital. The measurements have been carried out using Ekahau Sidekick spectrum analyser and Ekahau Pro software. Signal propagation has been modelled in the control ward of the Emergency department because many coexisting systems are used with critical requirements of data communication over there. The analytical models have been developed to understand the radio-frequency (RF) signal propagation in the entire building. Measurements have also been carried out on the entire first floor, in the Department of the Abdominal Diseases on the ground floor and in the Children's wards on the third floor.

The multi-slope path-loss propagation models with shadowing have been generated based on the Received Signal Strength Indicator (RSSI) measurements for typical hospital environment at the 2.4 GHz and 5 GHz Industrial, Scientific, and Medical (ISM) band. The measurements have been carried out within the two predefined routes. The models have also been compared to the empirically derived path-loss models. The probability of signal outage has been calculated for both measured routes.

The aggregate interference has been measured within the routes that cover the area where remarkable signal variations and the high level of interference has been indicated based on the heatmaps of Ekahau. The use of Ekahau Sidekick and Ekahau Pro software in the coexistence study has been described. The noise floor has been determined based on the averaged values of the six measurement campaigns. The local changes in signal strength of the desired signal and aggregated power of interference have been studied. The Signal-to-Interference Ratio (SIR) models have been generated within the measured routes.

The rapid decreases of Signal-to-Noise Ratio (SNR) have been indicated on all measured floors of building J2. They have been studied and their effect on the network performance has been evaluated. The evaluation has been done by comparing the measured values of RSSI, SNR and SIR to the requirements of the respective Modulation and Coding Scheme (MCS). The link margins have been calculated based on the chosen bit error probability and the given SNR requirement of the respective MCS. The comparison between the measured RSSI readings and the required threshold of the respective MCS has been done using the defined shadowing as a link margin.

It has been shown that the measured difference between the signal strength of the 2.4 GHz and 5 GHz bands has been caused by the reduced transmit power at the 2.4 GHz band. Based on the SIR measurements, it has been shown that the access points of the neighbouring building have contributed locally to the measured aggregate interference in the Control ward. However, the primary reason for the decrease of SIR at the 2.4 GHz band has been the decrease of desired signal power that has been contributed by the above mentioned reduced transmit power. The strong SNR drops have been indicated on every measured floor before the roaming has occurred.

Key words: path-loss, interference, signal-to-noise ratio.

Savolainen M. (2021) Sairaalan langattoman järjestelmän arviointi signaali-kohina-suhteen avulla. Oulun yliopisto, tieto- ja sähkötekniikan tiedekunta, elektroniikan ja tietoliikennetekniikan tutkinto-ohjelma. Diplomityö, 108 p.

TIIVISTELMÄ

Tässä diplomityössä on tutkittu Pohjois-Karjalan keskussairaalan (PKKS) langatonta verkkoa (IEEE Std. 802.11) äskettäin avatussa sairaalan laajennusosassa (J2-rakennus). Mittaukset on toteutettu käyttäen Ekahau Sidekick spektrianalysaattoria ja Ekahau Pro -ohjelmaa. Päivystyksen valvontaosasto on valittu tutkimuskohteeksi, koska siellä käytetään paljon eri teknologioihin perustuvia järjestelmiä, joiden välinen tiedonsiirto on luonteeltaan kriittistä. Luotujen mallien avulla rakennuksen langatonta toimintaympäristöä tutkitaan RF-järjestelmän (Radio-Frequency) näkökulmasta myös muissa mittausten kohteina olleissa tiloissa. Mittauksia on tehty myös valvontaosaston ulkopuolella 1. kerroksessa sekä 3. kerroksen lastenosastoilla ja Vatsakeskuksen tiloissa pohjakerroksessa.

RSSI-mittausten perusteella on luotu radiotiehäviöihin perustuvat etenemismallit molemmilla käytössä olevilla ISM-taajuuskaistoilla (Industrial, Scientific and Medical bands). Varjostuminen ja etenemishäviökertoimen muutokset on otettu huomioon etenemismalleissa. Mittaukset on suoritettu ennalta määritellyillä reiteillä. Luotuja malleja on verrattu myös tutkimuskirjallisuudessa esitettyihin, empiirisesti johdettuihin etenemishäviömalleihin. Signaalikatkoksen todennäköisyys on laskettu molemmille reiteille 2.4 GHz:n taajuuskaistalla.

Vastaanotetun häiriötehon summa on mitattu koko mallinnettavan tilan alueelle ulottuvien mittausreittien pohjalta. Mittausreitit on määritelty Ekahau Pron tuottamien kuuluvuus- ja häiriökarttojen avulla ottaen huomioon havaitut signaalitason vaihtelut. Ekahau Sidekick -spektrianalysaattorin ja Ekahau Pro -ohjelman käyttöä on kuvattu tämän tutkimuksen kontekstissa. Kohinataso on määritelty kaikissa kuudessa mittauskampanjassa mitattujen kohinatehoarvojen keskiarvona. Paikallisten hyötysignaalinvoimakkuus- ja häiriöteho-vaihteluiden vaikutusta verkon suorituskykyyn on tutkittu ja molemmat mittausreitit kattavat SIR-mallit (Signal-to-Interference Ratio) on luotu.

Kaikissa tutkituissa kerroksissa havaittuja äkillisiä signaali-kohinasuhteen vaihteluita on tutkittu ja niiden vaikutusta järjestelmän suorituskykyyn on arvioitu. Mitattujen hyöty- ja häiriösignaalivaihteluiden arviointi on toteutettu vertaamalla mittaamalla saatuja SNR-(Signal-to-Noise ratio), SIR- ja RSSI-arvoja (Received Signal Strength Indicator) eri tiedonsiirtonopeuksia käyttävien MCS-indeksien vaatimiin signaalinvoimakkuus- ja signaali-kohinasuhteen arvoihin. Kynnysarvoille on laskettu linkkimarginaalit käyttäen mitoitusvaatimuksena valittua bittivirhetodennäköisyyden arvoa. Mitattuja RSSI-arvoja on verrattu käyttäen linkkimarginaalina etenemismallinnuksessa määritettyjä varjostumisvaikutuksen arvoja.

2.4 ja 5 GHz:n taajuusalueiden välillä mitatun signaalinvoimakkuuseron on tutkimuksessa saatujen tulosten perusteella osoitettu olevan seurausta alennetusta lähetystehosta 2.4 GHz:n kaistalla. SIR-mittausten perusteella on todettu viereisen rakennuksen tukiasemien kasvattaneen vastaanotettua häiriötehosummaa valvontaosastolla paikallisesti. Ensisijainen syy mitattuihin SIR-arvojen vaihteluihin ovat kuitenkin alhainen signaalinvoimakkuus 2.4 GHz:n kaistalla, mikä osittain johtuu edellä kuvatusta alennetusta lähetystehosta. Voimakkaita SNR-vaihteluita on mitattu kaikissa kerroksissa ennen kuin päätelaite kytkeytyy uuteen tukiasemaan.

Avainsanat: häviö, interferenssi, signaali-kohinasuhde.

TABLE OF CONTENTS

FOREWORD

Siun Sote is the consortium of municipalities that are responsible for social and health services in North Karelia. It has commissioned this work to study the wireless network in J2 building of the North Karelian Central Hospital (NKCH). The work has been done for Meita Oy, which is an in-house company of Siun Sote providing technology services to it.

I want to thank Adj.Prof. Matti Hämäläinen, the Supervisor of this thesis for the patient guidance which has not been limited only to the few mandatory Teams meetings. The counter questions of the internationally merited professional researchers have been more than the answers for me. I also want to thank Second Examiner, Dr. Heikki Karvonen, for his expertise during this project. Thanks also to Prof. Jari Iinatti for your promise to be as a technical advisor.

I want to thank all my colleagues in Meita Oy. Special thanks to ICT Head Designer Mr. Tomi Tikkanen and Director of Digital Services M.Sc. Pia Hiltunen of Siun Sote who have identified the need for RF analysis in the wireless networks of NKCH.

Hopefully, this work will also serve the needs of the construction and design processes of the new, more wireless, mobile, and flexible hospital that could serve the residents of the sparsely populated North Karelia in the best possible way also in the future.

Joensuu, February 14, 2021

Martti Savolainen

LIST OF ABBREVIATIONS AND SYMBOLS

ACI	adjacent channel interference
AP	access point
AP_t	access point with index t
ASK	amplitude shift keying
AWGN	additive white gaussian noise
BER	bit-error-rate
BLE	Bluetooth low energy
BSS	basic service set
CCA	clear channel assessment
CCI	co-channel interference
CSMA-CA	carrier sense multiple access with collision avoidance
CT	computer tomography
dB	decibel, the tenth of a logarithmic ratio between the two power levels
dBd	dipole antenna gain
dBi	isotropic antenna gain
dBm	decibel-milliwatts, unit of power that is expressed in decibels with reference to the power of one milliwatt
DFS	dynamic frequency selection
DSSS	direct sequence spread spectrum
ECG	electrocardiogram
EIRP	effective isotropic radiation power
ETSI	European Telecommunications Standards Institute
FCC	Federal Communications Commission
FCME	forward consecutive mean excision
GHz	gigahertz
GI	guard interval
ICMP	internet control message protocol
IoE	Internet of Everything
IoT	Internet of Things
ISI	intersymbol interference, distortion of a signal in which one symbol interferes with subsequent symbols
ISM	industrial, scientific, and medical
ITU-R	international telecommunication union radiocommunication sector
LNSPL	lognormal shadowing path loss model
LOS	line-of-sight
MAC	medium access control, a sublayer of the data link layer specified in the OSI-model
Mbits	Megabits
Mbps	Megabits per second
MCS	modulation and coding scheme
MCSj	modulation and coding scheme with index j, where j = 1 for the MCS of the highest order
MHz	Megahertz
MIMO	multiple-input and multiple-output, a method for multiplying the capacity of a radio link by using multiple transmission and receiving antennas
ms	millisecond
MSE	mean squared error
NKCH	North Karelian Central Hospital

NLOS	non-line-of-sight
NSS	number of spatial streams
OFDM	orthogonal frequency-division multiplexing
OSI	open systems interconnection, a model that characterises and standardises the communication functions of telecommunication or computing system
OQPSK	offset-quadrature phase shift keying
PDF	probability density function
PHY	physical layer that have been specified in the OSI-model
PSK	phase shift keying
QAM	quadrature amplitude modulation
QoS	quality of service
QPSK	quadrature phase shift keying
RSSI	received signal strength indicator
$RSSI_{low}$	RSSI that has been measured in the location where SNR_{low} has been measured
$RSSI_{MCS}$	the minimum value of RSSI that is required by the respective MCS index
$RSSI_{min}$	the sum of X_σ and $RSSI_{MCS}$
RF	radio frequency
SCP	spectrum channel power
SIG	Special Interest Group
SIR	signal-to-interference ratio
SINR	signal-to-interference plus noise ratio
SISO	single-input and single-output
SNR	signal-to-noise ratio
SNR_{high}	the local maximum of measured SNR that has been measured after the rise of SNR associated with indicated rapid decreases of SNR before roaming
SNR_{low}	the local minimum of measured SNR that has been measured before the rise of SNR associated with indicated rapid decreases of SNR before roaming
SSID	service set identifier
TBF	transmit beamforming
UNII	unlicensed national information infrastructure
VLAN	virtual local area network
WiFi	a trademark of the non-profit WiFi Alliance
WBAN	wireless body area network
WLAN	wireless local area network

B	bandwidth
B_{DS}	bandwidth of desired receiver
B_I	bandwidth of interferer
C	channel capacity
d	distance between transmitter and receiver
d_0	reference distance measured from a transmitter
d_{pt}	perpendicular distance from the route to AP_t
E_b	bit energy
f	frequency
f_L	lower frequency of bandwidth
f_U	upper frequency of bandwidth
G_t	gain of a transmitter antenna
G_r	gain of a receiver antenna
k	Boltzmann's constant, 1.38065×10^{-23} m^2 kg s^{-2} K^{-1}
L_o	overall losses of a radio link

L_p	path loss of a radio link
M	order of modulation
n	path-loss exponent, may also be described as a slope of a logarithmic path loss in a function of the distance between the transmitter and the receiver
n_SISO	path loss exponent of SISO system
N	number of bits per symbol
N_0	spectral noise density
N_r	number of receiving diversity antennas
p	probability
P_b	bit-error probability
$P_\mathrm{b(reqd)}$	required bit error probability
$P_\mathrm{b(reqd)j}$	required bit error probability of $\mathrm{MCS_j}$
P_I	interference power
$P_\mathrm{i(high)}$	local maximum of measured P_I associated with indicated rapid decreases of SNR before roaming
$P_\mathrm{i(low)}$	local minimum of measured P_I associated with indicated rapid decreases of SNR before roaming
P_N	averaged noise power
P_r	received power
$P_\mathrm{r(high)}$	P_r that has been measured in the same location as $\mathrm{SNR_{high}}$
$P_\mathrm{r(low)}$	P_r that has been measured in the same location as $\mathrm{SNR_{low}}$
P_s	symbol error probability
P_t	power of a transmitter
Q	q-function
R	gross bit rate
R_B	maximum data rate, bit rate
$R_\mathrm{b(MCS)}$	maximum data rate of respective MCS
S	logarithmic value of signal power
S_m	mean value of signal power
T	temperature
T_b	bit time, duration of bit
T_c	coherence time
T_s	symbol time, the duration of a symbol
U	link margin
U_j	link margin for the respective MCSj
$\langle v_n^2 \rangle$	mean-square voltage of noise
z	random variable of normal distribution
β	threshold value of SINR
γ_b	SNR per bit
γ_s	SNR per symbol
η	spectral efficiency
λ	wavelength
σ	standard deviation
σ^2	variance
Σ	sum
X_σ	expression of shadowing effect with mean value of zero and standard deviation of σ

1 INTRODUCTION

"The design of any digital communication system begins with a description of the channel and a definition of the system requirements." [1]

The ubiquitous networking is a trend, not just a vision anymore. Still, we are not there yet. The wireless networks are needed in the industry, in the logistics, in the public administration and finally in the hospital environment too. The Internet of Things (IoT) has been turned to the Internet of Everything (IoE). Almost every area of human life has been discussed as a potential node in a huge global network of interlinked world. In fact, the mobility or the human-to-object communication that is independent on the location is a premise for the daily life. There are no borders in the world of human-to-human communication. The idea of a common global village has long been a dream of the distant and somehow unrealistic future that exists only in the science fiction movies. Who can remember how long the humanity has been entering to the new era of the technology that is a solution to all problems of a daily life? Why do we still struggle with such problems as: "my computer crashed when I tried to install a new application" or "why isn't the toaster warm", not to mention the "why did I lose the connection"?

As many times as we get frustrated with the daily technical problems, we must ask ourselves: did we do everything right? Was it plugged? Until we can get the next level of technology, we should ask if wireless communication can ensure mobility in our organization. We should ask ourselves what are we doing for the problems that seem to be out of control? Are we trying to maintain an illusion of automatically fixing problems or are we accepting that the current technology simply seems incapable of solving the problems by waiting for new updates, new technologies and new protocols?

The goal of this study is to map out the possible problems related to the wireless network in a hospital environment. However, the focus is not on the problems, but trying to find solutions to them. The approach of this work is from a physical layer point of view as it could be expressed in the "OSI language" (Open Systems Interconnection). The radio frequency (RF) design aspect has not traditionally been a very typical way of looking for the network issues in a hospital environment. However, a well-designed radio link is still the foundation of a wireless network that could serve clients in the best possible way. This is extremely important in a hospital environment where the amount of critical data communication is huge. Although the groundwork was already done when the network was designed, the maintenance of the network is a process that requires a continuous updating of the correct snapshot. "Why did I lose the connection" should lead to questions about the maintenance process of the network. In that process the RF point of view should not be forgotten.

Siun Sote has set the goal of developing North Karelian Central Hospital (NKCH) more and more in the direction of wireless connectivity in the future. The major reforms related to the new patient information system require the optimal operation of the wireless network infrastructure. The exponential growth of connecting the medical devices and the continuously increasing amount of transferred data set higher requirements not only for data security issues and in the framework of higher service level requirements but also to the highly technical disciplines covering [1]:

- Modelling the radio-wave propagation.
- Link-budget analysis.
- The coexistence issues related to the interference and spectrum management.
- The operational characteristic of radio communications protocols.

The wireless network is a RF system in which the idea of "one-size-fits-all" is not valid. The local conditions of propagation and coexistence as well as the requirements of the communications' protocols must be considered over the whole lifecycle of the system. The dynamic nature of the

shared, continuously changing RF environment means that “there is a thin line between a successful wireless network and a shining example of the tragedy of the commons” [1]. The wireless network in the hospital environment is a system with shared resources of the Industrial, Scientific, and Medical (ISM) frequency bands and the common physical space where medical devices with extremely critical requirements for data transfer must (co)exist with the systems of different technologies.

The IEEE Std. 802.11 (WiFi) [3] based Wireless Local Area Network (WLAN) has been studied in this work to figure out the challenges with signal propagation and coexistence of the newly opened part of the NKCH. The overall view of the RF-system on the ground floor and the 2nd floor of the building J2 of the hospital has been done as site surveys. The control ward of the emergency department has been chosen as the scope of more detailed study because there are many devices with critical data transfer requirements and the room geometry consists of challenging structures in the signal propagation point of view. The short site-surveys of the children’s ward on the third floor and the department of the abdominal diseases on the ground floor have been included in this work as example cases.

“The channel description includes received power, available bandwidth, noise and other impairments, such as fading” [1]. The coexistence has been chosen as an approach of this work because it includes all these aspects. The evaluation of performance has been carried out by received signal strength indicator (RSSI), signal-to-noise ratio (SNR) and signal-to-interference ratio (SIR). Hopefully, the channel description of the control ward may serve as a tool for the designing process that continuously must seek the choices that best match the channel and meet the performance requirements of a challenging hospital environment. [1]

2 RADIO SIGNAL PROPAGATION

2.1 Path loss

The path loss is based on the free-space attenuation formula of the Friis' equation which is a description of the $\frac{1}{r^2}$ -attenuation of the signal in the free space and may be expressed as

$$\frac{P_\mathrm{r}}{P_\mathrm{t}} = \left(\frac{\lambda}{4\pi d}\right)^2 \cdot \frac{G_\mathrm{t}G_\mathrm{r}}{L_\mathrm{o}} = \frac{G_\mathrm{t}G_\mathrm{r}}{L_\mathrm{p}L_\mathrm{o}}, \tag{1}$$

where λ is a wavelength of the transmitted signal, d is the distance between the transmitter and the receiver, G_t and G_r are the antenna gains of the transmitter and receiver antennas, L_p and L_o represent the path loss and other losses that are not related to propagation, respectively. [4]

Based on eq. (1) L_p may be expressed as [4]

$$L_\mathrm{p} = \left(\frac{4\pi d}{\lambda}\right)^2. \tag{2}$$

Eq. (2) expresses the free-space path-loss that has been referred in this work by $L_{\mathrm{p(free)}}$.

Because in this work the received power has been measured as Received Signal Strength Indicator (RSSI) readings that includes the effect of G_r and only the losses that have been related to the propagation has been considered, the received power P_r may be expressed based on eq. (1) and eq. (2) as

$$P_\mathrm{r} = G_\mathrm{r}\frac{P_\mathrm{t}}{L_\mathrm{p}}. \tag{3}$$

2.1.1 Transmitted power

The power P_t that has been generated in the transmitter has been led to the antenna that cannot amplify the signal of the transmitter because it is a passive device. However, the antenna may concentrate the power in the given direction. The directivity describes the power density in the direction of the maximum radiation in proportion to the radiated average power density in decibels. The isotropic antenna is an ideal construction that can radiate the same amount of energy in all directions, so the directivity is 0 dB. In this work, the access points of the studied system have an ideally omnidirectional radiation pattern in the horizontal plane. However, in practise they have some directivity too. The antenna gain may be expressed in dBi when it describes the ability of antenna to concentrate the radiation in proportion to the isotropic antenna. The antenna gain may also be defined in proportion to the dipole antenna, when it is expressed in dBd. If the dissipative or impedance losses of the antenna system are to be considered the antenna gain is a product of the antenna directivity and the loss factor that accounts for the losses. [1][4]

The effective isotropic radiated power (EIRP) is defined as a product of the transmitted power and the antenna gain. The EIRP is typically expressed as a logarithmic product of the power of the transmitter and the antenna gain as

$$\mathrm{EIRP[dB]} = P_t[\mathrm{dBm}] + G_t[\mathrm{dBi}], \tag{4}$$

where EIRP[dB] is the logarithmic value of EIRP, P_t[dBm] is the power of the transmitter in dBm and G_t[dBi] is the logarithmic antenna gain in proportion to the isotropic antenna. [1]

The EIRP varies according to the used Modulation and Coding Scheme (MCS) as it may be seen in the specifications of the access point Cisco 1852 that has been used in the studied system (Appendix 4). In the system under study, the settings of the WLAN controller have been adjusted to allow the maximum transmit power and the values of EIRP in the Appendix 4 have been calculated based on this.

2.1.2 Path loss

The large-scale variation is dominated by the attenuation of the signal as a function of the distance between the transmitter and the receiver and it follows the free-space attenuation. The path loss L_p of eq. (1) describes the attenuation as the function of the distance and it may be expressed in the logarithmical form as

$$L_{\mathrm{p}}[\mathrm{dB}] = -10n\log_{10}\left(\frac{\lambda}{4\Pi d}\right), \tag{5}$$

where L_p[dB] is the path loss attenuation expressed in decibels and n refers to the path loss coefficient [1][4].

The signal is said to be a line-of-sight (LOS) signal if there are not any objects or constructions in the direct signal path. In the opposite case it is called non-line-of-sight (NLOS). The free-space propagation is a special case of LOS propagation where the path loss coefficient $n = 2$. When $n > 2$, the attenuation of the signal has been contributed by obstacles. Although the theoretical minimum of path loss coefficient is reached in the free-space conditions when $n = 2$, it may be lower in some cases. Because of canyon effect, $n < 2$ is possible under the indoor circumstances where signal LOS propagates, e.g., in the long corridor [4]. When n increases as a function of distance, the signal is said to be attenuated and vice versa. [4]

"The concept of free space assumes a channel free of all hindrances to RF propagation" [1]. The phenomenon of the free space is a very theoretical simplification of reality because there are always obstacles that affect the signal propagation near the signal path. The free-space path loss is although needed when the reference path loss of eq. (6) is calculated. The received power at the distance d from the transmitter may be expressed as

$$P_{\mathrm{r}}(d) = P_{\mathrm{r}}(d_0) - 10n\log_{10}\left(\frac{d}{d_0}\right), \tag{6}$$

where $P_{\mathrm{r}}(d_0)$ is received power at the reference distance d_0. [1][4]. The reference distance of 1 metre is typically used indoors [4][6].

The path loss in the distance d may be defined empirically by measuring the received signal power at the distance d and subtracting it from the effective radiated power EIRP as [1]

$$L_{\mathrm{p}}(d) = \mathrm{EIRP} - P_{\mathrm{r}}(d). \tag{7}$$

Eq. (7) gives the reference path loss when $d = d_0$.

As it may be seen from eq. (6), there is a linear dependence between the path loss and the logarithmic distance where n represents the slope of the line. The slope n may be determined by measuring the received power at the reference distance d_0 and the respective values of path loss in the distance of d. The slope can be determined by linear regression from the cloud of the empirically derived values of $L_{\mathrm{p}}(d)$.

Because the path loss coefficient may not necessarily remain constant within the whole distance *d*, it must be determined piecewise (Figure 1).

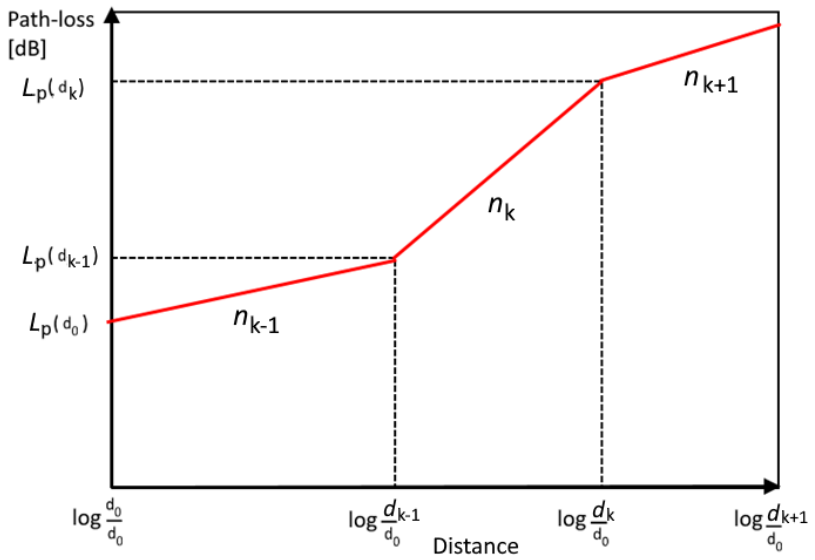

Figure 1. The changing slope n_k of the multi-slope path loss model where k = 1,2,3.

The multi-slope path loss model of Figure 1 represents the principle of determining the slopes of the piecewise linear curve. The reference path loss of the slope n_k may be determined as

$$n_k = \frac{L_p(d_{k-1})}{10[\log_{10}(d) - \log_{10}(d_{k-1})]} = L_p(d_{k-1}) \frac{1}{10 \log_{10}(\frac{d}{d_{k-1}})}, \quad (8)$$

where for n_k: d is the distance from the respective reference distance d_{k-1}, $L_p(d_{k-1})$ is the corresponding reference path loss and n_k is path loss coefficient with k = 1, 2, 3. [6]

2.2 Path loss propagation with shadowing

The obstacles near the signal path contribute to the random decrease of received signal strength. This variation is called a fading. The slowly changing random signal variation that has superimposed on the propagated signal is called slow fading. The slow fading is also called shadowing which refers to the shadowing effect of the obstacles that appear on the signal path. Shadowing has also been called log-normal fading because it is random and typically follows a log-normal distribution around the local mean value. The shadowing effect typically increases with distance because of the cumulative effect of the obstacles. [4]

The propagation model that considers these both effects is called the log-normal shadowing path loss model (LNSPL). It may be expressed as

$$L_p(d)[\text{dB}] = L_p(d_0) + 10n\log_{10}\left(\frac{d}{d_0}\right) + X_\sigma, \quad (9)$$

where X_σ represents the shadowing effect [4][8][8]. LNSPL is a path loss model where the accuracy is improved by considering the shadowing effect. It is a simple model that can be generalized to different environments. The Gaussian random variable X_σ describes the shadowing with a mean value of zero and a standard deviation σ [dB]. The allowable path loss that may be tolerated to meet the sensitivity requirements of the receiver can be expressed as a sum of the path loss and the shadowing.

The shadowing effect must be calculated based on the measurements in a wide range of locations and with different distances between the transmitter and the receiver. [4][8]

The shadowing that is assumed to be superimposed around the mean values of the model may be defined as

$$X_\sigma[\text{dB}] = z \times \sigma_s[\text{dB}], \tag{10}$$

where z follows the normal distribution. Typically, the coverage probability of 95% is assumed which gives for the normal distributed variable $z = 1.645$. The standard deviation σ_s is based on the squared errors and the sample variance of the measured values in proportion to the modelled ones that have been calculated based on the generated path loss model. [10]

The X_σ a value of 10 dB is often used both in office and hospital environments. Although the standard deviation of 8 to 10 dB has typically been used for the log-normal distribution the standard deviation of 12 dB has been defined empirically for the shadowing in the case of indoor propagation. When considering the indoor propagation, the uncertainty of the X_σ is 87% compared to the best case of 8 dB when it is 81%. That indicates the stronger variation of the shadowing effect in the environment where more obstacles are located near the signal path. The indoor shadowing in the order of 20 dB has also been reported in some publications [10]. [4]

There are few aspects that must be considered when modelling the propagation by LNSPL. Firstly, because the parameters of eq. (9) are defined by the linear regression, the amount of the measured data must be large enough. In other words, the sum of squared errors must be minimised when fitting the line to the measurement results. The inaccuracy of the LNSPL model will raise if there are external factors that affect the results of the RSSI measurements. [8]

Secondly, there have been some critics in the literature against the use of RSSI-values in the defining the path loss model. If there are coexisting devices in the neighbourhood that operate at the same frequency range the RSSI-values may cause errors to the model. Although the coexistence issues will be discussed later in this work it is worth mentioning that there have been reported the differences of 4.2 dB between the RSSI readings of interfered and non-interfered frequencies. Another aspect that must be considered and that has a major role in estimating the n is related to the problem that is caused by the fact that only the RSSI values of the received signal can be detected. The comparisons that have been done based on the mathematical models argue that the error in n is 0.25% when the threshold has not been accounted for the modelling of the path-loss whereas the error in the presence of the sensitivity threshold has increased to 10.55%. This can be eliminated by keeping the distance between the transmitter and the receiver under the limit where the power of the transmitted signal equals the sensitivity of the receiver. [8]

The shadowing is calculated by the variance of the measured path loss values. They are compared to the mean values that are based on the propagation model that has been derived from the empirical measurements. [6]

Based on eq.(9) it may be seen that path loss and a shadowing are summed together. According to the eq.(10) the statistical variation of the shadowing is described by the standard deviation σ around the modelled mean value. It may be computed by a minimum mean square error (MMSE) method. The MMSE may be expressed by the error equation as

$$F(n) = \sum_{i=1}^{k} \left(L_{\text{p}_{\text{meas}}}(d_\text{i}) - L_{\text{p}_{\text{model}}}(d_\text{i}) \right)^2, \tag{11}$$

where $L_{\text{p}_{\text{meas}}}(d_\text{i})$ refers to the measured values of power in dB, $L_{\text{p}_{\text{model}}}(d_\text{i})$ refers to the calculated value based on the propagation model, d_i is the distance of the measurement location from the transmitter and n is the propagation coefficient [6]. Although the propagation coefficient may be derived by linear regression as it has been discussed earlier, it can also be determined by

differentiating the eq. (11) in proportion to n. Then propagation coefficient with the minimum mean square error may be found by the equation where [6]

$$\frac{\partial F(n)}{\partial n} = 0 \ . \tag{12}$$

The square error function of eq. (11) may also be used in determining the standard deviation σ. If it is divided by the number of samples the variance σ^2 relative to the chosen propagation model will be resulted as

$$\sigma^2 = \left(\frac{1}{k}\right) \sum_{i=1}^{k} \left(L_{\mathrm{p_{meas}}}(d_\mathrm{i}) - L_{\mathrm{p_{model}}}(d_\mathrm{i}) \right)^2, \tag{13}$$

where k is the number of samples [6]. Eq. (12) gives the variance and by taking the square root the standard deviation σ is the result. [6]

2.2.1 Outage probability

When the log-normally propagated signal is received, the effect of shadowing may cause the transmitted power to fall below the sensitivity of the receiver. The outage probability $p_{\mathrm{out}}(P_{\mathrm{min}}, d)$ under the circumstances of path loss and shadowing can be calculated as

$$p(P_\mathrm{r}(d) \leq P_{\mathrm{min}}) = 1 - \mathrm{Q}\left(\frac{P_{\mathrm{min}} - (\mathrm{EIRP} - L_\mathrm{p}(d))}{\sigma_{\psi_\mathrm{dB}}}\right) \tag{14}$$

where $P_\mathrm{r}(d)$ is a received power at a distance d, P_{min} is sensitivity of the receiver, $\sigma_{\psi_\mathrm{dB}}$ is standard deviation of the shadowing and $L_\mathrm{p}(d)$ is path loss in the distance d from transmitter [6]. Typically, the outage probability should be under 1% for reliable communication [6].

2.2.2 Fast fading

The previously discussed shadowing is also called a slow fading. It is “the change in the average signal level over large distances due to … visual obstacles” [4] whereas the fast fading refers to the rapid changes in the signal power and phase that are caused by multipath mechanisms. The multipath is typically indicated within the displacement of the half of the wavelength. Because the fast fading occurs randomly it must be studied by considering the statistical properties of the varying signal strength. The probability density functions (PDF) of Rayleigh and Rician distributions are typically used depending on whether there is a dominant signal that contributes the signal changes or not. The dominant contribution may typically be LOS-signal. [4]

When the receiver is in motion with respect to the transmitter the signal properties may also be changed by the Doppler shift. In the frequency selective channel, the various frequency components of the propagating signal may be attenuated in a different way. The effect of the Doppler shift, or spread as it is also called, is described as a change of the frequency that is caused by the motion of the receiver when the channel is frequency selective. The maximum change in the frequency, f_m, can be described by a ratio of velocity of a receiver and wavelength. When the receiver is in motion there is both time and frequency dispersion that results the spread in time of the modulation whereas the frequency dispersion may be detected as the attenuation of the signal at the given frequency. The multipath mechanisms may result in the attenuation that changes in time. So, there may be times when the frequency selective fading does not occur, or it may be occurred only in the portion of the frequency region. If the resulting time spread is smaller than the symbol duration the fading is said to

be flat otherwise it is frequency selective at that moment. The changes of the channel that occur during the symbol time, T_s, of the signal results the symbol distortion. [4]

The frequency band where the attenuation of the frequency components remains unchanged is called a coherence bandwidth of the channel. If the coherence bandwidth is smaller than the modulation bandwidth, the time dispersion results inter-symbol interference (ISI) that in turn degrades bit error rate (BER) reducing the quality of the received signal. The coherence time, T_c, describes the time when the channel remains constant or in other words, it is a measure of the speed that is expected for the change in channel characteristics, and it may be approximated as an inverse of the Doppler shift. If the $T_c << T_s$, the channel fades rapidly and the fast fading is said to be occurred. When it is vice versa, the slow fading is resulted. [4]

2.3 Other empirical indoor path-loss models

Several more sophisticated propagation models have been generated. Some of them not only consider the multipath but also include algorithms that can compute the propagation by the accuracy of the single ray. They can be classified as empirical, deterministic, and semi-deterministic models. In some publications the models are classified in the deterministic and the statistical models. The deterministic models are based on the theoretical work and they typically require a complete description of the environment that is included in the parameters that the algorithms are using. However, most of them may also be called semi-empirical because the empirical measurements are needed in generating the model. The deterministic models enable the visibility of every path between the receiver and the transmitter by an algorithm that traces or launches a set of rays in the environment of propagation by solving Maxwell's equation according to the integral or differential solution. Other types of the deterministic algorithms are models that compute a 2D or 3D grid-based description of the environment using Maxwell's equations in both time and frequency domains. [10][10]

The statistical description of the multipath propagation is typically based on the Rayleigh distribution when the environment is strongly shadowed and on the Rician distribution when there is one dominating signal path as it is, for example, in the case of LOS propagation. Although most of the models have been developed for the cellular systems there still are some models that are suited for studying the indoor propagation where the distances are short compared to the outdoor propagation environment. [4]

Because the propagation is strongly dependent on the obstacles on the signal path or near it, the hospital environment forms specific conditions for propagation. The attenuation effect of the obstacles depends also on the material properties of the obstacles causing the varying RF-transparency of wall structures within the signal path. The special wall materials and constructions that are used especially in the hospitals may contribute a remarkable attenuation of the signal. Such wall structures are used, e.g., in the walls of X-ray or Computer Tomography (CT) rooms. Normally, they include an additional lead shield of 0.5 to 2.5 mm inside the wall construction depending on the strengths of the X-ray device. The attenuation of the X-ray room may be in the order of 60 dB which may lead to the crucial attenuation of the signal. On the other hand, the attenuation of an ordinary patient room with the wall construction of plasterboards is only 10 dB or less. Furthermore, there may be cabling, ducts of the hospital gases and pipelines in the hollow of the wall structures that may have a strong effect on the radio wave propagation that are not only causing the signal attenuation but also contributing the multipath propagation. [12]

Some empirically derived propagation models that have been developed for the indoor propagation will be presented here. The propagations models that are generated for the indoor environment are more complex because of a large number of obstacles near the signal paths, varying room geometries and the floors of the building that strongly affect the propagation. However, their use is typically limited to the context where the measurements have been carried out. [4][10]

The indoor path loss model for Picocells that may be used in WLANs at the 2.4 GHz frequency band has been presented as [4]

$$L_{\mathrm{p}}(d) = \bar{L}_{\mathrm{p}}(d_0) + 10n \log_{10}(d) + L_{\mathrm{f}}(b) + \mathrm{X}_{\sigma}[\mathrm{dB}], \tag{15}$$

where $\bar{L}_{\mathrm{p}}(d_0)$ refers to the reference path-loss at the distance of 1 metre that is 38 dB, n is path-loss coefficient of 3.0, d is distance [m], $L_{\mathrm{f}}(b)$ refers to the signal attenuation through b floors and is 15 + 4(b-1) and X_{σ} is shadowing of 10 dB. The form of the model in eq. (15) has been generated for residential, office and commercial environments. [4]

ITU-R (International Telecommunication Union - Radiocommunication sector) Model Recommendation for indoor propagation model has been presented as

$$L_{\mathrm{p}}(d) = 39.6 + 10n \log_{10}(d)\,, \tag{16}$$

where n is 3 for office environment, 1.8 for corridors, 4 for longer NLOS distances and $d > 1$ m [4]. The canyon effect causes a low value of n in the case of $n = 1.8$ which is below the free-space path loss.

The path loss model of IEEE 802.15.2-2003 has been generated for wireless sensor networks at the 2.4 GHz band. It has been published with two different forms where path loss coefficient and reference path loss have been determined for distances 0.5 m < d < 8 m as [4]

$$L_{\mathrm{p}}(d) = 40.2 + 20 \log_{10}(d), \tag{17}$$

and for distances $d > 8$ m as [4]

$$L_{\mathrm{p}}(d) = 58.2 + 33 \log_{10}\left(\frac{d}{8}\right). \tag{18}$$

2.4 AWGN noise process

"The noise refers to unwanted electrical signals that are always present in electrical systems " [1]. The mean-square voltage of the noise may be written to the form that expresses the spectral noise density as

$$N_0 = \frac{N}{B} = kT, \tag{19}$$

where N is averaged thermal noise power, B is the bandwidth of the receiver, k = 1.38065 x 10^{-23} m^2 kg s^{-2} K^{-1} (Boltzmann's constant) and T is antenna temperature [12].

The bandwidth of the noise that is seen at the detector is broader than the signal bandwidth in analogue receivers. However, the bandwidth of the noise equals the bandwidth of the signal in digital receivers because matched filters and correlators make more accurate filtering possible. So, it results that the noise power may be calculated as a product of spectral noise density and the bandwidth of the signal power. [12]

In the additive white gaussian noise (AWGN) channel the power spectral density $G_{\mathrm{n}}(f)$ of the thermal noise is flat until 10^{12}Hz and may be expressed as [1]

$$G_{\mathrm{n}}(f) = \frac{N_0}{2}\,. \tag{20}$$

Because of the flat distribution over the spectrum, the noise may be called as white noise. In principle, the bandwidth of the white noise is infinite. However, the limited bandwidth of the real systems results that the averaged power of white noise may have a finite value when the noise has passed through it as it has been discussed above. The averaged power of the white noise may be expressed as

$$P_{\mathrm{n}} = \int_{-\frac{B}{2}}^{\frac{B}{2}} \frac{N_0}{2} \mathrm{d}f \,, \tag{21}$$

where B is a bandwidth of the noise signal when $B < \infty$ [1].

The AWGN process may be described as a Gaussian random process with zero mean value and standard deviation, σ, of 1. If the noise properties of the radio link may be approximated as AWGN channel, the received signal may be expressed as a sum of the modulated signal power and the random noise power that has been added to the received signal before the reception. [6]

Because the AWGN process is a random process, any two white noise processes are uncorrelated if two samples were taken from the noise signal so that one sample is taken from the time-shifted (with $\tau > 0$) signal of another signal. With an assumption that they both are Gaussian distributed they are said to be independent. As a result, every transmitted symbol has been independently affected by the noise when the signal has been detected.

2.5 Signal-to-noise ratio

If the radio link may assume to be AWGN process as it is the case in most digital communication systems, the noise power may be assumed uniformly distributed with the spectral density of $N_0/2$ within the bandwidth of the receiver that is $2B$. Then SNR may be expressed as

$$\mathrm{SNR} = 10 \log_{10} \left(\frac{P_{\mathrm{r}}}{N_0 B} \right), \tag{22}$$

where P_{r} is received power [6]1.

If the aggregated power of interference may be assumed to follow the Gaussian distribution it may be summed with the noise power and the resulting logarithmic equation for signal-to-interference-plus-noise ratio (SINR) may be expressed as

$$\mathrm{SINR} = 10 \log_{10} \left(\frac{P_{\mathrm{r}}}{\Sigma P_{\mathrm{i}} + P_{\mathrm{n}}} \right) \geq \beta, \tag{23}$$

where ΣP_{i} refers to the aggregated power of interference, P_{n} is the averaged noise power and β is a threshold value of SINR. When the power of the received desired signal has been expressed only in proportion to the ΣP_{i}, the ratio may be called as signal-to-interference ratio (SIR). [6][14]

The SIR model that considers the bandwidth of the affected receiver has been published to figure out the interferences in WBANs where several pairs of Bluetooth and Zigbee nodes may interfere with each other. The logarithmic expression of the model has been presented as [6]

$$\gamma[\mathrm{dB}] = P_{\mathrm{S}} - L_{\mathrm{p}}(d) - \sum_{i=1}^{n} \left(W_{\mathrm{D,I}} P_{\mathrm{i}} - L_{\mathrm{p}}(d_{\mathrm{i}}) \right), \tag{24}$$

where γ is SIR, P_s is the useful signal, $L_{\mathrm{p}}(d)$ is the path loss in the distance d between the two affected nodes, P_{i} is the power of the i:th interferer, and d_{i} is the distance from the i:th interferer to the affected receiver. $W_{\mathrm{D,I}}$ has been expressed as [6]

$$W_{\mathrm{D,I}} = \begin{cases} 1, & \text{if } B_{\mathrm{I}} \leq B_{\mathrm{DS}} \\ \frac{B_{\mathrm{DS}}}{B_{\mathrm{I}}}, & \text{if } B_{\mathrm{I}} > B_{\mathrm{DS}} \end{cases}, \tag{25}$$

where B_{I} is the bandwidth of the interferer and B_{DS} is the bandwidth of the desired receiver.

The aggregated interference power in the eq. (23) and (24) refers to the power of all unwanted signals that have been received. In this work the fixed value of β has been used. The threshold β must be exceeded to meet the SINR-related quality requirements of the link. There have been some discussions about the fixed threshold in the literature and the model of graded threshold has also been presented. The fixed threshold has been criticized in throughput point of view because the links with the values of SINR less than β may still be useful in data transmissions of lower requirements. [14]

Because SNR is based on the averaged power, the energy of the signal is more practical in digital communications. However, the SNR is still an appropriate metric when the properties of RF system are analysed. [1]

The energy of one bit may be expressed as

$$E_{\mathrm{b}} = ST_{\mathrm{b}}, \tag{26}$$

where S is signal power and T_{b} is a bit time [1]. For binary modulation bit time T_{b} equals to symbol time T_{s}. If T_{s} is $1/B$, SNR for binary signalling may be expressed as SNR = E_{b}/N_0 [6].

If all received power is assumed to be in the modulating signal and the noise power follows Gaussian distribution with the characteristics of AWGN noise process, the energy of bit related to the noise power may be expressed as

$$\frac{E_{\mathrm{b}}}{N_0} = \frac{ST_{\mathrm{b}}}{\frac{N}{B}} = \mathrm{SNR}\,\frac{B}{R_{\mathrm{b}}}, \tag{27}$$

where N is the averaged noise power and R_{b} is the bit rate [1].

The bit energy per noise has typically been expressed in decibels when it may be expressed as [1]

$$\frac{E_{\mathrm{b}}}{N_0}[\mathrm{dB}] = 10\log_{10}\left[10^{\frac{\mathrm{SNR}}{10}}\left(\frac{B}{R_{\mathrm{b}}}\right)\right]. \tag{28}$$

The ratio of E_{b} to N_0 has sometimes been called as SNR per bit. If the bit energy has been replaced by the energy of the received symbol and binary modulation has been used, the SNR may be written in the form of

$$\mathrm{SNR} = \frac{E_s}{N_0 B T_s} = \frac{E_b}{N_0 B T_b}, \tag{29}$$

where E_s refers to the energy of the received symbol [6]. Based on eq. (27), SNR may be expressed using the SNR per bit of eq. (28) in decibels as [1]

$$\mathrm{SNR}[\mathrm{dB}] = 10\log_{10}\left[10^{\frac{E_{\mathrm{b}}}{10N_0}}\left(\frac{R_{\mathrm{b}}}{B}\right)\right]. \tag{30}$$

Eq. (27) may be re-written in the form that expresses the received power as a product of SNR per bit and the data rate as [6]

$$\frac{P_r}{N_0} = \frac{E_b}{N_0} R_\mathrm{b} \ . \tag{31}$$

Although the equations above assume that all received power is in the modulating signal, they may be used if the difference has been considered as signal losses in the carrier. [1]

2.6 Capacity of the channel

Shannon's theorem sets the theoretical limit for the capacity of the channel. It gives the maximum capacity for a Gaussian channel. The channel capacity, *C*, is given as a function of the signal-to-noise ratio as [1]

$$C \leq B \log_2(1 + \mathrm{SNR}) \ . \tag{32}$$

Dividing both sides of eq. (32) by *B*, the spectral efficiency may be expressed as

$$\eta = \frac{C}{B} \leq \log_2\left(1 + \frac{E_\mathrm{b}}{N_0}\frac{R_\mathrm{B}}{B}\right) \tag{33}$$

where R_B is the maximum data rate [1]. The lower limit of SNR per bit may be expressed by spectral efficiency as

$$\frac{E_\mathrm{b}}{N_0} \geq \frac{2^\eta - 1}{\eta} \tag{34}$$

The Shannon capacity equation indicates that it is possible to find a coding and modulation scheme that in the conditions of bandwidth limited signal gives a maximum data rate that equals the channel capacity over the AWGN channel with an arbitrary low value of bit error probability [4].

The SNR may be expressed as a product of the ratio of averaged signal power and noise density and the spectral efficiency of the modulation scheme as

$$\mathrm{SNR} = \frac{E_\mathrm{b}}{N_0}\frac{R_\mathrm{B}}{B} \tag{35}$$

where R_B/B is the spectral efficiency or an information bit rate per unit bandwidth occupied and is expressed in bps/Hz [4]. It describes the spectral efficiency of the modulation scheme for which the symbol rate may be expressed as

$$T_\mathrm{s} = \frac{R_\mathrm{B}}{\log_2 M} \tag{36}$$

where *M* is the order of modulation [4]1.

2.7 Error performance of the wireless system

The error performance of digital communication systems may be studied from various perspectives. It may be studied from SNR or inter-symbol interference (ISI) point of view, but it may also be evaluated as bit error probability or bit error rate as well. The term error performance refers to the performance degradation of digital communication systems that may be caused by losses or noise in

the channel that results in the degradation of SNR and finally increase of symbol error and bit error probability. [1]

Eq. 27 describes the dependence between the SNR of digital communication system on the received E_b/N_0. Ultimately, the error performance has been contributed by the signal attenuation, the noise power, or interferences of the channel. The propagation models that have been discussed earlier or link budget analysis have typically been used to figure out the losses of the channel that may result in the degradation of SNR. However, as it will be described in Figure 3, the chosen operation point is based also on the bit error probability that typically has been used as a design criterion. [1]

The two parameters that refer to the probability of bit error are discussed. The bit error ratio (BER) is a metric that describes the number of bit errors in proportion to the received bits. The bit error rate describes the number of bit errors in proportion to the studied time interval. The expectation value of the BER is called bit error probability (P_b or P_e). It has been used to approximate the real BER and it is an important measure of the required quality of digital communication that may be used to describe the error performance of the system. [1][4]

The BER defines a tolerance for the error performance of the system. The requirements of the used modulation and coding scheme (MCS) depend on the SNR and the received signal strength P_r which are affected by EIRP, losses and noise parameters of the channel. On the other hand, also the required BER is depending on the SNR, which results together with the previously described dependence in restrictions for the use of MCS. So, e.g., if also maximum data rate has been used as design criterion, BER should be defined for given data rate. In this work BER has been defined for the maximum data rate of the used modulation and bandwidth. The SNR sets the upper limit for the achievable BER and when it increases when the received power gets closer to the receiver sensitivity and if the required SNR could not be guaranteed, the coding may be used for error correction. Although Shannon's theorem defines the absolute minimum for the appropriate SNR, the required BER defines it from the practical error performance point of view. [1][8][14]

Secondly, the MCS has been discussed as it determines the required SNR and signal strength of the channel. The maximum capacity of the studied network may be attained by 256QAM (quadrature amplitude modulation) modulation at the 5 GHz frequency band and 64QAM modulation at the 2.4 GHz band. MQAM modulation scheme is based on the modulation of amplitude and phase. Symbol 'M' expresses the order of the modulation that indicates the number of locations in amplitude – phase axis that have been used in the constellation of one symbol. The square root of M represents the number of locations in the symbol. They have been ordered in the square shape so that one symbol may transfer $\sqrt{M}$ of binary coded data bits. However, the data transfer capacity increases with increasing value of M at the expense of the bit error probability. As it may be seen in the figure below, when the number of locations has been increased the error margin between the locations decreases (Figure 2). This sets the higher requirements for the radio link, especially in the SNR point of view. [1][14]

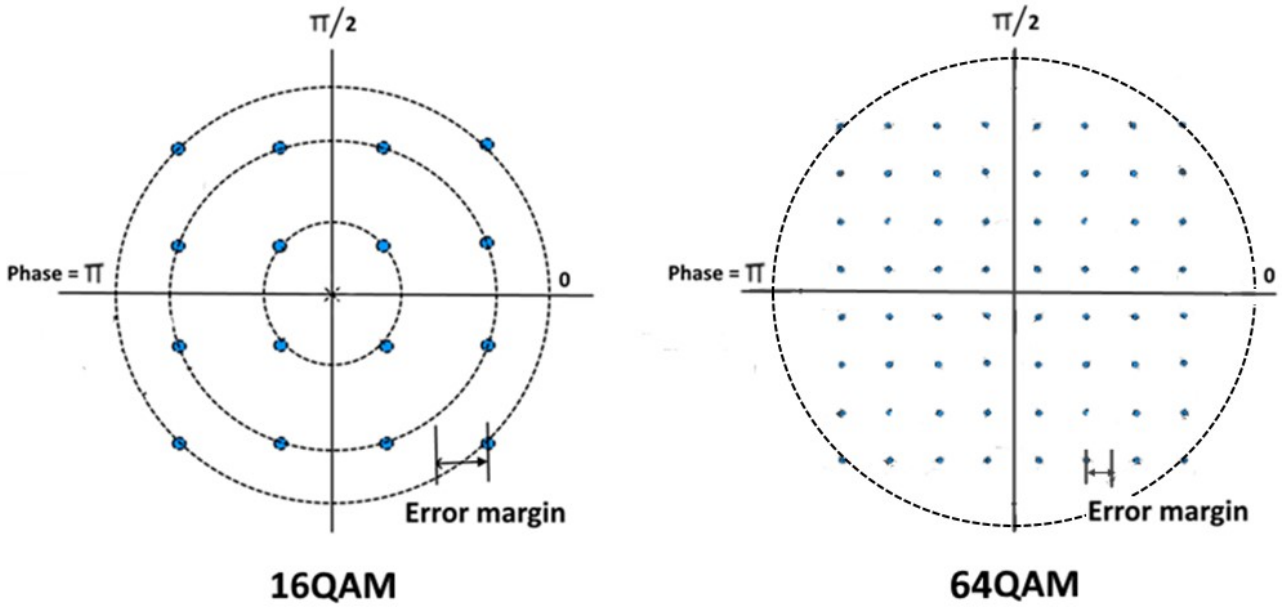

Figure 2. The error margin of the modulation scheme.

The spectral efficiency increases with the increasing order of MQAM modulation scheme. As it has been discussed earlier, there is an upper limit for the increased spectral efficiency. Although the capacity of the channel may be raised by increasing the data rate, based on eq. (32) the upper limit has been dictated by the E_b/N_0. When the MQAM modulation scheme has been discussed, the capacity of higher order modulation requires more SNR or otherwise the data rate must be decreased. However, the transmit power should simultaneously be reduced to avoid the distortion caused by the high peak to average ratios. In the case of IEEE 802.11n this means that a decrease of 4-5 dB is needed in the transmit power when MCS has been increased from MCS indices MCS0 to MCS7. The properties of the respective MCS index may be seen in the Appendix 2. The resulting theoretical decrease of coverage is in the order of 10 to 40 metres depending on the channel model. [16]

If the SNR requirement of the used MCS has not been met in the channel, the coding has been used. The MCS indices defines the used coding with the specific redundancy of the respective MCS resulting in the varied requirements of the headroom. This may further increase the required bandwidth in the given data rate. [1]

The transmitted error bits may be corrected by using the coding scheme known as forward error correction (FEC) that has been defined by the PHY level protocol. Higher bit rate requires more coding resulting the increased overhead. However, the efficient modulation scheme is more beneficial than the coding scheme when the BER must be increased. [10]

2.7.1 Link margin

The gains and losses of the propagated signal in decibels has been summed up to figure out the resulting link margin, *U*. When the sensitivity requirement of the receiver has been given, the maximum of allowable path loss may be calculated by the link budget. In this work, the link margin has been evaluated primarily from the signal-to-noise ratio point of view.

Although the SNR describes the quality of the radio link, E_b/N_0 has been used when the error performance of digital communication has been studied because digital signal is not a power signal. In Figure 3 $(E_b/N_0)_{reqd}$ expresses the minimum E_b/N_0 that is needed for the reliable communication in the AWGN channel when the required P_b has been given (Operating point 2). However, the measured value of E_b/N_0, $(E_b/N_0)_{meas}$, is lower than $(E_b/N_0)_{reqd}$ resulting in higher P_b than the required value (Operating point 1). Because of this, coding must be used. The coding pushes the curve towards the

origin resulting the reduction of the required $(E_b/N_0)_{reqd}$ that is called coding gain. This may be seen in Figure 3 as transition from Operating point 1 to Operating point 2. As a result, required P_b may be attained by the lower value of E_b/N_0. Because of the redundancy that it requires, the more bandwidth is though needed.

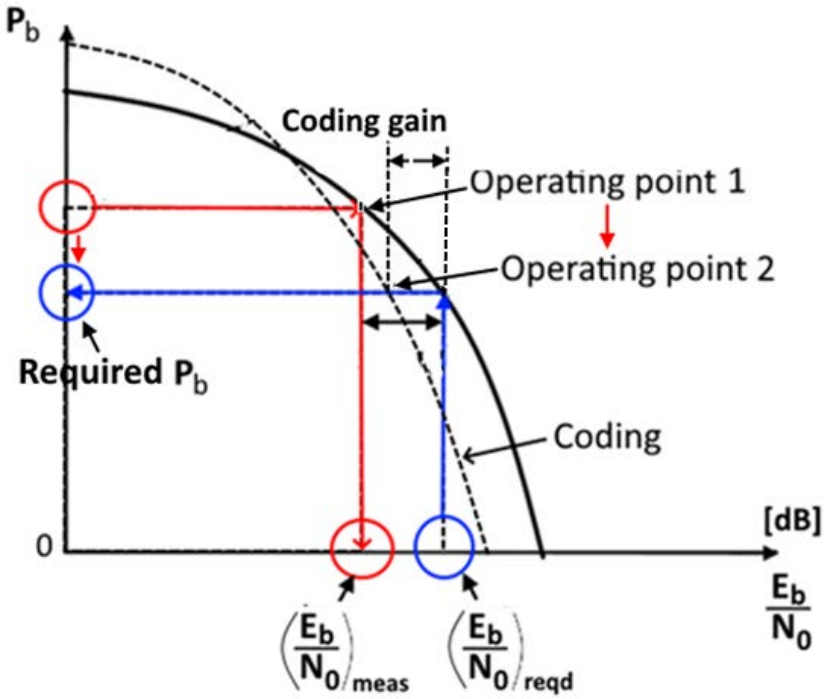

Figure 3. The gap between the required $(E_b/N_0)_{reqd}$ and measured $(E_b/N_0)_{meas}$ and of coding gain.

The gap between the required and measured E_b/N_0 may also be decreased by increasing the EIRP or by reducing the data rate because E_b/N_0 is inversely proportional to the data rate. The increase of bandwidth results also the increase in E_b/N_0 but because the signal is bandwidth limited in this case, it may not be used. As it has been discussed above, the optimization of the parameters may be needed to guarantee the required error performance. If the required value of $(E_b/N_0)_{reqd}$ cannot be maintained within the link, the access point obviously reduces the data rate by decreasing the MCS. If the data rate cannot be decreased, the coding may be used to keep the required error performance. [1]

The required BER has typically been defined as 10^{-3} when the sensitivity of the client has been measured 1. However, in this work the required value of P_b has been defined as 10^{-2} [6]1. There must also be a link margin between the measured and the required signal-to-noise ratio to ensure the given value of BER because there will always be some changes in the signal-to-noise ratio. The system required error performance yields the value of the required BER based on the required throughput of the system. The used modulation and the coding scheme set the requirements for the BER but also for SNR and the RSSI. The fading must be considered in the calculation of link margin as well as noise floor. The sufficient link margin depends on how accurately the system has been described in the link budget analysis. The changing interference conditions, the suboptimal behaviour of the RF system or varied noise properties of the receiver must be considered when the link margin is determined. In some cases, U of a few decibels may be sufficient, but it must be considered case by case. [1]

When the link margin of this work has been calculated, these maximum values of data rates have been used as a reference to compare the empirically derived values of data speed. There are variations in the RF conditions that might not have been considered in the modelled path loss although the shadowing has been included in the model. The variations may result the decrease of data rate or signal outage that has been discussed earlier. The devices that will be added in future and changes in

the building constructions as well as wireless infrastructure may change the conditions of RF system. This results that the determination of a proper link margin must be done carefully, and it be defined as in the worst case. [1]

2.8 Requirements of the wireless network

The Quality of Service (QoS) defines the requirements of the network. The QoS features of IEEE 802.11 standards have primarily been ensured at the MAC (medium access control) layer and some of the standards have launched only because of enhancing the QoS properties. Specifically, IEEE 802.11e has been focused on QoS by defining the MAC routines that work with any PHY (physical layer) implementation. Because the scope of this study is the discussion of the PHY layer from the aspect of the RF system, the more detailed discussion of the QoS will be ignored in that context. However, an insight to the QoS from the RF point of view has been presented in Figure 4 although the MAC layer mechanisms have been needed for admission control and scheduling of data packets. [18]

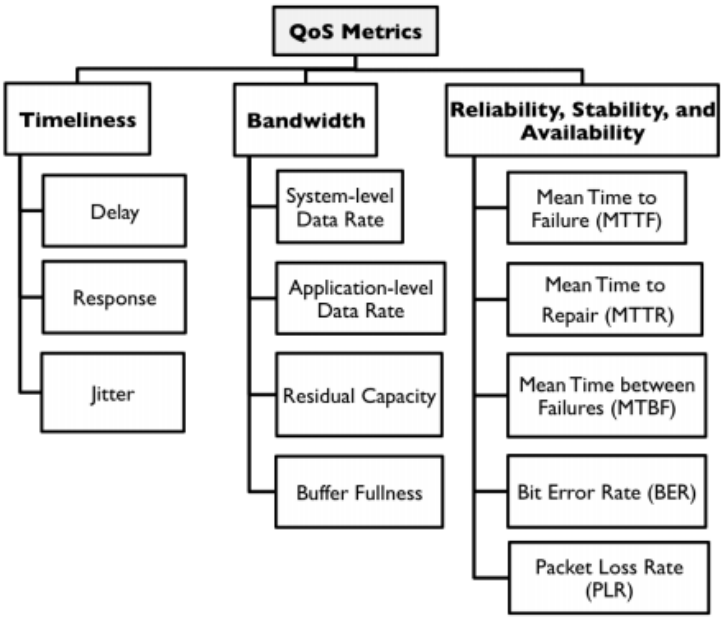

Figure 4. QoS metrics of the IEEE 802.11.

QoS issues deal with resource allocation regardless of the standard that the wireless system is based on. As it may be seen in Figure 4, the timeliness, bandwidth, reliability, stability, and availability have been presented as shared resources. If the allocation of the resources has not been managed in a proper way, the extraordinary loading or the deteriorated parameters of the RF system may result in some of the consequences that have been listed under the respective resource in Figure 4. [18]

There are QoS techniques that use algorithms to mitigate the detected interference by joint channel assignment and routing. The channels have been assigned based on the network topology and the traffic information has then been used to assign the channels in a proper way. The algorithm may also create multiple routes to raise the throughput in the network. [18]

The new QoS techniques may also enhance the coexistence of different technologies like IEEE 802.11 and IEEE 802.15.4 by using the cognitive wireless networks. They involve means for adaptation of distributed wireless resources that will be more important with the trend of increasing deployment and diversification of wireless technologies. Specially, in the hospital environment where

the issues of coexistence between the WBANs and the IEEE 802.11 may arise, the traditional QoS may not be implied without considering the application specific nature of the QoS criteria. For example, because the WBANs typically operate at low duty cycles and there may be a remarkable periodic variation in the traffic, the implementation of strict QoS may lead to suboptimal use of the shared resources. It may result in the network instability as well as link and power failures in the WBAN. Because the mobility of the typical patient monitoring device in the WBAN is extremely important, the routing problems resulting from the network instability may be fatal. [18][19]

The QoS requirements vary to a great extent among the different user groups. This is challenging from the system design perspective. The queuing delays and number of packet retransmissions are typical examples of the QoS criteria that are strongly case specific. Next, some aspects of QoS requirements for medical WBANs will be discussed. [20]

2.8.1 QoS requirements of the medical WBANs

The special requirements for the wireless networks in hospitals have been discussed in many standards by IEEE and some ongoing projects of ETSI. The comprehensive survey on the QoS of hospital environment is not in the scope of this study because QoS has primarily been defined by the parameters of the MAC level. The QoS of IEEE 802.11 WiFi has been shortly discussed above and some typical specifications and requirements of the medical WBANs will next be briefly reviewed.

The typical medical applications that use the nodes of WBANs on the human body or inside it has been used in the measurement of ECG (electrocardiogram), oxygen saturation, blood pressure and in pacemakers and glucose sensors. The data rates of them are typically at maximum in the order of few kbps and duty cycles per device are under 1% except in ECG where it is tenfold. On the contrary, the requirements for low latency may be crucial in some medical devices. [19]

The requirements of WBANs have been defined in IEEE 802.15.6. The scalability of the networks should be up to 256 nodes and the data rate of 10 kbps to 10 Mbps should be supported. Packet error rates for octet payload should be under 10% for 95% of the best performing links. The performance of links has been considered so that at a given SNR of 5% for the channels that have given the worst PER should not have been calculated. The latency should be under 125 ms and jitter under 50 ms. According to the standard, the coexistence must be supported in the environment where the various technologies are cooperating. The coexistence problems may arise also because of the vendor dependencies of complex systems that should have been coordinated in a better way. [19]

2.8.2 Required error performance of the studied system

The requirements of the WLAN in NKCH have not been available for this study so they could not have been used as reference values. Hence, the error performance of the system under study has been discussed based on the chosen bit error probability, the required SNR and RSSI level of the respective MCS.

The system performance is typically defined also from the bit error point of view. As it has been discussed earlier, the given bit error probability may be used to describe the designed operation point of the system. In this work P_b has been used as it is a function of the signal-to-noise ratio that has a major significance in evaluating the operation of the RF system. [1]

The P_b has been presented as a function of SNR per bit in Figure 3. The used modulation defines the lower limit for the tolerated value of SNR from the modulation point of view and the upper limit has been dictated in principle by Shannon's theorem in eq. (31) but in practice the measured value of SINR sets the upper limit. The required BER has been approximated by P_b. On the other hand, since the performance of the existing RF system has been analysed, the SNR requirements of the MCS have been used in this study as performance criteria and the performance has been first evaluated by

comparison of the SNR that has been measured in the respective locations and the SNR required by the MCS. The difference between them may be called a safety margin or link margin which refers to the typical design process where the margin must be added to ensure the proper operation of the RF system. In this work the safety margin has been evaluated to figure out if the requirements of the MCS have been met in the respective locations within the measured routes under the circumstances where signal fluctuation and variation of aggregate interference may be occurred. The shadowing contributes typically the signal fluctuation in the order of 10 dB indoors although the higher values have also been reported, as it has previously been discussed [10]. [4]

First, the error performance probability has been expressed as a symbol error probability P_s that has been required by the used modulation and coding scheme. The symbol error probability for coherent modulation using MQAM scheme may be expressed as

$$P_s = 1 - \left(1 - \frac{2(\sqrt{M}-1)}{\sqrt{M}} Q\left(\sqrt{\frac{3\overline{\gamma_s}}{M-1}}\right)\right)^2 \tag{36}$$

where M is the order of modulation and $\overline{\gamma_s}$ refers to the total average symbol energy of the MQAM constellation [6]. If symbol energy has divided equally among the bits, the Gray encoding has been used so that the occurrence of one symbol error means that there has been occurred exactly one bit error, the approximations of SNR per bit γ_b may be expressed as

$$\gamma_b \approx \frac{\gamma_s}{\log_2 M}, \tag{37}$$

and for the probability of bit error P_b as

$$P_b \approx \frac{P_s}{\log_2 M}, \tag{38}$$

where γ_s is SNR per symbol and P_s is the symbol error probability. [6]

In this work Q-function has been approximated as [21]

$$Q(x) \approx \left[\frac{1}{\left(1-\frac{1}{\pi}\right)x + \frac{1}{\pi}\sqrt{x^2+2\pi}}\right] \frac{1}{\sqrt{2\pi}} e^{-\frac{x^2}{2}}. \tag{39}$$

where a = 1/ π, b = 2 π and $x \geq 0$ for "the best lower bound approximation" [21] for Q-function. The bit error probability for BPSK and QPSK modulation may be approximated as [6]

$$P_b \approx Q\left(\sqrt{2\gamma_b}\right). \tag{40}$$

The P_b has been studied in proportion to the order of MQAM modulation by calculating the bit error probabilities for respective order of modulation (Table 1). When SNR has been kept constant, the bit error probability of the MQAM modulation increases with the order of modulation because error margin between the adjacent states of the amplitude-phase constellation decreases. As it may be seen in the Table 1, the P_b of 256QAM is worse than P_b of 16QAM by almost the order of the modulation with the same E_b/N_0.

Table 1. The calculated values of P_b for the respective order of MQAM modulation

	M = 4	M = 16	M = 64	M = 256
E_b/N_0 [dB]	15	15	15	15
P_b x 10^{-2}	0	0.02	1.1	4.9

Based on the above-mentioned dependence between P_b and order of QAM and eq. (23) it may obviously be deduced that if data rate were decreased, the required E_b/N_0 may be decreased too. If although the received E_b/N_0 stays constant it results in the decrease of bit error probability. So, the error performance of the modulation may be enhanced by decreasing the data rate which practically means the reduced MCS index.

The SNR and RSSI requirements of the respective MCS have been given in the table of Appendix 2. The probability of the bit error for MQAM modulation has been calculated using the equations (36-38) above and for the QPSK using eq. (40). The results have been presented in Table 2 for IEEE 802.11n with three spatial streams and for the IEEE 802.11ac with four spatial streams (Table 3). The spatial streams refer to the MIMO (Multiple-In Multiple-Out) technique where transmission has been multiplexed to multiple simultaneous streams that use the same time – frequency resource. The short guard interval (GI) of 400 ns have been used by both technologies. The SNR values have been converted to the form of bit energy per spectral noise density using eq. (27) where the bandwidth of 20 MHz and the maximum data rate of respective MCS have been assumed.

Table 2. The calculated bit error probabilities that correspond to the minimum requirement of the SNR for MCS of IEEE 802.11n that have been used in the control ward

	MCS23	MCS22	MCS21	MCS20	MCS19	MCS18	MCS17
SNR_{reqd} [dB]	25	20	18	15	11	9	5
Data rate [Mbps]	217	195	173.3	130	86.7	65	43.3
E_b/N_0 [dB]	15	10	9	7	5	4	2
Modulation	64QAM	64QAM	64QAM	16QAM	16QAM	QPSK	QPSK
P_b x 10^{-2}	**1.098**	**2.533**	**5.406**	**0.667**	**0.566**	**2.334**	**2.265**

Table 3. The calculated bit error probabilities that correspond to the minimum requirement of the SNR for respective MCS of IEEE 802.11ac that have been used in the control ward

	MCS8	MCS7	MCS6	MCS5	MCS4	MCS3	MCS2	MCS1	MCS0
SNR [dB]	29	25	20	18	15	11	9	5	2
Data rate [Mbps]	346.7	288.9	260	231.1	173.3	115.6	86.7	57.8	28.9
E_b/N_0 [dB]	17	13	9	7	6	3	3	0.4	0.4
Modulation	256QAM	64QAM	64QAM	64QAM	16QAM	16QAM	QPSK	QPSK	BPSK
P_b x 10^{-2}	**4.327**	**1.147**	**3.004**	**4.242**	**0.817**	**3.330**	**0.713**	**18.356**	**18.356**

As it may be seen from Tables 2 and 3, the required SNR has been decreased with the decreasing MCS index. However, if the maximum data rate of MCS has been required with the minimum SNR of the respective MCS, it results the increase of P_b respectively. Because P_b is typically given in the requirements of the system it may not be allowed to increase as it has been done in the tables above. So, SNR must exceed the level that is required by the bit error probability of the system if the maximum data rate of respective MCS were to be maintained. There are two ways of doing that. First, the signal attenuation must be compensated by increasing the EIRP if it is possible and secondly, the noise level including the interference must be kept under the threshold of SINR. These two aspects will be considered in the link margin analysis of Chapter 6.

3 COEXISTENCE OF WIRELESS SYSTEMS

3.1 Coexisting wireless technologies on the ISM bands

The 900 MHz, 2.4 GHz and 5.8 GHz frequency bands are used for unlicensed industrial, scientific, and medical purposes (ISM). The Unlicensed National Information Infrastructure (UNII) at the 5 GHz frequency region has also been used in the unlicensed wireless communication. The wireless networks that are based on the IEEE 802.11 standard, use the ISM frequency band of 2.4 GHz and the UNII band of the 5 GHz frequency region. The users of the network on these bands are secondary users which means that they must accept the interference from the primary users when they are active. The power of the transmitter is restricted in proportion to the bandwidth to mitigate the interference issues and is governed by FCC (USA) and ETSI (Europe). [6]

The shared frequency spectrum at the 2.4 and 5 GHz will be discussed next. Because the IEEE 802.11n and IEEE 802.11ac have been used in NKCH, the short description of the properties that relate to the coexistence will also be presented. The two wireless technologies that have been widely used in the hospital environment will shortly be described too.

3.1.1 IEEE 802.11 (WiFi) channel allocation

The ISM band of 2.4 GHz and the UNII band of 5 GHz are used in the WLANs. The 2.4 GHz frequency band has been divided into 11 channels outside the U.S. The bandwidth of the channel has been defined in the standard as 22 MHz with centre frequencies ranging from 2.412 to 2.462 GHz (Figure 5). In practise the bandwidth is not so wide, for example -10 dB bandwidth may typically be 16 MHz. [14]

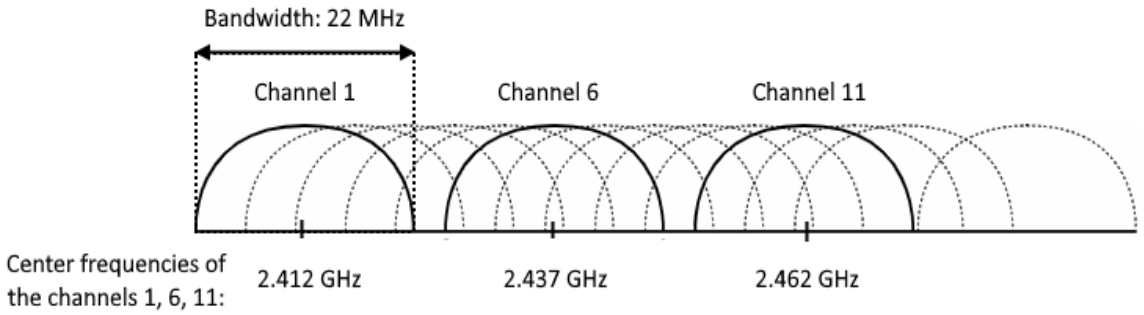

Figure 5. The channel allocation of 802.11 (WiFi) at the 2.4 GHz region of the ISM bands.

The frequency region at the 5 GHz has been allocated to the UNII-1, UNII-2a, UNII-2c and UNII-3a allocations. For each of them the respective power restrictions have been applied by FCC (in USA) and ETSI (in Europe). The regulatory EIRP of 100 mW to 200 mW has been accepted on UNII-1 and UNII-2a indoors. On the UNII-2Ext. The EIRP of 1000 mW has been accepted by ETSI. The DFS (Dynamic Frequency Selection) channels that use the allocations UNII-2a and UNII-2c or UNII- 2-Extended as it may also be called are used by radar systems. [14]

The bandwidth of the channels at the 5 GHz region is 20 MHz in the case of unbounded channels. If more bandwidth is needed the single channels of 20 MHz may be bonded together to get the bandwidths of 40, 80 and 160 MHz. The channels ranging downwards from the second row in Figure 6 have been reserved for these bandwidths [22]. The centre frequencies of the channels with bandwidth of 20 MHz have been shown in the figure too1. [14]

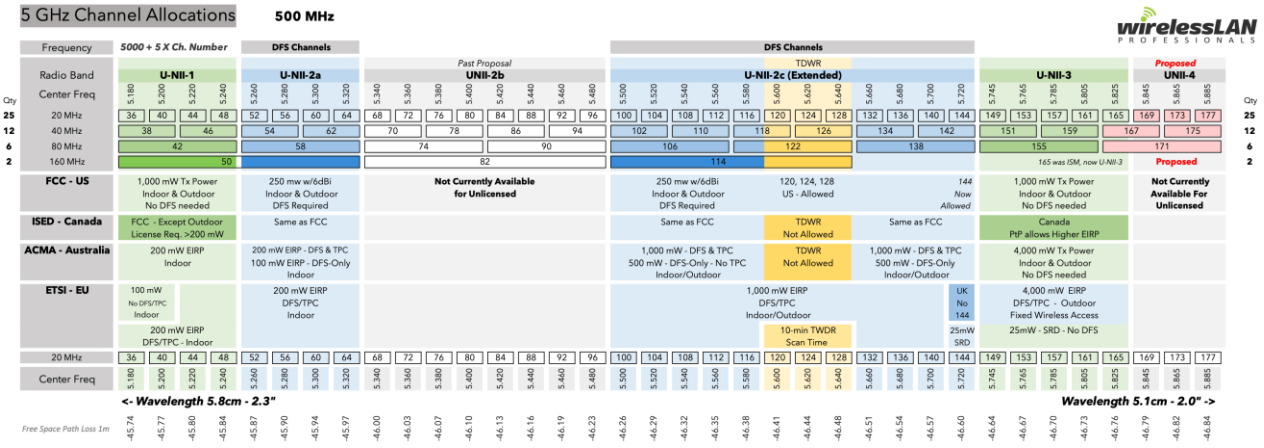

Figure 6. The channel allocation of the 5 GHz band.

The orthogonality of the channels means that they do not collide with each other, so they are said to be non-overlapping channels [23]. At the 2.4 GHz frequency region there are only three orthogonal channels 1, 6 and 11 which means that in the case when the number of clients has increased the utility of the network decreases and it may result in the degradation of the performance. There have been developed algorithms that optimize the channel allocation process by also using the overlapping or partially overlapping channels. The optimized channel allocation algorithms have been widely studied in many publications. The comparison of the different approaches has been presented in [23]. It has been argued that although the use of non-orthogonal channels would increase the options of channel allocation the co-channel interference typically prevents the channel allocation algorithms to use more than three channels. Furthermore, many researches have proved that there will be no increase in performance when the number of channels has been increased using the non-orthogonal channels. [14] [23]

3.1.2 MU-MIMO and beamforming of 802.11n/ac technology

Traditionally Local area networks (LAN) have been used to connect the computers of the single facility or small house. Today, the network may be called a LAN although it has been extended to larger facilities or covers the multisite campus. Ethernet technology has been a major technology in wired LANs while the wireless LANs (WLAN) have been dominated by IEEE 802.11 technologies. Many generations of IEEE 802.11 standards have been developed when at the same time the network capacity and number of connected devices have continuously increased. The generations of the IEEE 802.11a/b/g/n/ac/ax standards are backward compatible. The technologies and standards have not been described in this work because the specifications and more detailed descriptions are open and widely available on the internet. However, a few aspects that are related to the interference mitigation and coexistence capability of the 802.11n/ac have been described. [14]

The 802.11n has been used in NKCH at the 2.4 GHz band with two or three spatial streams. The 802.11ac has been used at the 5 GHz frequency band with three to four spatial streams. IEEE 802.11n/ac technologies support the use of a downlink beamforming and Multi-User MIMO (MU-MIMO). The use of multi-spatial transmissions increases the gain of the transmitted signal by using the superposition of multipath propagated signals. This results in the higher data rate over the extended range, and finally the better system performance. [20]

The transmit beamforming (TBF) combines constructively the signals that are in phase and destructively the signals that are out of phase. This technique results in increased gain when the interferences that have been detected in the direction of the receiver may not be harmful. MU-MIMO feature refers to the ability to send data to more than one client at time. The IEEE 802.11ac uses four spatial streams in the studied J2 of NKCH. Access point performs a channel sounding routine and

after the responses from beamformees performs poll among the nodes that have responded. Finally, it generates a matrix that will be processed by MAC level. The packet transmissions to the clients are based on the matrix and the negotiations of parallel transmissions. [20]

The regulatory constraints restrict the benefits of beamforming the most. Specially, for long links the reduction in data throughputs of more than 50% have been reported compared to the situation where the regulatory constraints are not considered [24]. Because of many time-varying losses that are caused by mobility and interference, the wireless channels typically suffer the inconsistent throughput. [20]

3.2 Wireless technologies of medical devices in the ISM bands

The medical devices that use the IEEE 802.15.1 and IEEE 802.15.4 technologies have been widely used in the hospital environment. Wireless Personal Area Networks (WPAN) and the Wireless Body Area Networks (WBAN) use typically Bluetooth (IEEE 802.15.1) and Zigbee (IEEE 802.15.4) technologies. There are also other special transmission techniques that have been used in WBANs of the hospitals like Wireless Medical Telemetry Services (WMTS), Ultra-wideband (UWB) or Medical Implant Communication Services (MICS). The more detailed study of the technologies is out of the scope of this work. [25][26]

Many physiological signals from the patients are transmitted in the WBAN. There is increasing tendency in the hospitals towards the continuous monitoring of the vital signs of a human body by using the short-range WBANs. The IEEE 802.15.6 standard defines the requirements of the WBAN so that the coexistence of 10 WBANs with up to 256 nodes must be implementable. The requirements of the transmission techniques that are used in WBAN depend on the application. WBAN traffic can be on-demand, emergency traffic or normal traffic that is the patient monitoring after a certain time on the regular basis. For example blood pressure or heart rate may be monitored by emergency traffic and the alarm is triggered when they are below the threshold. [25][26]

When the critical data is transmitted in the WBAN or WPAN, the mitigation of the interference is of crucial importance in their neighbourhood. They could be interfered by the WLAN specially if they are located near the access points, because the power levels of WLAN transmitters are high compared to the short-range systems with high sensitivities typically. Additionally, the WBANs are often operating with low duty cycles but depending on the application with the fast rate too. Although the interference mitigation techniques of the WLAN like beamforming helps to lower the risk for harmful interference the frequency hopping technique of Bluetooth systems is the primary contribution to the coexistence between the two short-range technologies. [26]

3.2.1 IEEE 802.15.1 (Bluetooth)

The Bluetooth system is based on the piconet that consists of connected devices, nodes. One of the nodes has been designated as a master and the rest of the nodes in the piconet are slaves. The number of nodes has not been limited by the standard but the resources of the network and the properties of the connected device [44]. Bluetooth uses the same frequency band as IEEE 802.11 WLAN at the 2.4 GHz band. It implements frequency-hopping technique which means that the signal is transmitted within the range of about 79 MHz at the 2.4 GHz frequency band by changing the carrier frequency with 1 MHz spacing. The range covers the frequencies from 2402 MHz to 2480 MHz. The master may be changed so that any of the slaves may be a master. The piconets may also be combined forming ad-hoc networks called scatternets. [27][28]

Depending on the power of the Bluetooth transmitter and the conditions of the propagation the range of a typical Bluetooth transmitter of 10 m may be extended to 100 m. The transmit power has been restricted according to the five classes where the highest permitted power of transmitter is 20 dBm and the lowest -3 dBm. [28]

The Bluetooth LE (BLE) is a technology with a reduced power consumption and it has appeared since the Bluetooth 4. The use of BLE has been increased also in the hospitals where the low power wireless technologies have been widely adopted. The Bluetooth SIG (Special Interest Group) has promoted health care profiles that use BLE technology together with The Continua Health Alliance that is an international non-profit open-industry group of healthcare and medical industries. The health care profiles of BLE covers, e.g., the measurement of blood pressure, temperature, and glucose profile. [28][29]

The mutual interferences between piconets have been found to be tolerable and coexistence with IEEE 802.11 has shown to be dependent on the data rate [30].

3.2.2 IEEE 802.15.4 (Zigbee)

The IEEE 802.15.4 standard defines MAC and PHY layers for the wireless technology called Zigbee. The Zigbee alliance is responsible for creating the flexibility and interoperability that is needed by the applications that implement the technology. From the coexistence point of view Zigbee is a potential risk for WLAN because it uses the same ISM frequencies ranging from 2400 to 2484 MHz too. The band has been divided into 16 channels that are used by Zigbee. The separation between the channels is 5 MHz and the bandwidth is 2 MHz. Because of the low transmit power the interference risk of Zigbee is although marginal for WLAN. There have been published researches that have indicated that Zigbee may be interfered by WLAN transmitters particularly when the Zigbee is close to them. Because the small-ranged wireless technologies have typically been used in patient monitoring appliances they may be moved in the neighbourhood of the WLAN transmitters which may increase the risk for interference. [31][32]

The Zigbee uses Offset-Quadrature Phase-Shift Keying (OQPSK) and Direct Sequence Spread Spectrum (DSSS) technologies which eases the operation in environments of low SNR. The multiple access technique that it uses implements Carrier Sense Multiple Access with Collision Avoidance (CSMA-CA) principle and with checksum at the end of each packet it verifies that the packet has been delivered. If the collision has occurred three times, it starts the procedure that completes the transmission. Because the Zigbee is often used also in the applications of the house automation where the data needs to be transmitted remarkably seldom and it is silent most of the time, the interferences may only be indicated by long-time measurement periods. [32]

The data rate of Zigbee is low. The open-air data rate without considering the packet overhead and processing delays is 250 kbit/s at the 2.4 GHz which is too low for video signal but enough for temperature measurement that is a typical Zigbee application. In principle it is 250 kbps but because of retries and encryptions/decryptions it is in the order of 25 kbps in practise. The effective throughput is also reduced by half-duplex transmissions of Zigbee. The low data rates and utilization degree of the shared ISM frequencies enhance the coexistence with other technologies although the coexistence issues with other technologies have been reported. [31][32]

3.3 Coexistence

The number of wireless devices that operate at the same ISM bands has strongly increased in the hospitals. This has contributed to the aggregate interference that may have a remarkable effect on the medical wireless systems. The increase of aggregate interference is related to the limited resources of the ISM band at the same time with continuously widening use of wireless systems. Specially, in the hospital environment this may lead to severe problems because many critical patient monitoring systems have typically been operated at the ISM bands. The 2.4 GHz band is the most susceptible to interference in a hospital environment due to the large number of available wireless technologies and devices. [6][33]

The coexistence in the context of wireless systems may be defined as “the ability of a device to operate successfully in a shared environment” [34]. The coexistence of two wireless devices may also be discussed from the performance point of view by defining the devices “as coexisting if they can be brought near one another without significant degradation in their performance” [27]. The coexistence may be viewed also from the opposite perspective. The distance between two coexisting devices is actually “the distance between two devices in order to interfere if they operate at the same frequency and at the same time” [19]. The aspects of the definitions above may be combined by recognizing the requirements of the “shared environment” from the aspect of the performance of a single device that operates close to the other devices that are using the same resources of the “shared environment”.

The spectral occupancy is a stochastic metrics that describes the use of the frequency resources that have been used by the wireless system. It is based on the principle of dividing the spectrum to the frequency channels of fixed bandwidth and measuring the averaged power that has been received on the respective channel. The spectral occupancy may be studied, e.g., by comparing the measured power to the threshold that has been obtained by the median forward consecutive mean excision algorithm (Med-FCME) and if the averaged power of the band has been over the threshold, the channel has been defined occupied. The occupancy may then be evaluated by calculating the number of occupied channels through the number of sweeps. [37]

The interference in the hospital environment has been studied by modelling the aggregate interference as a stochastic phenomenon in the spectrum occupancy point of view. The aggregate interference over the whole time and frequency dimension or the frequency channels of the lowest and highest interference have been modelled using the large amount of the samples that have been measured over the whole week. The results of the research work have led to the conclusion that there may simultaneously be interference-free channels in the ISM band while the other channels with higher occupancy “would severely hamper the proper working of mission-critical medical services”. [33]

The coexistence considerations are of crucial importance when the new device is deployed in the wireless system. The spectral environment must be considered from the aspect of the new device as well as the existing system point of view. The risks, reliability and performance aspects should also be weighted in relation to the other existing systems that are used in the environment. The coexistence capability requires that the RF aspect has been considered in understanding the sensitivity of the deployed device to the transmissions of the systems that already are in use. Furthermore, all interferences are not consequential though they may be embarrassing. It is not appropriate to apply the same requirements of coexistence in public spaces and intensive care rooms. The coexistence of the new device must be tested in the existing environment after its use of spectral resources have been understood. It must also be surveyed after the deployment because the wireless environments are dynamic, and they are constantly changing. The network loading may strongly be varied resulting in the potential risks for successful communication. This may result in corrupted data or totally block the communication. [34]

The coexistence may be discussed from the single device point of view or between the wireless systems that share the common resources, whether it is the shared frequency spectrum or the common physical room where the systems exist in parallel. The systems or devices may represent different technologies, or they may be implemented by the same technological standards. Two WBANs may interfere with each other as it may be with two access points of WLAN. A microwave oven, electric motor, or a node of Bluetooth system close to the WLAN access point may cause coexistence challenges that might be difficult to detect without the spectrum survey. Which one of them is interferer and which one is interfered may be depended on several features of the coexisting systems and devices. The transmitted power or the sensitivity of the receivers may contribute to the coexistence issues as well as the amount of the traffic or duty-cycle of the coexisting systems. The short distances between the systems may contribute occasional interferences when the device is in

motion as it may be happening when the patient has been moved with monitoring her or his vital functions simultaneously by short-range technology. Additionally, because of lower duty-cycle of typical measurement of vital parameters, it may be interfered by access points of WLAN more probably than vice versa. [34][35]

Because the power levels of IEEE 802.11 network are higher than most coexisting networks that are used in the hospital environment, the access points of the WLAN may primarily be seen as interferers. In this work the coexistence has been studied from the perspective of IEEE 802.11 system only and because of some limitations of the used measurement devices the coexistence of the access points has been prioritized. This means that potential interferers are primarily the other access points of the network. However, because the higher transmission power of the access points may interfere with wireless systems of shorter coverage and they coexist typically in the hospital environment, the systems will be shortly described. [19] [27] [33] [34]

The simulation studies of coexistence between the WBANs have shown that without synchronization of nodes the collisions may be resulted with adjacent WBANs. The coexistence problems have also been reported between the Zigbee based WBANs and especially IEEE 802.11b/g-based WLANs. High Packet Loss Ratio (PLR) has been resulted when the WBAN nodes on the human body have been moved in the neighbourhood of WiFi access points. The finding has been done even in the case when the centre frequency of Zigbee is far from the active access point. [19]

The OFDM (orthogonal frequency-division multiplexing) is a multiplexing technique that has been used in IEEE 802.11 standards beginning from the IEEE 802.11a. It tries to prevent multipath effects because the multipath delay is proportional to the frequency, the number of multipath components and symbol time of the serial stream that has been divided among the symbol time of the parallel symbols of the subcarriers. Delay spread is inversely proportional to the coherence bandwidth. In addition to the fact that closely spaced subcarriers increase the spectral efficiency which is desirable from the spectral occupancy point of view, the OFDM subcarriers increase the amount of channel parameters that channel sounding of TBF must process. On the other hand, the OFDM makes the WLAN transmissions more resilient in the conditions of high interference. [20]

From the technological point of view, the MU-MIMO and beamforming have enhanced the WLAN coexistence as it has been described above. The simultaneously increased gain and ability to mitigate the interferences have been caused by beamforming. The TBF feature of IEEE 802.11n/ac technology has improved their ability to maintain high data rate performance even in the low SNR conditions especially in the medium-ranged distances. The use of transmit beamforming increases the signal strength by 2-4 dB which results in an increase of 10-35 m in the coverage. [16][20]

From the perspective of coexistence, the criteria of channel access are vital. All IEEE 802.11 standards implement the CSMA-based collision avoidance by Clear Channel Assessment (CCA) mechanism. It implies three modes of collision avoidance that defines the criteria of channel access. The modes use thresholds of -96 dBm, -80 dBm and -62 dBm depending on the given sensitivity level of the clients. [16]

There are various WLAN technologies that are used in parallel in the NKCH. So, the coexistence of them must be considered. Although the IEEE 802.11 standards are backward compatible, it has been proved that deterioration of the throughput might have occurred when the earlier technologies with lower data rates have been allowed in the network where the IEEE 802.11n/ac technologies have been used. The possible coexistence issues of different WLAN technologies should be indicated by the throughput measurements that would have been carried out by iPerf. IPerf is a software tool that may be used to measure the throughput of the network based on the transmitted data stream between the client and server. IPerf may be operated either in server or client mode. However, because it had not been available in the network, the measurements could not have been carried out. [16]

3.4 Interference modelling

Several models have been discussed in the literature with a different approach to the basic idea of using the SINR or SIR without considering the noise, in the modelling of the interference. The interference models may be defined in primary and secondary interference models. They may be classified in the two categories depending on whether they are considering only the interference between the two links with a common endpoint or the nodes of the whole network. [36]

The SINR model has been used based on both empirically derived path losses based on the measured distances and the models that use the power of the received signals. The attenuation of the walls and building structures may also be considered in the interference models. Because the distances are usually difficult to measure, the SINR model that is based on the measured aggregate power is more practical than the distance-based model with modelled path loss. [14][32]

The network throughput is inversely proportional to the system interference. The partially overlapped interference model has been generated based on the idea of using also the non-orthogonal channels of WLAN and adopting it to the SINR model to raise the throughput. The generated heuristic algorithm is based on the channel-overlapping attenuation coefficients. The model also gives a channel assignment procedure that makes it possible for two nodes that are close to each other to communicate with themselves by using the adjacent channel in the conditions where there are enough overlapped frequency bands between the transmitting and receiving channels. [1]

The graded SINR model describes the packet retransmission rate (PRR) as a function of SINR where the strict threshold of the traditional SINR model has been replaced by a smooth transition region. The transition region ranges from β_0 to β_1 with $PRR(\beta_0) = 0$ and $PRR(\beta_1) = 1$ and there is $\beta_0 < \beta_Q < \beta_1$ so that $PRR(\beta_Q)$ meets the minimum link quality requirement. In the simulations of the model, it has been proved that throughput has been increased by using the 5 dB to 10 dB marginal below the threshold β_1 for the transmissions of lower requirement. However, there are still many challenges in the model especially from the aspect of the varied node density. [1]

The more systematic approach to the coexistence evaluation of the wireless systems has been presented in the model where the coexistence has been studied by measuring the channel power over the whole spectrum during long measurement campaigns. The spatio-temporal spectrum occupancy has been determined by first dividing the spectrum based on the systems that have been expected to utilize it. Then each of the channels has been searched for the samples that have exceeded the predefined threshold. If the number of samples exceeding the threshold is over 50%, the channel is defined as occupied. [37]

The noise threshold can be defined iteratively by FCME method. It has been applied for each individual sweep because there are periods of time when the measurement has not been going on, but the noise floor still fluctuates. After the iterations, the threshold has been found and it is implemented in a way that all amplitude samples that are below the threshold have assumed to be noise and those over threshold includes interference. [33][37]

4 MEASUREMENT INSTRUMENTS

The measurement campaigns have been carried out using Ekahau Sidekick spectrum analyser that has been connected with USB A-micro-B cable to the HP Elitebook laptop. The measurement software Ekahau Pro runs on the laptop. The measurements have been done as hybrid measurement which means that both passive and active site-survey have been done simultaneously. [38][39]

Ekahau Sidekick is a professional site-survey, troubleshooting device that has primarily been intended for IEEE 802.11 environment. It has also been featured with simulation tools that make it appropriate for the designing purposes. Sidekick is a spectrum analyser with two radios which makes it possible to survey both 2.4 GHz and 5 GHz frequency bands simultaneously. The sweep time has been announced in the specifications as maximum sweep speed that is 25 sweeps per second in both 2.4 GHz and 5 GHz regions at the maximum accuracy which means the sweep time of 40 ms. The frequency resolution of Sidekick is 39 kHz at both frequency regions and there are two integrated omni-directional antennas inside. The sensitivity of the Sidekick is -95 dBm and the maximum power that can be measured is -20 dBm. The frequency range of Sidekick covers the frequencies from 2400 to 2495 MHz and from 5000 MHz to 5950 MHz. [38][39]

Figure 7. Ekahau Sidekick spectrum analyser.

Ekahau Sidekick supports all WiFi standards from IEEE 802.11a to IEEE 802.11ax. It is battery powered but cannot be used when charging. The charge is normally enough for an eight hours measurement. The packet capturing may be done by Sidekick at the single WLAN channel or at all channels of the respective frequency regions simultaneously. The captured packets should be studied by the third part programme, for example Wireshark. Although some packet capturing has been carried out also in this work to analyse the packet retransmission rates (PRR), the MAC level study has been out of the scope of this study. So, Sidekick has primarily been used as a measurement device of RF parameters in this work. The measurements of this study have been carried out as hybrid measurements so that the active site-survey has been done using the Intel Wireless-AC 9560 160 MHz network adapter of HP Elitebook laptop. The hybrid site-survey means that one device is measuring the received signals as accessed in the network and another measures all received signals that exceed the sensitivity of the device without associating the access point. The active device measures data rate in ping mode based on the beacon information of the accessed access point. The throughput cannot have been measured by the arrangement of this study because iPerf may not have been used. Ekahau Pro has only presented an estimated throughput based on the measured data rates. [38][39]

The readings of the measured metrics have been presented by Ekahau Pro that runs in the same HP laptop that also uses its network adapter in the hybrid measurement that has been discussed above. The sensitivity of the network adapter has been presented in Table 4 for both frequency bands and MCS indices of MCS0, MCS6 and MCS7. The bandwidth of 20 MHz has been primarily used in the

whole studied area of the J2 yielding the sensitivities from -74.9 to -93.9 dBm for IEEE 802.11n and sensitivities from -72.2 to -94.2 for IEEE 802.11ac. The announced lowest sensitivity has been used with the maximum data rate that is 217 Mbps for IEEE 802.11n and 367 Mbps for IEEE 802.11ac. The signal strength has been measured using the threshold setting of Ekahau Pro of -85 dBm which means that the signals that have exceeded the threshold have been shown by Ekahau Pro. Regardless of the adjusted threshold of Ekahau Pro, Sidekick measures spectrum without any threshold with the sensitivity of -95 dBm. The more accurate information about sensitivities of the device has not been available. Sensitivity has been presented on the respective WLAN channel in Table 4. [39][40]

Table 4. The sensitivity of the network adapter Intel Wireless-AC 9560 160 MHz

Sensitivity, [dBm]						
Technology	B [MHz]	Frequency band [GHz]	MCS index	Ch. 36-64	Ch. 100-144	Ch. 149-165
IEEE 802.11n	20	2.4	MCS0	-93.9		
			MCS6	-77.4		
			MCS7	-74.9		
	40	2.4	MCS0	-91.3		
			MCS6	-74.5		
			MCS7	-72.1		
IEEE 802.11ac	20	5	MCS0	-94.2	-94.6	-94.6
			MCS8	-72.2	-72.5	-72.3
	40	5	MCS0	-91.7	-92.2	-92.2
			MCS8	-69.2	-69.6	-69.4
			MCS9	-67.5	-68.0	-67.7

The distance measurement has been done by Kalei LDM-100 laser measurement device that measures the distances up to 100 metres with accuracy of +/- 1.5 mm.

5 MEASURED ENVIRONMENT

The measurements of this study have been carried out in the building J2 of NKCH that has been taken into use from the beginning of the year 2020 (Figure 8). There are three floors and the ground floor in the building J2. The emergency care ward is located on the first floor where the control ward is located. The intensive care department of the second floor has been out of the scope of this study. Measurements have also been carried out in the two children's wards on the third floor and the department of the abdominal diseases on the ground floor. Some signal strength measurements have also been carried out in the neighbouring buildings A, E and K (Figure 8).

The measurement environment in the control ward has not been the same in all campaigns. The number of patients has strongly varied in the emergency ward. The number of customers has varied not only on a weekly basis but also daily. Additionally, the Covid-19 pandemic has caused extraordinary conditions during the whole autumn 2020 when the measurements have been carried out, although the pandemic has not been as severe in North Karelia as it has been in the rest of Finland. This has been reflected especially in the emergency care department because customers have not sought hospital services as usual for some reason and the number of customers has been lower compared to the normal conditions.

Figure 8. The J2 building of NKCH campus.

The propagation and SIR have been modelled in the control ward of the first floor. The control ward is part of the emergency care department of the first floor. The control ward has been marked by red dashed line in the floor plan of the first floor of J2 (Figure 9).

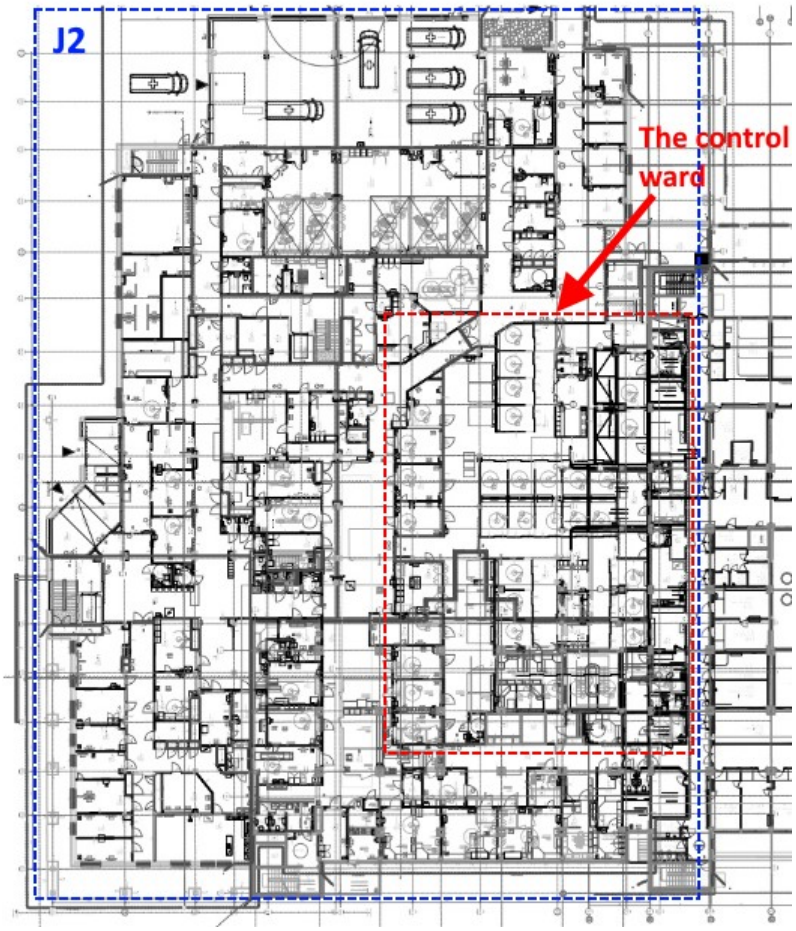

The Figure 9. The floor plan of the first floor of J2.

The measurements have primarily been carried out in the control ward although the entire first floor has been measured to figure out an overview of signal strength and interferences around the modelled control ward. The Cisco wireless system has been used in the whole building J2 with access points of Cisco 1850 series [41]. There are 28 access points on the third floor, 20 access point on the first floor and 17 access points on the ground floor. The building E may partly be seen to the right from the control ward in the floor plan of the figure above. During the first campaigns it has been almost empty but because of the renovation of the main entrance of the building A there have later been some activities also in the building E during two last of the six measurement campaigns. The Meru wireless system of the 2.4 GHz frequency band has been used in the neighbouring building E but it has been planned to be replaced by the new system of Cisco. Six access points of the Meru system have been received in the control ward from the building E.

5.1 Control ward of the emergency department

The control department consists of two rooms and the corridor-like room on the left side of the rooms totally including 35 places for patients (Figure 9). The rooms are separated with the load-bearing walls and connected with the corridor-like room that will be called corridor in this study. It has about ten places for short-time control of patients on one side and the doors to the medical examination rooms on the other side.

The measurement environment has varied the most in this room because of strong variation of the number of patients that have occurred on a weekly and daily basis. The Covid-19 pandemic has

caused the decreased number of patients in general during the time of the measurements, as it has been discussed previously. This may have affected the network load. However, the number of patients in the emergency care department and in the control ward has been strongly varied from day to day. The variation in the number of patients has affected the changes of the locations of medical appliances and movable patient beds too. The variation has not affected as much in the two rooms where the patient places have been surrounded by glass walls. Only variation that has occurred is the glass sliding door that has been open when the place inside has been unoccupied.

There are four Cisco 1852 access points in the control ward. Three of them use four spatial streams and one uses three streams. The short guard interval of 400 ms has been enabled in all four access points. The channel allocation and transmit power has been controlled by automatics according to the seller's recommendation. The channel options have been restricted to two at the 2.4 GHz band where only channels 1 and 11 (Figure 5) may be chosen by the automatics while all channels may be chosen at the 5 GHz band (Figure 6). The maximum transmit power has been enabled by the power settings of the WLAN controller.

5.2 Children's ward and the department of the abdominal diseases

In addition to the measurement campaigns on the first floor of the J2 building the measurements have also been carried out on the ground floor and on the third floor of the building. The floor plan of the third floor has been presented in the Figure 10.

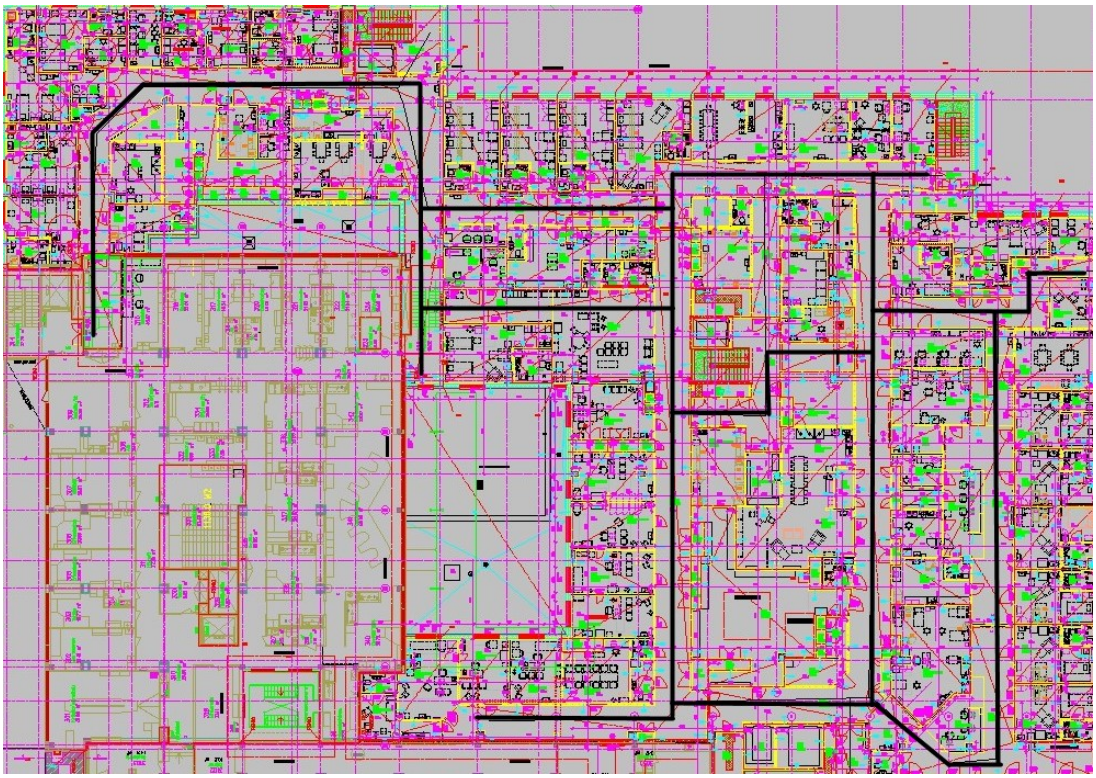

Figure 10. The measured routes on the third floor.

The measurements have been carried out in the two Children's ward that are located on the third floor. Also, the Maternity ward is located on the same floor, but the measurements have not been done there. The floor plan of the ground floor has been presented in Figure 11. The Department of abdominal diseases is located on the ground floor. It has been added to the targets of the single site-surveys because the problems with Ascom mobile clients that operate in the IEEE 802.11 network have been reported by the hospital personnel.

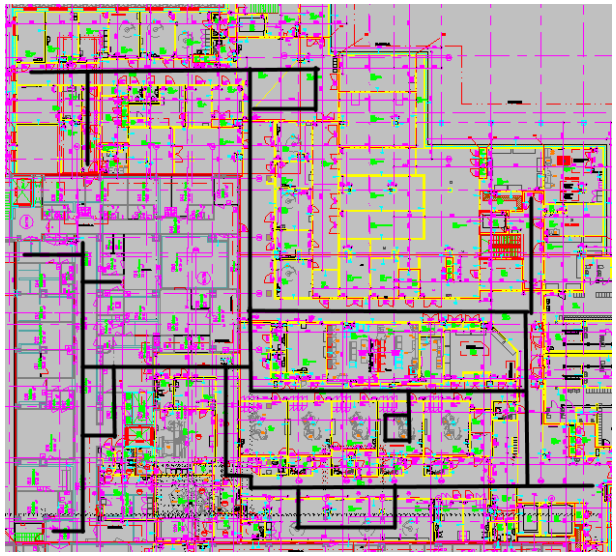

Figure 11. The measured routes on the ground floor.

5.3 WLAN Architecture of J2

The WLAN of building J2 has divided the distribution systems that have been named by the respective floor and the sequential numbering that refer to one of the distribution centres of the floor (Figure 12). For example, the distribution system 1J12 of Figure 12 refers to the distribution centre 12 of the first floor of J2. WLAN switches are located in the distribution centres where the signal has been distributed using the Ethernet network to the access points belonging to the respective distribution system. Basic Service Sets (BSS) have been formed around the access points that have been identified by sequential numbering in the respective BSS (Figure 12). [42]

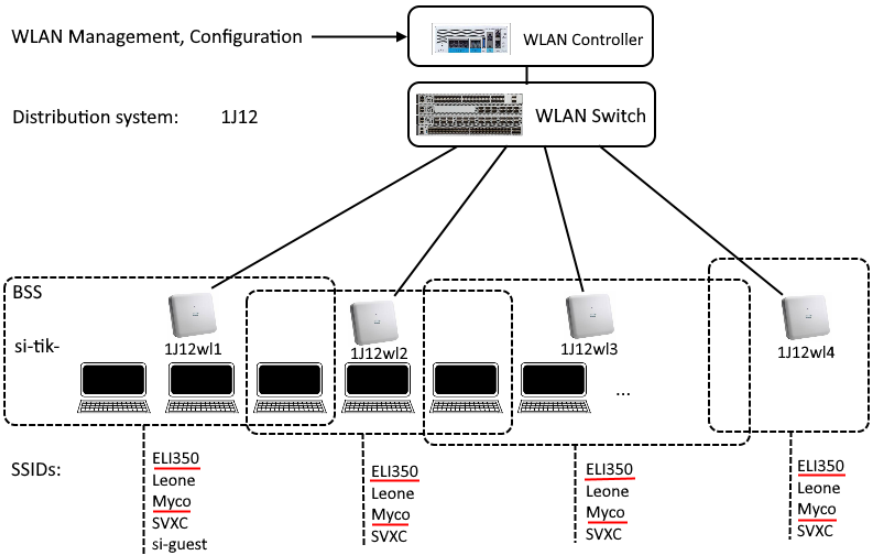

Figure 12. The architecture of WLAN in the building J2.

The services that have been distributed in the WLAN are identified by Service Set Identifiers (SSID). In this work, SSID ELI350 has primarily been studied because it has been served practically in all BSSs of the building J2 and because it includes many vital services, for example, the distribution of the patient monitoring like ECG. The Myco SSID has also studied on the ground floor and the third floor. The SSID Myco refers to the Ascom Myco mobile device that has been used for

communication by the hospital personnel. Also, the alarms are triggered using the SSID Myco. The WLAN of J2 has been implemented using the virtual local area networks (VLAN) where each SSID forms an independent VLAN. According to the established way of speaking among the professionals, the VLANs are called networks. So, also in this study the SSIDs are called networks when they unambiguously refer to the VLANs as it has been the case in the context of this study. The scope of this study has been restricted to the PHY point of view; the more detailed description of the WLAN architecture has been out of the scope. [42] [11]

6 IMPLEMENTATION OF THE MEASUREMENT CAMPAIGNS

The measurements have been carried out as hybrid measurements which means that passive and active site-surveys have been performed simultaneously. The passive site-survey measures all signal strength related metrics as signal-to-noise ratio, number of interfering transmitters etc. It receives signals from all access points that exceed the sensitivity of the network adapter. The active site survey has been performed in the accessed network where the latencies, packet loss and roaming areas may be measured based on the ICMP (Internet Control Message Protocol) echo requests. In this work active site-survey has been carried out in SSID ELI350 that covers the whole scope of the study and SSID Myco that has been measured on the ground floor and the third floor.

6.1 The overview of signal strength on the ground floor of J2

The signal strength has been measured on the whole first floor of J2 (Figure 9) by measuring the RSSI at 2.4 and 5 GHz frequency bands. RSSI have been measured by several site-surveys by walking slowly within the corridors and halls scanning all receivable transmitters. The patient rooms have not been entered, despite a few exceptions. Ekahau Pro shows the results in the heatmaps that have been presented in Figure 13 for both frequency bands. Two heatmaps of Ekahau Pro may be merged. The heatmap of Figure 13 is based on the two measurement campaigns that have been done in September 2020.

The heatmaps of Figure 13 show signal strength at the 2.4 and 5 GHz bands. It may be seen that the signal has been stronger at the 5 GHz compared to the 2.4 GHz band where it mostly has been under -55 dBm while the power level -50 dBm has mostly been exceeded at the 5 GHz band. The heatmaps may be used as coarse guidelines for estimating the variation of the signal strength and figuring out the possible outages when the sensitivity requirement of clients has been given. As it can be seen in the figure above, the power level of -67 dBm has been exceeded almost in the whole floor at the 5 GHz but when it comes to the 2.4 GHz band there have been three to four areas where the threshold of -67 dBm has not been exceeded. The threshold of -67 dBm refers to the Ekahau 'Best practise' value that has been used in the heatmaps in a way that the RSSI has been under the threshold of -67 dBm in grey-coloured areas. The difference between the signal strength of the 2.4 and 5 GHz band has been repeatedly indicated in the other measurement campaigns too.

Figure 13. RSSI readings at the 2.4 GHz (left) and 5 GHz frequency band (right).

Figure 14. The co-channel interferences at 2.4 GHz frequency band (left) and 5 GHz band (right).

Based on the measured signal strengths the number of co-channel interferences have been presented in Figure 14 for both frequency regions. The colour code is based on the criteria of Ekahau Pro where the different shades of grey describe the conditions where the requirements of Ekahau Best Practices have not been met. The suboptimal conditions at the 2.4 GHz band means that more than three co-channel access points have been received over the signal strength of -85 dBm and two or more access points at the 5 GHz band, respectively. Based on the heatmaps of the Figure 14 it can be seen that the defined criteria have not been met at all in the case of 2.4 GHz band and only on two thirds of the area at the 5 GHz band.

The interferences and signal strength will be studied in detail by measuring the signal strength of the useful signal, noise power and aggregated interference in the control ward of the emergency department and based on the measurements, generate the arrangement where the empirically derived SINR may be used to evaluate the possible effects of signal attenuation and interference on the error performance of the system. The signal propagation has been modelled at both frequency regions.

6.2 Arrangement of the measurements

The measurement campaigns of the control ward have been carried out as six separate series during the three months period beginning from September. The weekday and time of the campaigns have varied to get a better overview from the network under varying load. However, as it has been discussed earlier, the situation in the hospital has not been normal because of the Covid-19 pandemic and it has obviously resulted in somewhat smaller network load. The effect of the varying phases of the pandemic has been tried to prevent by extending the measurement campaigns over the period from September to November 2020. The measurements have been performed simultaneously at both frequency regions.

The access points of the control ward have been referred by AP1, AP2, AP3 and AP4 (Figure 15). The six measurement campaigns have been carried out by measuring the RSSI within the predefined routes that are called Route 1 and Route 2 (Figure 15). The AP1 has LOS within the distance of a few meters from the beginning of Route 1 while AP3 locates in the middle of the corridor with LOS until the distance of 15 m within Route 2.

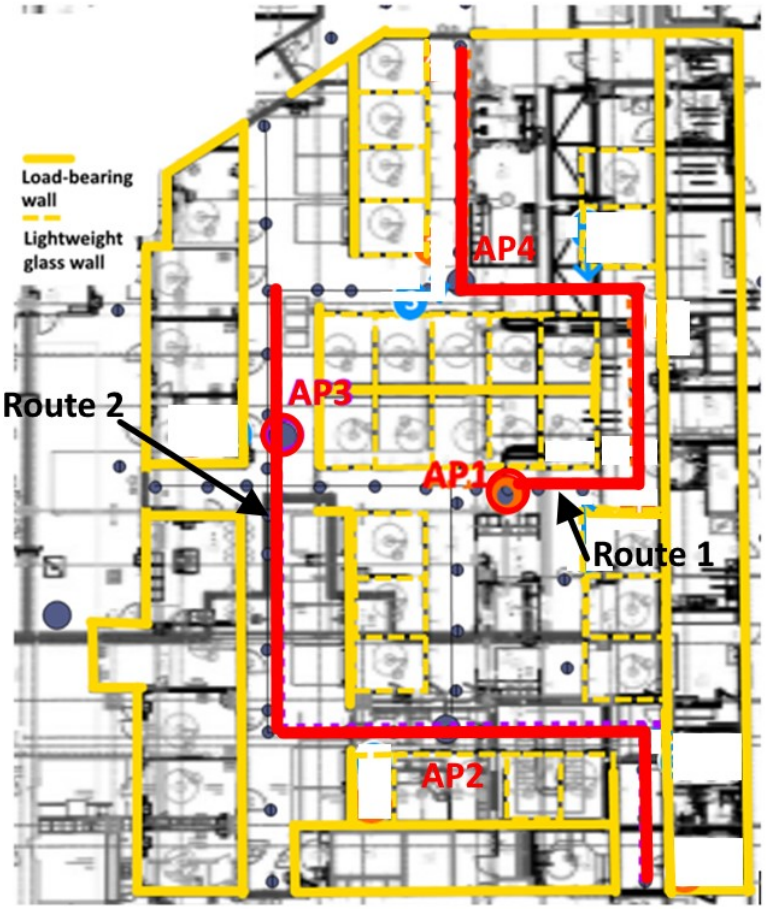

Figure 15. The control ward with the measured routes.

The distance of both routes is long enough for the signal to attenuate below the value of -80 to -85 dBm that is the minimum threshold of the measurement device. The studied routes have been chosen so that they cover most of the area of the control ward. The measurement locations outside the routes have been marked by the grey points (Figure 15). The routes have been defined based on the results that have been obtained by the measured signal strength (Figure 13) and the indications of the interferences from the access points of the neighbouring building E.

The distances from the access points have been defined based on the CAD floor plans so that the location might easily be identified visually when the measurement has been carried out. When there is a LOS connection between the transmitter and the receiver the distances have been measured also by laser device. The measurement devices have been placed in a cart that is used in the hospitals by doctors when they visit patients of a ward (Figure 16).

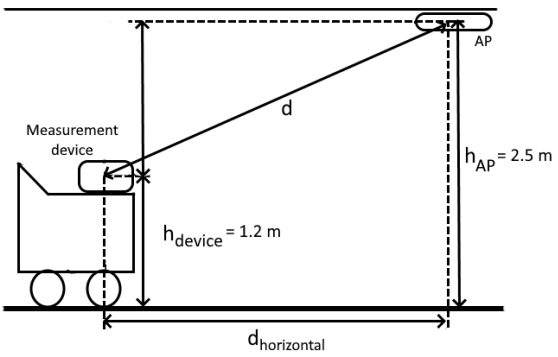

Figure 16. The measurement of the distance *d* from the access point.

The altitude of the measurement device in the cart is h_{device} and the altitude of the access point is h_{AP} as measured from the floor level. The distance $d_{\text{horizontal}}$ that has been measured from the floor plan is a horizontal distance between the measurement location and the access point. The access points have been mounted on the roof and the direct distance d from them to the measurement device has been calculated by Pythagorean theorem. When there is a LOS connection the laser distance measurement has been done. However, the distances have primarily been measured once when the fixed measurement locations have been determined and the check measurements by laser have only been made as needed.

There may have been some temporary barriers and moving obstacles that have limited the exact entrance to the location. When the measurement apparatus must have been moved from the fixed location under ongoing measurement, RSSI readings have been kept below the tolerance of 5 dBm.

6.3 Signal propagation in the control ward

The signal propagation is modelled by the lognormal shadowing path-loss model of eq. (8) where the reference path-loss $L_{\text{p}}(d_0)$, the propagation coefficient n and the shadowing effect X_σ have been empirically derived by the measured values of RSSI in the fixed locations within both routes.

The Ekahau Pro gives the readings immediately so that the measurement process may be controlled in real time. The results of the RSSI measurements of the single campaign have been presented in the form of a heatmap in Figure 17.

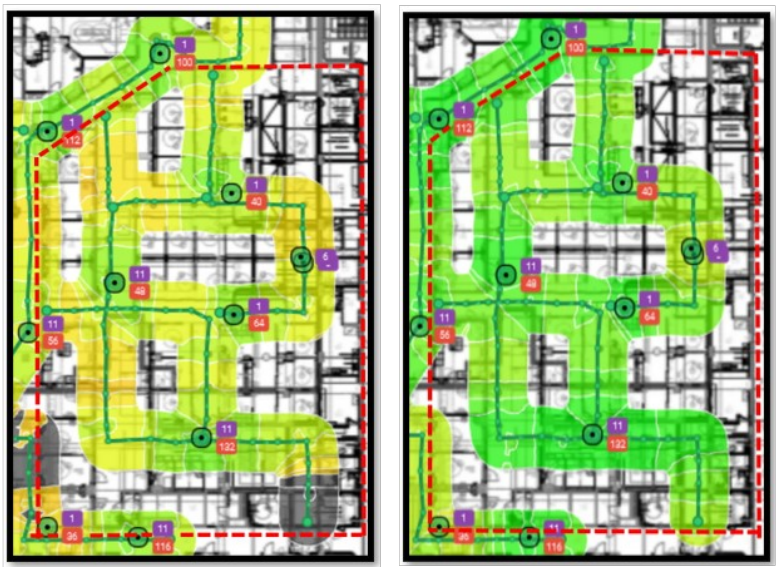

Figure 17. Screenshots from the heatmaps showing the RSSI readings of the single campaign at the 2.4 (left) and 5 GHz (right) region.

The heatmaps above show the places of access points with the channels for both frequency regions. The red dashed line has been added to the screenshots to crop the area of the control ward where the models have been generated. The RSSI readings have been measured continuously within the route and the green circles on the route refer to the locations where the moving measurement apparatus has been stayed for 10 to 15 s. Part of the locations that have been shown by green circles represent the same fixed locations that have been described earlier and that have been called as measurement locations (Figure 17). All calculations are based on the measurements at these locations.

The RSSI values of all six series have been averaged at every measurement location and the path-loss in the location has been calculated using eq. (6). The heatmaps could not be used because the

values of all measurement campaigns in the respective location have been averaged and the averaged RSSI values have been used to calculate the path-loss in the given location of the respective route and respective frequency range.

The EIRP has been calculated based on the specifications of the access points (Appendix 4) for both frequency regions because the power settings of the access points have been adjusted to the maximum power. The transmitter power may be varied depending on the channel as it may be seen in Appendix 6 but on the channels that have been used in the control ward the given values have been the same. The values of EIRP have been calculated based on the specifications for both frequency regions and the results have been shown in Table 5.

Table 5. The calculated EIRP of the access points AP1 and AP3 at the 2.4 and 5 GHz frequency region

Access point	**2.4 GHz** (AP1: Ch. 1, AP3: Ch. 11)				**5 GHz** (AP1: Ch. 64, AP3: Ch. 48)			
	MCS	P_t [dBm]	G_t [dB]	EIRP [dB]	MCS	P_t [dBm]	G_t [dB]	EIRP [dB]
AP1, AP3	20	17	3	20	27	18	5	23

At the 2.4 GHz region the access points transmit at the constant power P_t = 17 dBm at all channels when at the 5 GHz region the transmitted power depends on the channel when the beamforming has been used. At the UNII-1 and 2 channels Cisco 1852e transmits with downlink beamforming at the power of 18 dBm. This gives the EIRP of 20 dB and 23 dB on respective channels that have been used by AP1 and AP3 (Table 5).

The path loss in the reference distance has been defined for both modelled access points at both frequency regions by measuring the RSSI in the reference distance d_0. The typical indoor reference distance of 1 metre have not been possible for practical reasons and because of this the reference distances of 1.3 and 1.5 m have been used instead (Table 6). The reference path loss $L_p(d_0)$ has been calculated using eq. (6) and the results have been presented in Table 6.

Table 6. The empirically derived values of the reference path-loss for the respective route at both frequency regions

AP1 (Route 1)					AP3 (Route 2)			
d_0	1.3				1.5			
	2.4 GHz		5 GHz		2.4 GHz		5 GHz	
	f [GHz] (Ch.11)	EIRP [dB]	f [GHz] (Ch.64)	EIRP [dB]	f [GHz] (Ch.11)	EIRP [dB]	f [GHz] (Ch.48)	EIRP [dB]
	2.462	20	5.32	23	2.462	20	5.24	23
RSSI(d_0)	-47 dBm		-30 dBm		-44 dBm		-31 dBm	
$\boldsymbol{L_p(d_0)}$	**67 dB**		**53 dB**		**64 dB**		**54 dB**	
$L_{p(free)}(d_0)$	43 dB		49 dB		44 dB		50 dB	

The free-space path losses $L_{p(free)}(d_0)$ have been calculated using eq. (4) with n = 2 to compare them with previously derived $L_p(d_0)$ because the attenuation has been assumed to follow the free-space attenuation within the reference distance. As it can be seen from Table 6, there has been a remarkable difference between them at the 2.4 GHz band while the $L_p(d_0)$ at the 5 GHz band may be approximated by $L_{p(free)}(d_0)$.

The path losses at the respective locations of distance d within both routes have been defined empirically by averaging the measured values of RSSI(d) of six campaigns and calculating the value of path loss at the respective locations using the averaged RSSI readings and eq. (6).

The results have been presented as a function of the logarithmic distance that is expressed as $\log_{10}\left(\frac{d}{d_0}\right)$ where d_0 is a reference distance that has been measured from the respective access point. Because of the changing room geometry, the path loss coefficient changes within the measured route and the piecewise linear multi-slope path loss model must be used. The reference distances of the model have been presented in Table 7. Two slopes with respective reference distances d_0 and d_1 have been needed to describe the path loss attenuation within both routes.

Table 7. The reference distances of the path-loss models

	2.4 GHz		5 GHz	
Distances [m]	AP1 (Route 1)	AP3 (Route 2)	AP1 (Route 1)	AP3 (Route 2)
d_0	1.3	1.5	1.3	1.5
d_1	3.2	12.6	6.3	12.6

The results have been fitted to the line by linear regression. However, the complex estimation methods have not been used because there has not been a remarkable variation of the results and the number of the results have been moderately small. So, the fitting has been done visually.

The numbers in blue and orange circles at the beginning, at the point where the slope changes and at the end of the route refer to the locations in the floor plan (Figure 18). The marked points are blue when the measurement route of the 2.4 GHz has been described and orange at the 5 GHz band.

Figure 18. The measured routes with referred points of the respective curves of the Figures 18 and 19.

6.3.1 Generated path-loss models within Route 1 and Route 2

The piecewise linear path loss curves have been presented in Figures 19 and 20. The path losses of AP1 (Figure 19) have been measured within the orange route of Figure 18. The distance where the slope has been changed is not the same in the 2.4 and 5 GHz region (Point 2). The path loss has been under one between the points 1 and 2 which means that the signal practically has not been attenuated at all in the distances under 3.2 m at the 2.4 GHz whereas it has followed free-space attenuation at

the 5 GHz. The signal has attenuated faster between the points 2 and 3 at the 5 GHz than it has been done at the 2.4 GHz which has been indicated by the path loss coefficient n_2 of 3.3 at the 2.4 GHz and n_2 of 5.0 at the 5 GHz. This is in line with the presumption of the attenuation of the signal at higher frequency.

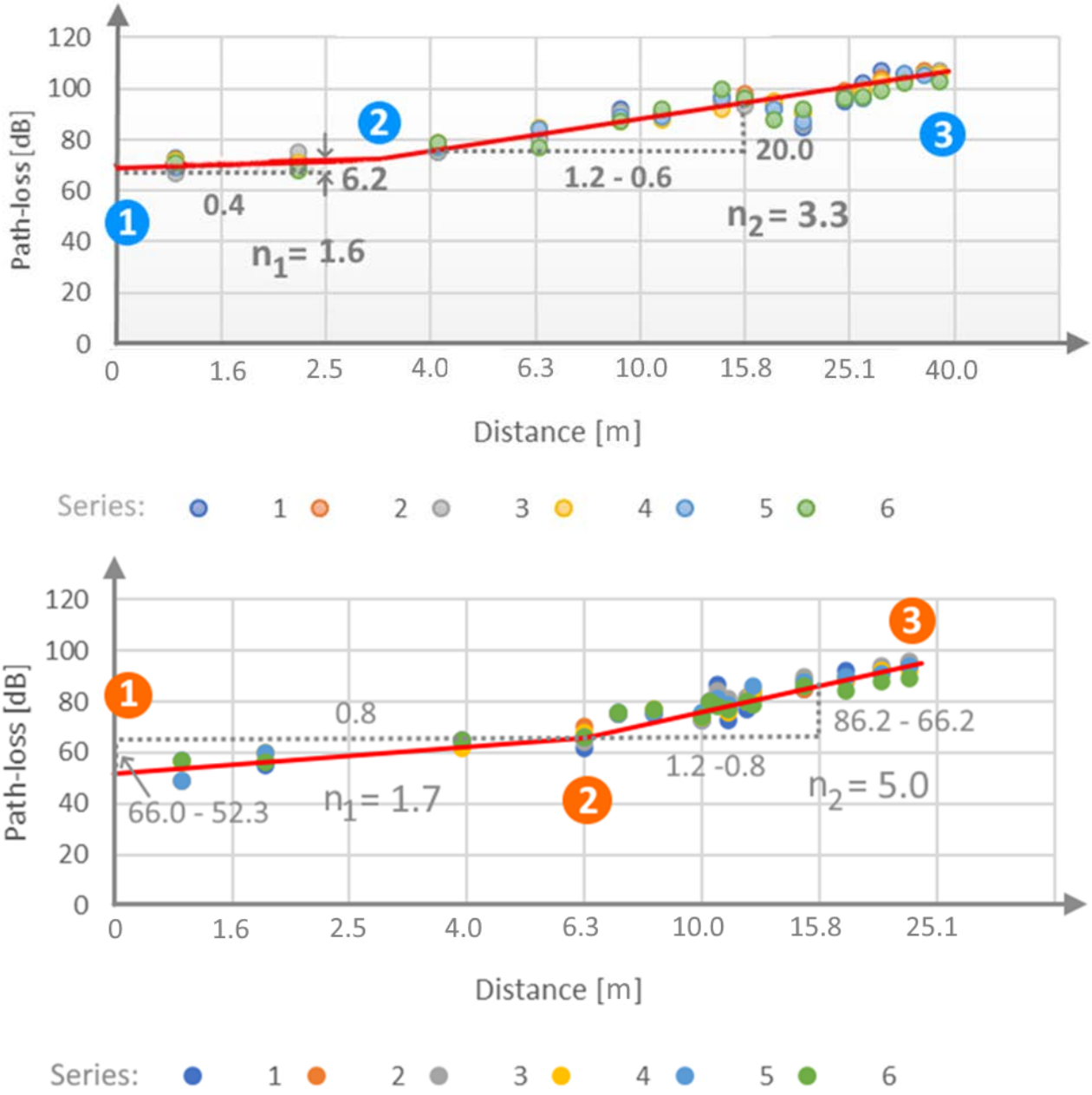

Figure 19. The path loss curves of AP1 at the 2.4 (upper) and 5 GHz region (lower).

In the case of AP3 the turning point of the slope has been in the same distance of 3 m (Point 2) at both frequencies. The path loss of signal from the AP3 has been near the free-space path loss in the distances less than 13 m. It may be seen in the floor plan (Figure 18) that there has been LOS connection in the long corridor until the point 2 has been reached. Entering the transverse corridor has raised the path loss coefficient to 5.0 at the 2.4 GHz band and 6.3 at the 5 GHz band. Because the threshold of the displayed RSSI readings in the Ekahau Pro has been adjusted to -85 dBm, the readings may only have been received until the distance of 22 m (Point 3) where the values of RSSI has gone out of range.

The path loss at the 5 GHz has followed the free-space attenuation law as it has been done at the 2.4 GHz until the turning point at the distance of 13 m (Point 2). After entering the transverse corridor, the slope has risen to $n_2 = 8.4$.

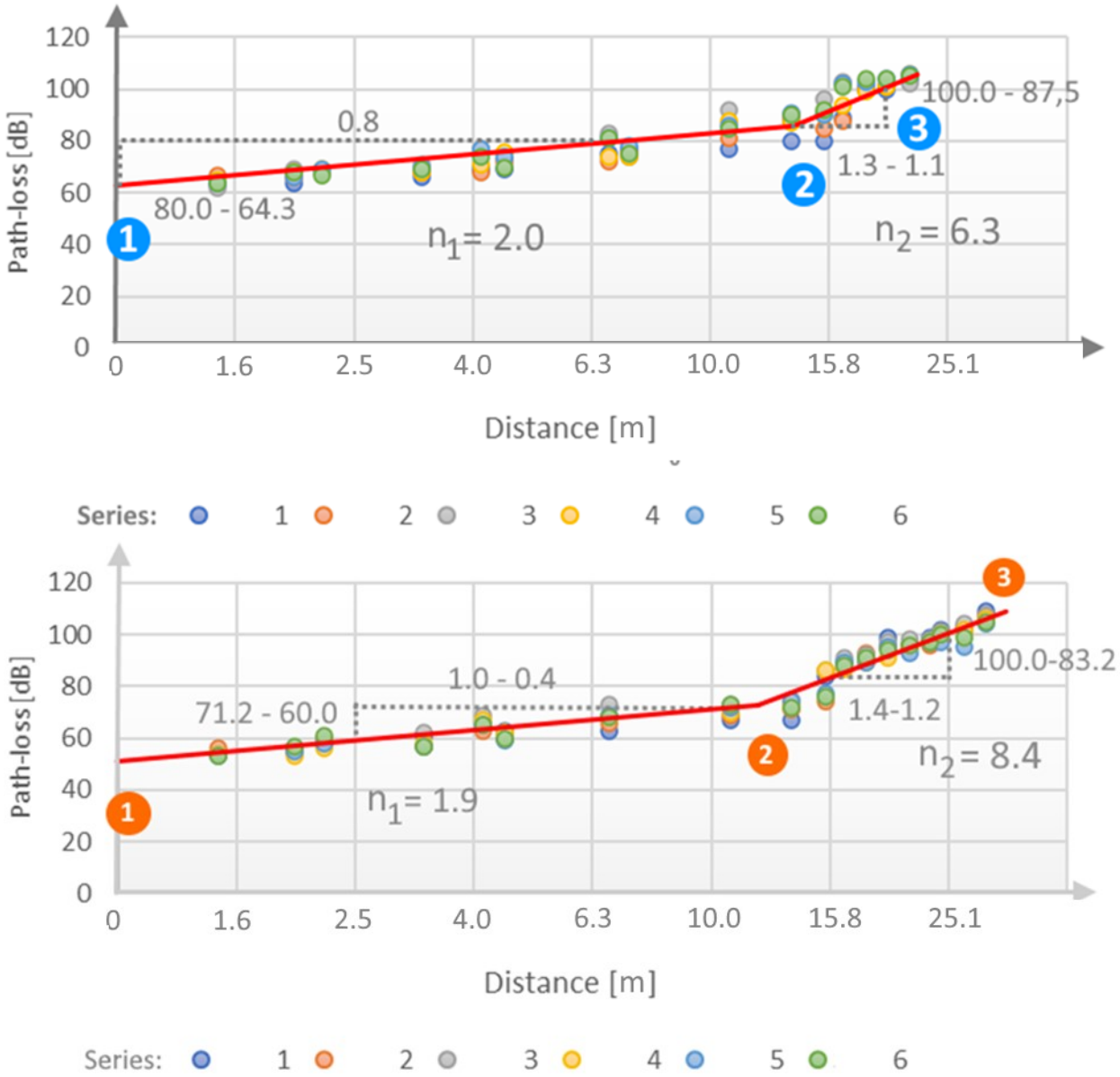

Figure 20. The path-loss curves of AP3 at the 2.4 (upper) and 5 GHz region (lower).

Based on the Figures 19 and 20 it may be concluded that the slope has risen when entering to the room behind a heavier wall structure (Point 2) and the path loss may be approximated as a free-space path loss in the shorter distances. The distances where propagation may be approximated as free-space propagation have varied so that in the case of AP3 the signal attenuation has followed the free-space attenuation until the LOS connection has been lost behind the corner of the transversal corridor. In the case of AP1 the attenuation of the signal may be approximated as free-space propagation until the distance of $d = 3.2$ m that refers to the Point 2 at the 2.4 GHz or $d = 6.3$ m that refers to the Point 2 at the 5 GHz (Figure 19). The signal has been attenuated faster at the 5 GHz band compared to the 2.4 GHz band which was to be expected. Because the path loss coefficients have equalled within the distances under 13 m, the difference of the respective reference path losses has remained in the distance of 13 m where the slope has been changed. Because of this, the path loss of 5 GHz signal

has been 10 dB lower compared to the path loss of 2.4 GHz signal although it should have normally been vice versa.

There is an open doorway between these two locations, and it seems like the path loss at the 2.4 GHz band has begun to rise immediately when entering the doorway in the distance of 3.2 m whereas the turning point of the path loss at the 5 GHz band has been reached until the LOS connection has been lost behind the massive wall in the distance of 6.3 m. The multipath at these locations should be studied to get the explanation for the different attenuation at the point from the propagation point of view. In principle, the complex glass wall structures together with the load-bearing pillars and walls in the vicinity of the doorway at the blue Point 2 (Figure 19) may result the attenuation that is depending on the frequency of the signal when the destructive interferences have been occurred by the multipath in the frequency selective channel. The attenuation after the Point 2 (of 2.4 and 5 GHz band) has been followed by the presumption of the frequency dependency of the path loss.

6.3.2 Shadowing effect of the generated models

The shadowing has been studied within both routes. To calculate the shadowing the mean squared error (MSE) of the measured path loss values in proportion to the modelled values have been computed. The calculations have been done for Route 1 and Route 2, respectively. The results of the calculations are based on the empirically derived path losses $L_p(d)$ within the respective route and the respective values that have been derived by the generated path loss models where the path loss coefficients have been defined as it has been previously discussed (Table 8). The results of the calculated values of the variance σ^2 and standard deviation σ have been presented in Table 8.

Table 8. The calculated values of the sample variance and standard deviation of the measured values of path-loss in proportion to the mean values of the generated path loss models

	Freq. range, [GHz]	Variance, σ^2	Standard deviation, σ	Shadowing, X_σ
Route 1 (AP1)	2.4	14.4	3.8	6.3
	5	8.6	2.9	4.8
Route 2 (AP3)	2.4	18.9	4.3	7.1
	5	12.2	3.5	5.8

Based on eq. (9), the shadowing effect X_σ may be calculated using the values of σ that have been presented in Table 8. The probability of coverage has been defined as 95% which gives for the lognormally distributed variable z value of 1.645. The shadowing has been calculated within both routes and at both frequency regions. The results have been presented in Table 8.

To compare the previously calculated values of shadowing the signal strength have been measured at the fixed distance of 12 m and 15 m from the AP1. The distances of 12 m (red circle) and 15 m (blue circle) have been chosen to study the effect of the load-bearing walls in front of them and to cover as large part of the control department as possible in any directions from the access point (Figure 21).

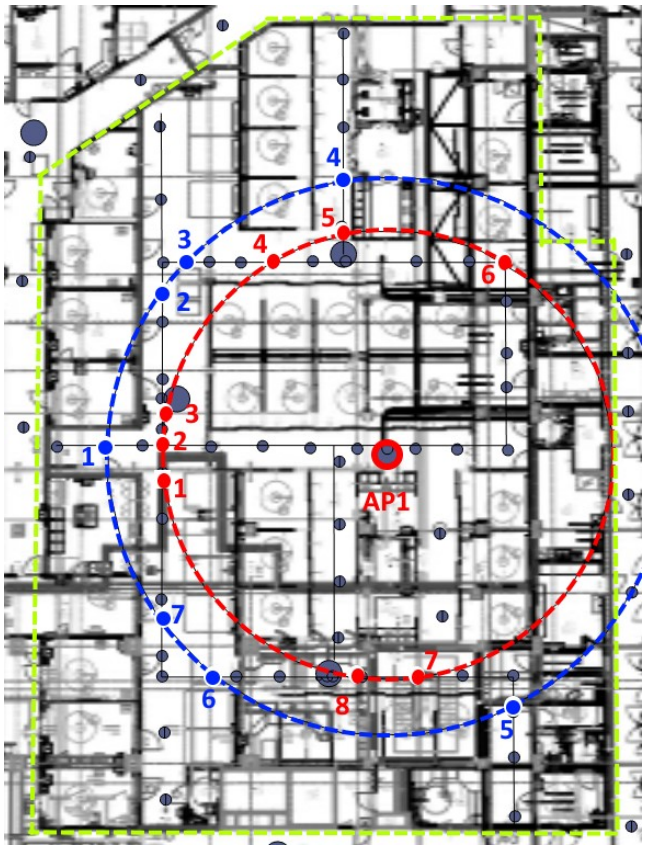

Figure 21. The measurement locations at the d = 12 m and d = 15 m from the AP1.

The signal strength has been measured regardless of the defined routes so that the most of measurement locations have been outside the predefined routes. The averaged results of the six measurement campaigns have been presented in the Table 9 together with the calculated values of the modelled path loss, sample variance, standard deviation, and the shadowing effect X_σ that has been calculated as an average of the shadowing in the distance of 12 and 15 metres. The calculated values have been based on the averaged values of the measured RSSI readings. The probability of coverage has been defined as previously using the value 1.645 as a lognormally distributed random variable.

Table 9. The derived path losses and the shadowing at the distances of d = 12 and d = 15 m from the AP1

Freq. range, [GHz]	Distance from AP1, d [m]	Measured path-loss, $L_{p_{meas}}(d)$ [dB]	Modelled path-loss, $L_{p_{model}}(d)$ [dB]	Variance, σ^2	Standard deviation, σ	X_σ, [dB]
2.4	12	88.8	85.4	69.0	8.3	13.5
	15	83.4	88.5	63.8	8.0	
5	12	73.7	77.0	35.6	6.0	8.8
	15	82.6	81.8	20.8	4.6	

Based on the values of X_σ that have been presented in the Table 8 and the Table 9 the comparison between the derived values have been done for the 2.4 and 5 GHz, respectively. The shadowing that has been defined within whole route has been shown remarkably lower values than the shadowing that have been defined in the fixed distance of 12 and 15 metres. This has been in line with the presumption because the cumulative effect of the obstacles increases with distance, as it has been

discussed earlier. The difference between shadowing of the respective frequency bands has varied a bit but the shadowing has been higher at the 2.4 GHz band than at the 5 GHz band. As has been discussed earlier, the shadowing of 9.8 to 19.7 dB has been defined for the desired coverage of 95% in the complex indoor environment at the 2.4 GHz band 1. The calculated values of Table 8 have been under the values of [10] although values of X_σ have been close to the lower limit of 9.8 dB at the 2.4 GHz band. However, it may be seen from Table 9 that when shadowing has been calculated based on the P_r that have been measured at the fixed distance of 12 and 15 m around the control room, X_σ has been within the variation of 9.8 to 19.7 dB (Table 9).

6.3.3 Comparison of the generated path-loss models

The generated multi-slope path loss models with shadowing have been presented for both route and frequency band in Table 10.

Table 10. The generated path loss models for the Route 1 and Route 2

	2.4 GHz	**5 GHz**
Route 1:	1.3 m ≤ d < 3.2 m : $L_{p1}(\text{dB}) = 67 + 8log\left(\frac{d}{1.3}\right) + 6.3$ 3.2 m ≤ d < 40 m : $L_{p2}(dB) = 70 + 33log\left(\frac{d}{3.2}\right) + 6.3$	1.3 m ≤ d < 6.3 m: $L_{p1}(\text{dB}) = 52 + 17log\left(\frac{d}{1.3}\right) + 4.8$ 6.3 m ≤ d < 25 m : $L_{p2}(\text{dB}) = 66 + 50log\left(\frac{d}{6.3}\right) + 4.8$
Route 2:	1.5 m ≤ d < 12.6 m : $L_{p1}(\text{dB}) = 64 + 20log\left(\frac{d}{1.5}\right) + 7.1$ 12.6 m ≤ d < 25 m : $L_{p2}(\text{dB}) = 88 + 63log\left(\frac{d}{12.6}\right) + 7.1$	1.5 m ≤ d < 12.6 m : $L_{p1}(\text{dB}) = 54 + 19log\left(\frac{d}{1.5}\right) + 5.8$ 12.6 m ≤ d < 30 m : $L_{p2}(\text{dB}) = 72 + 84log\left(\frac{d}{12.6}\right) + 5.8$

The generated models have been compared to the indoor path loss models that have been found in the literature and they have been presented in eq. (15), eq. (16) and eq. (17) [4]. The comparison has been done by calculating the path loss in the given distances of 2 m and 8 m on Route 1 and in the distance of 2 m and 15 m on Route 2. The distances have been chosen to cover the path loss variation in the cases of both slopes.

The ITU-R Model Recommendation of eq. (15) [4]1 also considers the canyon effect using the path loss coefficient of 1.8 for corridors. It has been used on the Route 2 with the distance of 2 m. The LOS path loss on the Route 1 has been compared using the coefficient of 3.0 that approximates the propagation in office environment. The path loss coefficient of 4.0 for the longer NLOS distances have been used on both route in the distances of 8 and 15 m, respectively. The IEEE 802.15.2-2003 [4] has been derived for the industrial environment primarily for the wireless sensor networks. It has been used in this work to compare the generated models in all cases based only on the measured distance. Eq. (16) has been used for the distances from 0.5 to 8 m and eq. (17) for distances over 8 m. The comparison between different models have been carried out and the results in decibels have been presented in Table 11.

Table 11. The comparison of the generated models, chosen empirically derived indoor path loss models and error between the measured and modelled values of path loss

Frequency band:	2.4 GHz				5 GHz			
Route:	Route 1		Route 2		Route 1		Route 2	
Distance:	2 m	8 m	2 m	15 m	2 m	8 m	2 m	15 m
ITU-R Model, [dB]	49	76	45	76	-	-	-	-
IEEE, [dB]	46	58	58	67	-	-	-	-
The values of generated models: [dB]	**68**	**83**	**66**	**93**	**55**	**71**	**56**	**78**
Measured values: [dB]	68	83	67	88	59	76.0	55	75
The error [%]:	**0.0**	**0.0**	**1.5**	**5.4**	**7.3**	**7.0**	**1.8**	**3.8**

The modelled values have also been compared to the averaged values of the six measurement campaigns and the error has been calculated for the respective values of the generated model. It may be seen from Table 11 that the generated models describe more accurately the averaged values of the measurements than the compared empirical ITU-R and IEEE models (Table 11).

It may be seen from Table 11 that the error has been increased within Route 1 at the 5 GHz and within Route 2 at the 2.4 GHz band when the distance has been 15m. The findings will be discussed in the conclusions (Chapter 7).

6.3.4 Probability of signal outage

The probability of signal outage has been calculated for Routes 1 and 2 at the 2.4 GHz band using eq. (14). The results of the calculations have been presented in Figures 22 and 23, respectively. Probabilities have been calculated using the sensitivity of -85 dBm that has also been used as a threshold in Ekahau Pro as it has been discussed earlier.

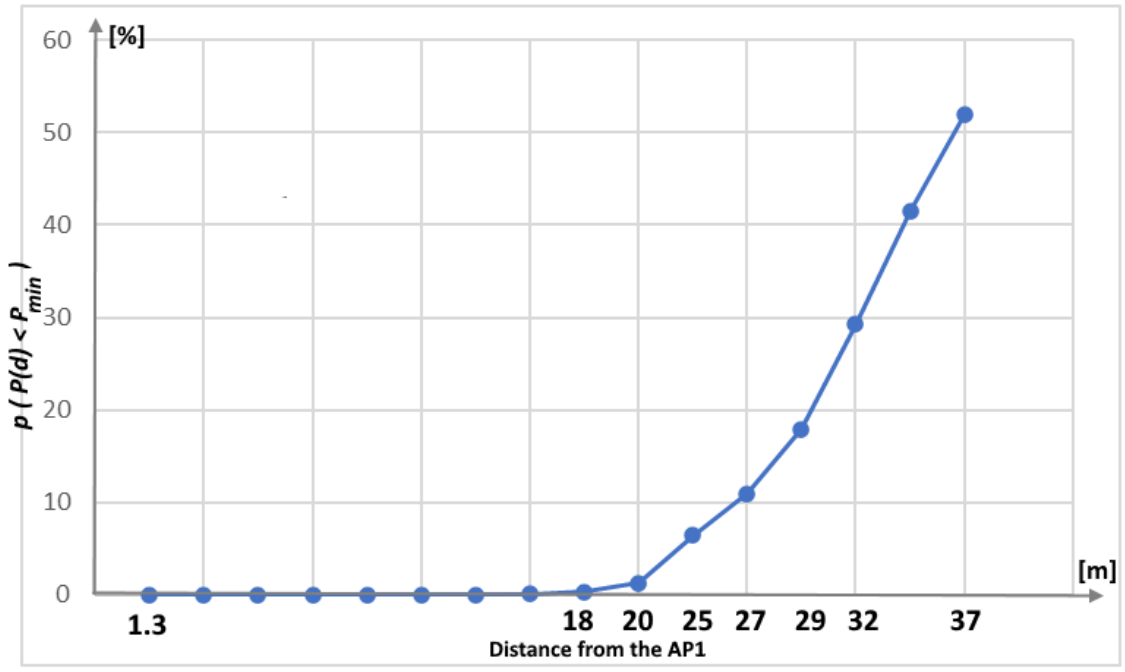

Figure 22. The probability of the signal outage for Route 1 at the 2.4 GHz band.

The typical requirement for the outage probability $p(P(\mathrm{d}) < P_{\min})$ of 1% has been used. It may be seen by comparing Figure 22 and Figure 23 that the probability has risen more at the end of Route 2 which has been in line with the path loss model that has been generated earlier. The design requirement of 1% has been met in the distances below 20 m on Route 1 and 17 m on Route 2.

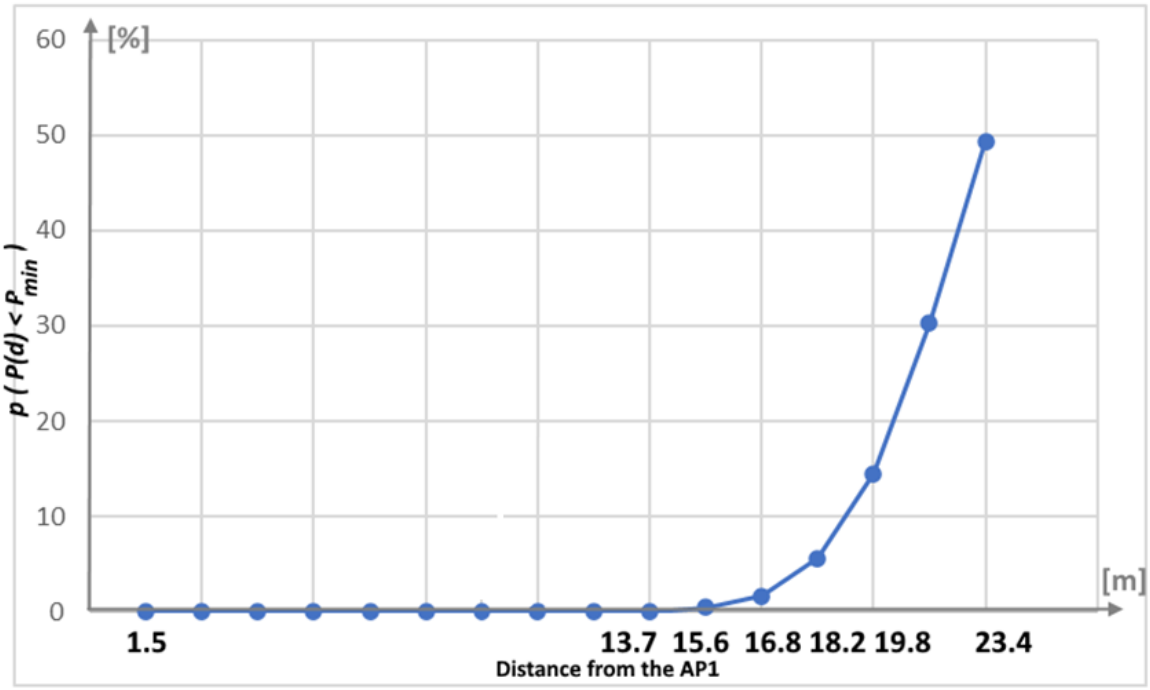

Figure 23. The probability of the signal outage for Route 2 at the 2.4 GHz band.

Although the generated models have been based on the measurements that have been carried out in the control ward, they may be applied with certain restrictions in the rest of the J2.

6.4 Coexistence in the control ward

The control ward has been chosen as an object of the interference study because there are a lot of patient monitoring appliances and critical data communication which may be extremely sensitive to interferences. Furthermore, based on the findings of the previously discussed overview of the interference conditions it may also be assumed that the potential risk for interferences in the control ward must be considered. The complex room geometry contributes the signal propagation which obviously may affect the signal-to-noise ratio and potentially increase the risk for harmful interferences.

The overview of interference conditions in the control ward have been studied using the channel interference parameter of Ekahau Pro. It shows the heatmap where the number of co-channel (CCI) and adjacent channel interferences (ACI) have been presented as the visualized outcome of the site-survey. The co-channel interference has been shown in the heatmap in a way that different colours of the heatmap represent the number of access points that are transmitting at the same channel as the associated access point. The program shows the list of interfering access points, their MAC names, channel and RSSI in a pointed location of the heatmap. The amount of the viewed access points is based on the threshold that can be adjusted. In this work the threshold is set to -85 dBm but may be changed to the arbitrary value between -100 dBm and -20 dBm. The overview of interferences has been studied also by the lists of interfering access points that may be shown in the chosen location of the heatmap. An example of the list from the arbitrary location in the control ward has been presented

in Figure 24. It may be seen from Figure 24 that the signals from the upper and lower floors have also been received in the chosen location.

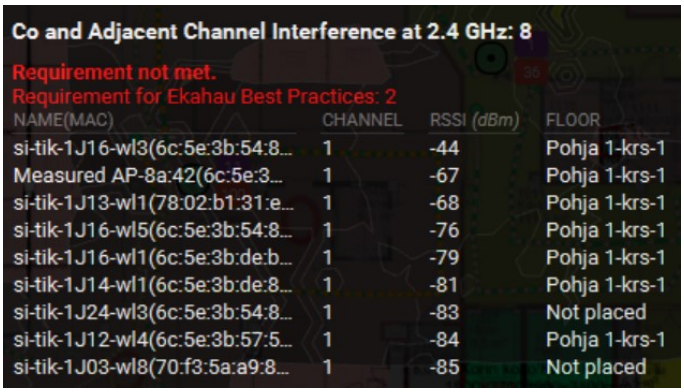

Figure 24. An example of the displayed list the of access points that have been received in the measurement location [Screenshot from Ekahau Pro]

During the campaigns, the RSSI readings have been measured as continuous site-survey measurement using the hybrid measurement principle that has been described earlier. The measurement has been carried out continuously by walking slowly within the predefined routes around the control ward. There have been 21 chosen locations where the measurement device has been stayed about 10 s. The distances from the locations to the associated access points have been measured in a way that has been described earlier. (Figure 25)

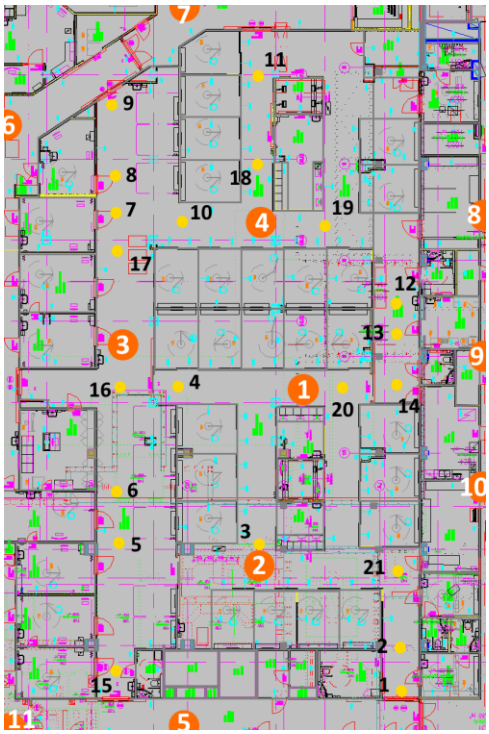

Figure 25. The locations of the interference measurements in the control ward.

The heatmap of Figure 26 is based on the two measurement campaigns that have been done in November 2020 and the visualized results represent the averaged outcome. It is worth mentioning that although the heatmaps of Figure 26 have been based on the averaged results of two independent campaigns, all other results of the interference measurements have been based on the six measurement campaigns that have been carried out in a period from September to November 2020.

The access points have been marked as blue circles and the results have been presented separately in the case of both frequency regions (Figure 26). The number of co-channel interference sources that have been received in the chosen location has been described by colours. So, black represents the area where seven or more interfering access points have been received and so forth according to the colour code at the bottom of the figure. The associated access point has not been included in the number of co-channel access points of the figure above. Because the threshold of -85 dBm has been chosen in Ekahau Pro, only the interferers that has exceeded the threshold have been shown in the heatmaps and the listings of Figures 24 and 26.

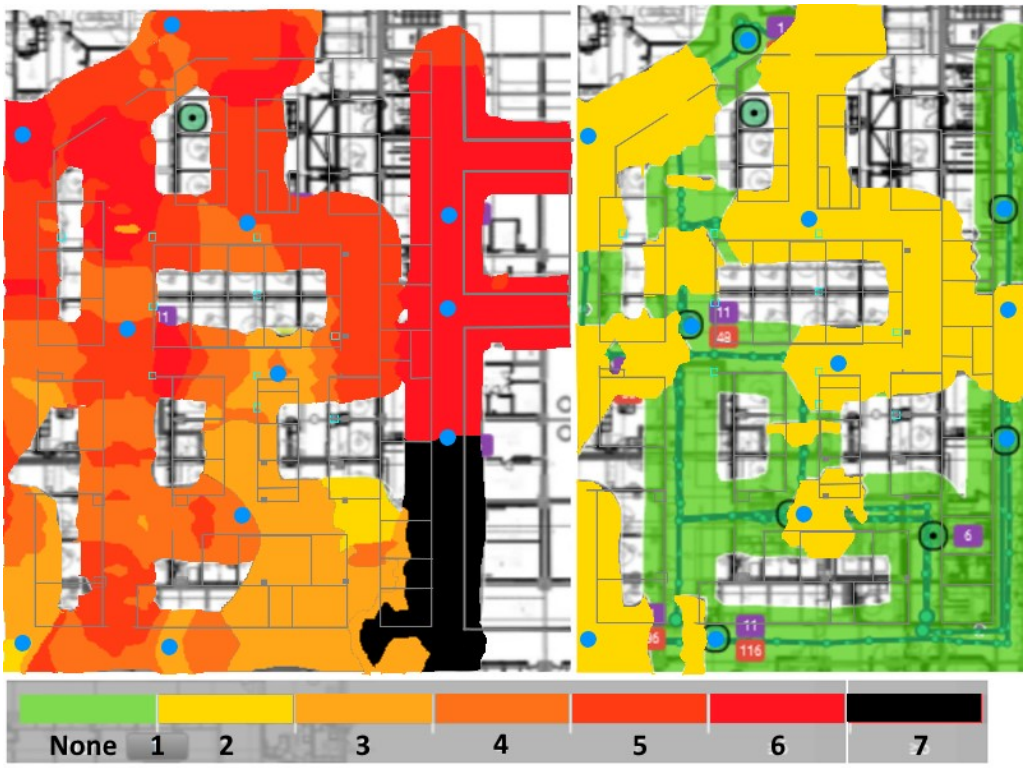

Figure 26. The co-channel interference in the control ward at the 2.4 GHz (left) and at the 5 GHz band (right).

The number of co-channel interferences has been higher at the 2.4 GHz than 5 GHz band. Based on Figure 26 it may be seen that there has been a remarkable difference in the amount of interfering access points at the 5 GHz band compared to the 2.4 GHz band. Two co-channel access points have been received at the half of the areal of the control ward at the 5 GHz while at the 2.4 GHz band the power of more than -85 dBm has been received from five or more co-channel interference sources at more than half of the areal. Obviously, this has been caused because only two channels have been used at the 2.4 GHz while at the 5 GHz band all four access points are using different channels. This may have some consequences on the transmitted power as well that has been assumed to be adjusted at the maximum level but has been controlled automatically based on the data that have been acquired about the interference conditions by access point. The channel allocation and power control mechanisms of the access points should be studied more in detail to figure it out. However, the issue is out of the scope of this study.

Although, the study begins with an overview of the CCI in the control ward, the interference has been studied in this work by SIR model without making difference between the sources of the interference. The measurement locations that have been used in all interference measurements of the control ward have been chosen from the locations of Figure 25. Although the locations have mostly been the same as the locations of the propagation measurements there have also been a few locations

outside the routes of the propagation measurements. The locations have primarily been chosen based on the previously discussed overview that have shown the locations of higher indicated interference (Figure 26). However, when locations have been defined for the study of SIR, the distribution of the locations along the routes and the local variation of the spectrum channel power of Ekahau Pro have also been considered.

6.4.1 Study of local SINR variations

In this work the coexistence has been studied from the signal-to-noise ratio point of view. As it has been discussed earlier, the allowable threshold of SINR depends on data rate and the modulation scheme that has been needed in the network. The empirical determination of SINR in the control ward has been done in two phases. First, an overview of interferences in the control ward has been provided. Secondly, the SINR has been determined partly in the same locations where the propagation models have earlier been generated. Variations of the SINR within the respective routes and the effects that the variations may have on the signal propagation will be analysed. Finally, the threshold values β will be determined for the modulation that has been needed in the network to meet the requirements of the IEEE 802.11n at the 2.4 GHz and the IEEE 802.11ac at the 5 GHz band with maximum data rate.

The interferences have been measured partly in the same locations where the RSSI values of the propagation measurements have been carried out. Although the measurement locations have primarily been chosen from the interference point of view, they have also been chosen to compare the modelled propagation and SINR within the routes where the propagation models have earlier been generated. Furthermore, the wide coverage of the locations has also been important to figure out the local variations of the interference whether the sources of interference have been the access points of the network or outside the network. The chosen measurement locations have been shown as yellow circles in Figure 26. The access points of the control ward and its neighbourhood have been shown as orange circles with white numbers. The numbers 1 to 4 refer to the same access points of the control ward that have also been measured when the propagation models have been generated.

The RSSI of the access points that have been measured in the respective locations have been averaged from the results of six measurement campaigns that have been carried out during the period from September to November. Based on the averaged RSSI readings the power of the access points has been summed up except the one that has been accessed. The noise has been measured simultaneously with the RSSI measurements and the resulting noise readings of the measurement campaigns have been averaged in the respective locations. The client chooses the connected access point according to the device specific roaming criteria in WLAN. In this work the strongest received signal has been assumed to be the signal of the accessed access point to avoid the device dependency in the determination of SINR. If the strongest signal has been changed between the locations of the route the first measurement location in the direction of route has been assumed to be the location with a changed access point although the clients in general tend to stay accessed regardless of the local variation of the strongest signal as it has been discussed earlier. In the locations outside the routes the accessed access point has been assumed to be the one with the strongest signal in the location.

The SINR has been calculated in all numbered locations from 1 to 21 using eq. (23) where P_r refers to the received power from the accessed access point and noise power P_n refers to the averaged value of noise as it has been measured in the respective location. The results in all 21 locations have been presented in Figure 26.

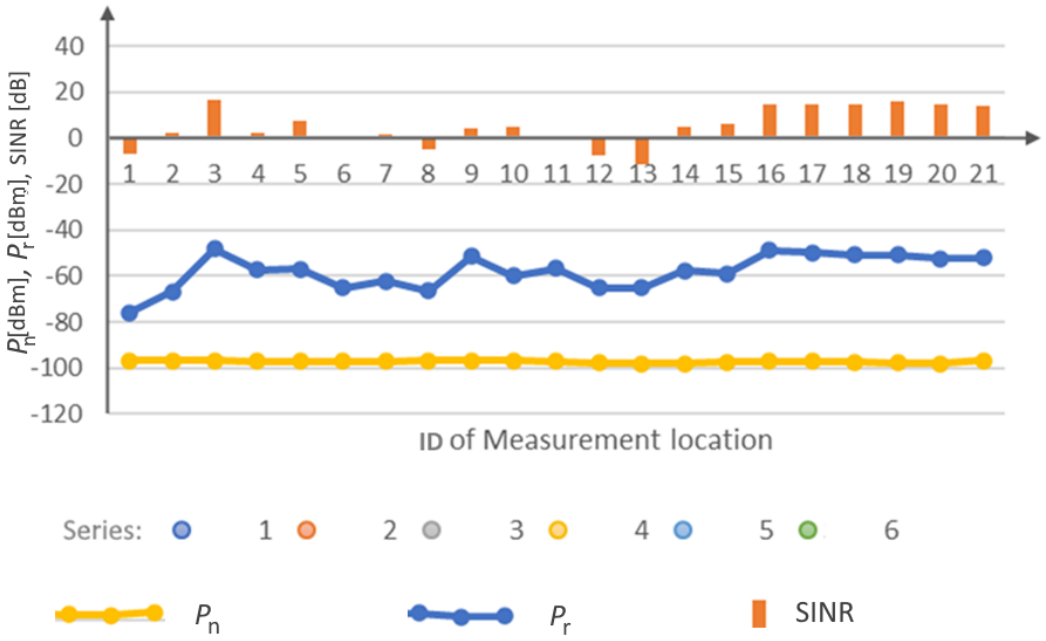

Figure 27. The P_n, P_r and SINR in the measurement locations of the interference measurements in the control ward at the 2.4 GHz band.

The numbered locations from 1 to 21 refer to the locations that have been presented in the Figure 25 and they do not follow exactly the routes or any other order. There has been only slight variation in the noise power P_n. It has varied between -96.8 and -98 dB and the averaged value has been -97.2 dBm. Based on the value of averaged noise power the noise floor has been determined to be -97 dBm.

The signal of the accessed access point has been about -60 dBm everywhere except close to the locations 1 and 2. There has been extraordinarily strong attenuation of the 2.4 GHz signal between the locations 1 and 2 which has also been indicated in the path-loss model of the Route 2 as it has been discussed earlier. So, as it may be seen in the figure above, the signal strength of the accessed AP2 has been sinking dramatically after the location 3. It may be calculated from the figure that the SNR has been mostly in the order of 40 dB except between locations 1 and 6 where it has been in its minimum of 21 dB. In principle this may be an acceptable value with low order modulation, but the primary problem has been the low SINR in these locations. On the other hand, from the perspective of the given QoS requirements the SNR has been too low as it will be seen later. The low value of SINR in turn has been caused by both local attenuation of the accessed signal and increase of aggregated interference. The weak signal in the locations 1 and 2 has resulted in the client connecting the access points of the upper floor and the neighbouring building.

The low values of SINR in the locations 1, 2 and 4 as well as between the locations 6 and 13 where SINR has been under 0 dB indicate the power of aggregated interference that has been higher than the power of the accessed access point. There has been strong variation of the SINR between the maximum of 16 dB and minimum of -11 dB. The reasons for variation of SINR and its effects on the capacity of the channel will be studied more in detail within the routes where the propagation model has been generated.

Evaluating the local SIR variations within the modelled routes

The change in measured values of the received power P_R, the measured power of the aggregated interference P_I and the calculated values of SIR have been studied piecewise for both routes at the 2.4 GHz and 5 GHz frequency regions. The measured P_R is based on the propagation models that

have been generated earlier for the respective routes at both frequency bands. The changes have been compared to each other to figure out the primary reason for the local variation of SIR.

The study of SIR variations within the routes has been done without considering the client specific roaming criteria. The access point with the strongest signal and the shortest distance from the measured route is assumed to be accessed. The shortest distance from the route has been defined by the perpendicular distance d_{pt}, d_{pu} or d_{pv} from the measured route (Figure 28). Red vertical lines of the figure show the roaming lines where the power of the formerly accessed signal has been exceeded by the access point with the shortest perpendicular distance as it has been defined in the Figure 28. The signal has been called the desired signal and in Figure 28 it has been changed from the signal from the AP_t to the AP_u in the roaming line before the location x_k because the distance $d_{pu} < d_{pv}$ (Figure 28). The power of the desired signal in the location x_k has been referred as $P_r(x_k)$ while the other received signals in the location x_k have been called as interfering signals that contribute the aggregate power of interference in the location that has been referred as $\Sigma P_i(x_k)$. Now, SIR in the location x_k may be defined as $SIR(x_k)$ and it may be calculated based on the averaged values of measured $P_r(x_k)$ and $\Sigma P_i(x_k)$ using the eq. (23).

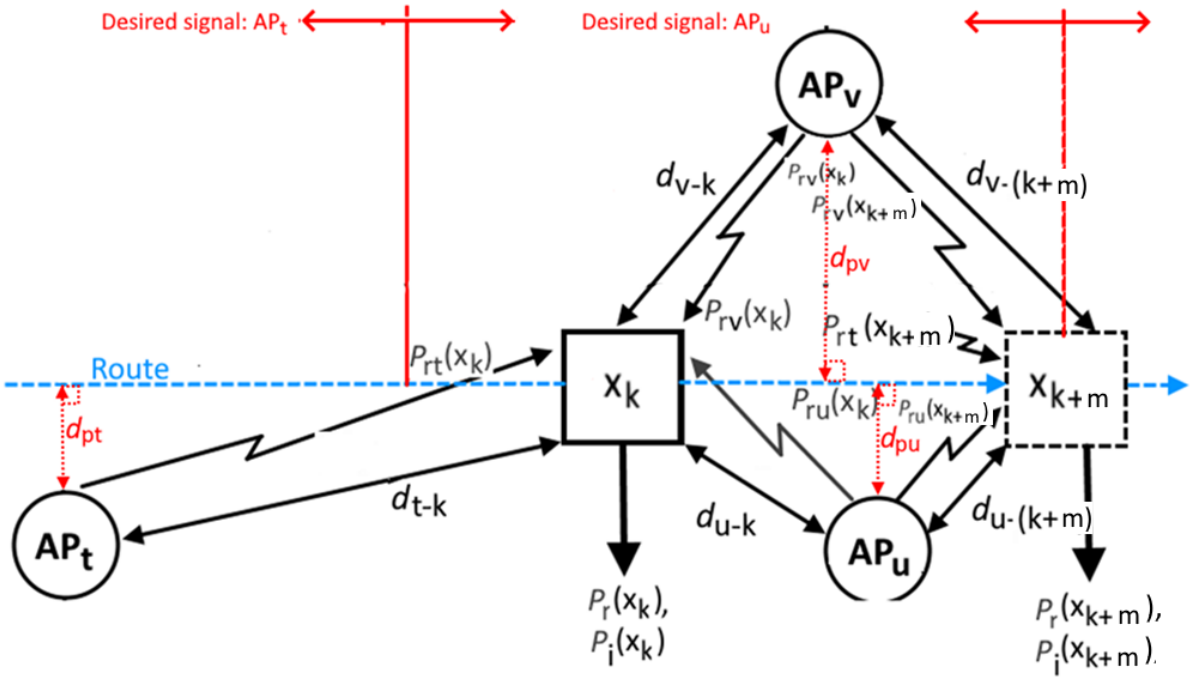

Figure 28. The distances and signal strengths of desired and interfering signals from access points in the neighbourhood of the measured route.

There are two measurement locations in the Figure 28 within the route that have been referred by x_k and x_{k+m} where $k = 1, 2, 3, \ldots, k = 1$ for the beginning of the studied route and $m = 1,2,3,\ldots$ So, e.g., if the distance between two consecutive measurement locations is to be studied, $m = k+1$. The desired signal, as it has previously been defined, and aggregate power of interference have been measured in the locations x_k and x_{k+m} and the results have been referred as $P_r(x_k)$, $P_r(x_{k+m})$, $\Sigma P_i(x_k)$ and $\Sigma P_i(x_{k+m})$, respectively. SIR has been calculated in a similar way as it has been calculated in the location x_k too.

The projections of the distances $d_{t\text{-}k}$, $d_{u\text{-}k}$ and $d_{v\text{-}k}$ between the measurement location and the associated access points have been shown in Figures 29 – 32 by red arrows. Index t, u and v refer to the index of associated access point and k refers to the respective measurement location x_k.

Measurement locations x_k have been presented by the numbers in blue circles of Figures 29 – 32. So, e.g., if the client has remained accessed on the AP_2 in the measurement location x_3, the projection of the distance between the client and associated access point has been referred by $d_{2\text{-}3}$ (Figure 28). The received power from the respective access point in the location x_k has been referred by $P_{rt}(x_k)$, $P_{ru}(x_k)$ and $P_{rv}(x_k)$. The desired signal power $P_r(x_k)$ is one of them and the rest of the signals represent together the sum of the power of interfering signals $\Sigma P_i(x_k)$ in the given location as it has been described earlier.

Because SIR variation within the route is to be studied, the change of SIR, ΔSIR has been calculated based on the previously defined $SIR(x_k)$ and $SIR(x_{k+m})$ by subtracting $SIR(x_{k+m})$ from $SIR(x_k)$. The results have been presented in Tables 12, 13, 14 and 16 together with the calculated values of $P_r(x_k)$, $\Sigma P_i(x_k)$, $P_r(x_{k+m})$ and $\Sigma P_i(x_{k+m})$ which have been based on the averaged values of the measured signal strengths in the respective location. The change of P_r and ΣP_i over the studied distance have been calculated by subtracting $P_r(x_{k+m})$ from $P_r(x_k)$ and in the case of ΣP_i accordingly. The change has been referred by ΔP_r and $\Delta(\Sigma P_i)$ in the Tables 12, 13, 14 and 16 when the change has been defined positive in respect to the increasing distance as it has been shown by the values of x-axis of the Figures 29 -32.

The Route 1 has been studied at the 2.4 GHz in Figure 29. It may be seen from the figure that there are five measurement locations that have been marked by numbers in the blue circles within the route. They refer to the previously described measurement locations x_k. As it has been discussed above, the distances from the location x_k to the associated access point have been marked by the distances $d_{t\text{-}k}$, $d_{u\text{-}k}$ and $d_{v\text{-}k}$, where index t refers to the AP_t and index u to the AP_u, and k refers to the respective measurement location x_k. In the case of Figure 29, AP_t is AP1 and AP_u is AP4 and AP_v refers to the access point of the neighbouring building that has been located close to the measured route.

As it has been presented by the dashed vertical line of Figure 29, the desired signal has been changed from AP1 to AP4 in the location x_3 (indicated by number three in blue circle). Based on the discussion above, the roaming has been assumed to be occurred in x_3 because the power $P_{r1}(x_3)$ from AP1 has been exceeded by the power of $P_{r3}(x_3)$ from AP4 with the shortest perpendicular distance d_{p3} as it has been measured from the route to the access point. However, in the location x_3 of Route 1, the strongest signal has been received from the access point AP_v of the neighbouring building with the shortest distance $d_{v\text{-}3}$ (Figure 28) from the measurement location x_3. The respective perpendicular distance d_{pv} from the measured route to AP_v has though been higher than the perpendicular distance d_{p3} from the AP4, though the distance from AP4 to x_3 has been higher. As a result, the signal from AP4 has been defined as desired signal in x_3. Because desired signal has been determined using the perpendicular distance from the access point of the highest received signal strength, the projection of the distance $d_{t\text{-}k}$ (in the case of AP_t) has only been used to show the access point that has been associated along the route until the local minimums or maximums of SIR. The whole route has been shown in the thumb nail from the CCI heatmap (Figure 25) that has been included in the figure for guidance. (Figure 29)

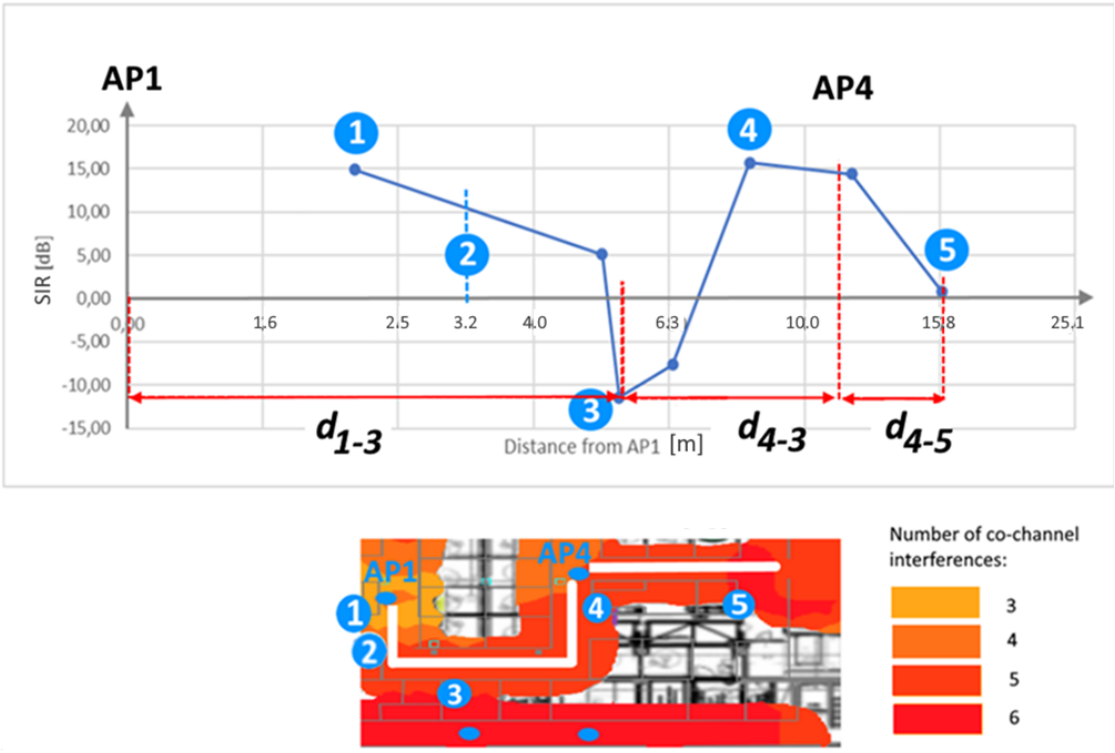

Figure 29. The SIR within Route 1 at the 2.4 GHz band.

The analysis of the SIR variation within the Route 1

The previously discussed comparison for Route 1 at the 2.4 GHz band has been presented in the Table 12. The roaming from the AP1 to AP4 has occurred in the location marked by number three. The comparison between the propagation model of the respective route (Figure 18) and Table 12 shows that ΔP_R has decreased slowly under distance of 0.7 which corresponds to the propagation conditions of the first slope when the path loss has practically followed the free-space attenuation (Figure 27).

Table 12. The piecewise study of the Route 1 at the 2.4 GHz band

Studied distance between the points x_k and x_{k+m}	ID of the accessed AP	$P_r(x_k)$ [dBm]	$\Sigma P_i(x_k)$ [dBm]	SIR(x_k) [dB]	$P_r(x_{k+m})$ [dBm]	$\Sigma P_i(x_{k+m})$ [dBm]	SIR(x_{k+m}) [dB]	ΔP_r [dB]	$\Delta(\Sigma P_i)$ [dB]	ΔSIR [dB]
1 - 3	AP_1	-52	-67	15	-65	-54	-11	-13	13	-26
3 - 4	AP_4	-65	-54	-11	-51	-66	15	14	-12	26
4 - 5	AP_4	-51	-66	15	-57	-57	0	-6	9	-15

The variation of noise power has been assumed negligible and the defined noise floor of -97 dBm has been used. Based on the table above it may be seen that the rapid decrease in SIR of 26 dB between the points 1 and 3 has been caused by both strongly increased path loss of 13 dB and aggregated interference of equal amount. The slope of the path loss curve has been changed after the corridor has been entered and the increased attenuation effect of the surrounding load-bearing walls have contributed to the further rising path loss. This has occurred simultaneously with the increase of aggregated interference that has been dominated by the access points of the neighbouring building close to the corridor.

Within the distance from Point 3 to Point 4, SIR has risen to the same level as it has been in point 1. It may further be seen from Table 12 that the decrease in aggregate interference and useful power have almost equally contributed the increase of SIR by 26 dB. The distance from the access points of the neighbouring building to the points 1 and 4 is equal which obviously means that the increase of aggregated interference must equal to the decrease of the interference between the points 3 and 4 which has been the case. Looking at the thumbnail of Figure 29 the symmetrical geometry of the load-bearing walls in respect to the locations of the Point 1 and Point 4 may easily be seen. This has resulted in the symmetrical change in path loss because the access point near the Point 1 has been located symmetrically with the access point near the Point 4 in respect to the Point 3 where the accessed access point has been changed. This has been indicated in Table 12 by decrease of SIR between the points 1 and 3 that has equalled to the increase of SIR between the points 3 and 4.

After reaching the maximum value in the Point 4, SIR has been decreased toward the Point 5. Based on Table 12 the reason for the decrease may primarily be explained by the increase in aggregate interference. The increase in path loss has had a minor contribution to the decreased SIR because the signal has LOS propagated from the access point near point 4 through the straight corridor between the access point and Point 5. The degradation of SIR has obviously not stopped in Point 5, but it has been continued until the new access point has been accessed. The endpoint of Route 1 has been so close to Point 5 that further study of SIR variations might not have been justified. The SIR variations at the 5 GHz band have been analysed in Figure 30 and Table 13, respectively.

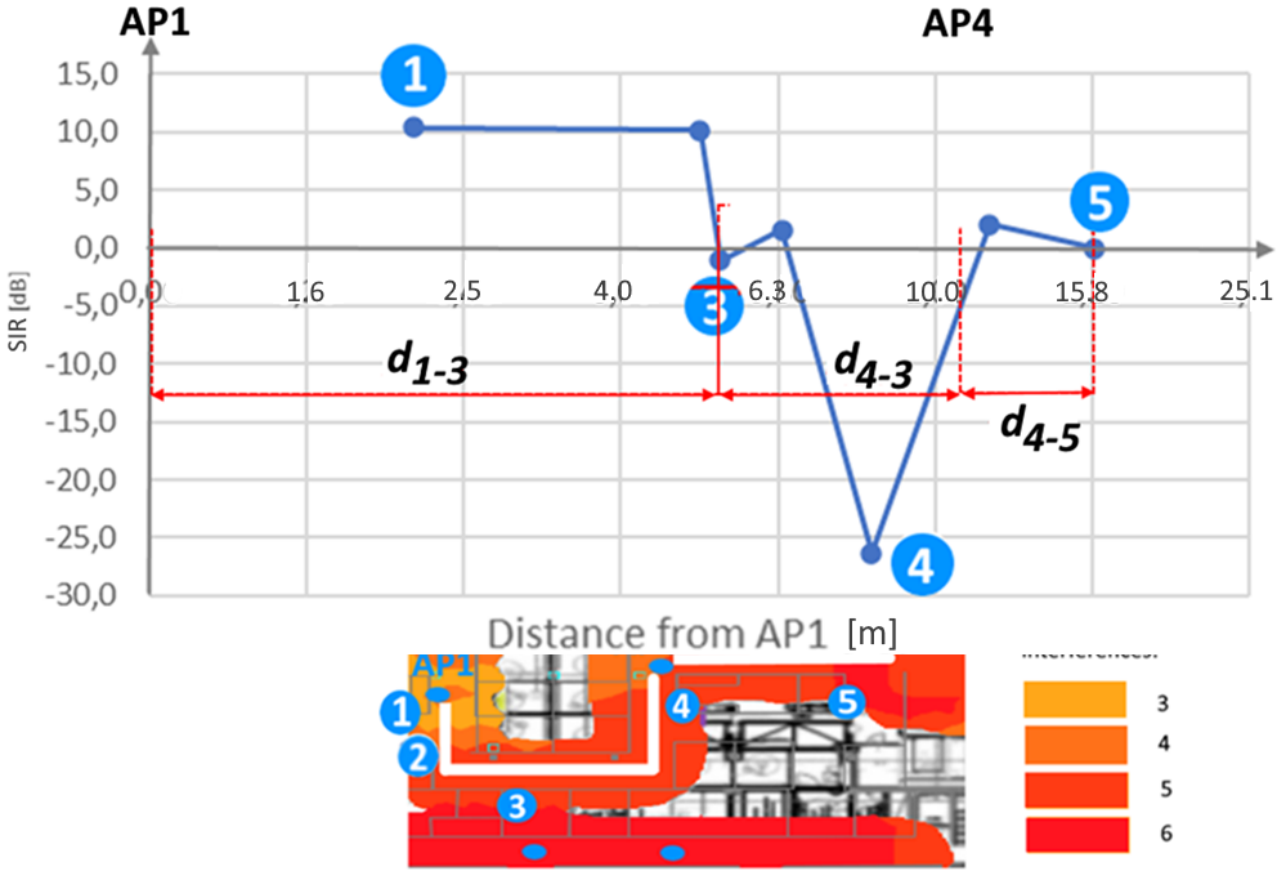

Figure 30. The SIR variations within Route 1 at the 5 GHz band.

At the 5 GHz band SIR has mostly variated less than at the 2.4 GHz band. However, there have been measured strong variations at the 5 GHz band too. At the 5 GHz the transmitters in the neighbouring building have not interfered because they are using only 2.4 GHz band which may be seen in Table 13 where the path-loss has clearly dominated the contribution to the fallen SIR. The

load bearing wall on the left from the locations 12 and 13 have obviously caused the decrease in signal power before the roaming point of the location three. As a result of a remarkable attenuation SIR has dropped close to 0 dB. After the corner of the route, under the conditions of LOS from the AP4 signal has although continued to fall and SIR has reached the minimum of -26.3 dB in the point four. It has been the absolute minimum of SIR in the whole control ward. The minimum of SIR in the distance of 8.3 m has been caused by the extraordinarily strong aggregated power from the other access points of the control ward and neighbouring corridors. This has been indicated also in Table 13 where the aggregated power has increased 34 dB from the point three to the point four. The aggregate interference has although fallen in the next measurement location that has been close to the AP4. The previous decrease in aggregated power has been completely compensated in the location.

Table 13. The piecewise study of the Route 1 at the 5 GHz band

Studied distance between the points x_k and x_{k+m}	ID of the accessed AP	$P_r(x_k)$ [dBm]	$\Sigma P_i(x_k)$ [dBm]	SIR(x_k) [dB]	$P_r(x_{k+m})$ [dBm]	$\Sigma P_i(x_{k+m})$ [dBm]	SIR(x_{k+m}) [dB]	ΔP_r [dB]	$\Delta(\Sigma P_i)$ [dB]	ΔSIR [dB]
1 - 3	AP_1	-39	-49	10	-53	-52	-1	-14	-3	-11
3 - 4	AP_4	-53	-52	-1	-44	-18	-26	9	34	-25
4 - 5	AP_4	-44	-18	-26	-45	-45	0	-1	-27	26

The analysis of the SIR variation within the Route 2

The piecewise analysis that has been described above has also been applied for the SIR variations within the Route 2 (Figure 31).

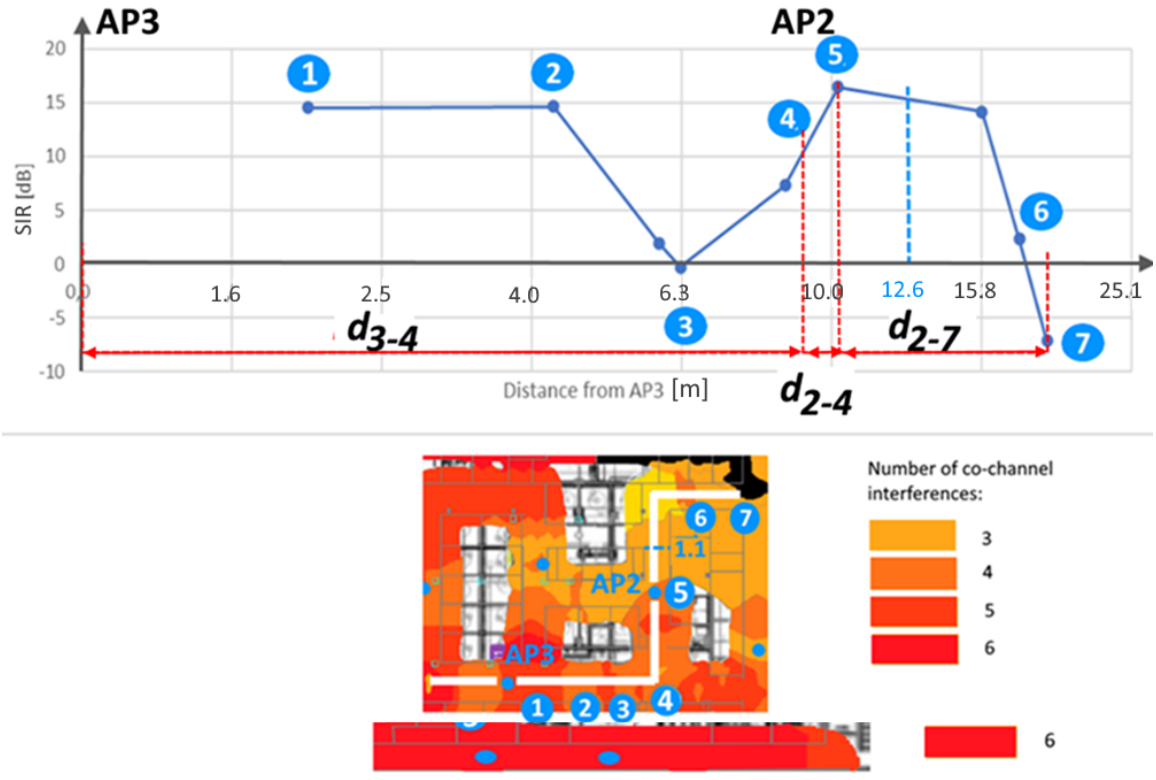

Figure 31. The SIR variations within the Route 2 at the 2.4 GHz band.

The accessed AP3 has changed to AP2 between the points 3 and 4. SIR has risen because of the increased signal strength that has been caused by the changed access point. It may be seen from the thumbnail of the heatmap in Figure 31 that the transverse corridor has been entered after the corner in the Point 4 and the strengthening LOS signal from the AP3 has caused an increase of SIR by 9 dB while the aggregated interference has remained constant. The AP2 is close to the Point 4 where the SIR has reached its local maximum. In the distance of 12.6 m measured from the AP2 where the slope of the modelled path-loss has been changed the strong attenuation of the accessed signal from AP2 has occurred. This has caused a rapid decrease in SIR that has fallen below 0 dB close to Point 6 and has reached the minimum value of Route 2 at the level of -7 dB. As it has been discussed earlier in the case of Route 1 the geometry of the load-barrier walls in the centre has obviously contributed a remarkable attenuation of the signal close to Point 3 of Route 1. The similar geometry in respect to the access point AP2 may be seen after Point 5 at the end of Route 2. This might have caused similar effects between the points 5 and 7 of Route 2 as well.

As it may be seen from Table 14, SIR variations between all five distances that have been studied within Route 2 have primarily contributed by changes in path loss of the accessed access points. The aggregated interference has been at a moderately high level within the whole route with minor changes locally. It may be seen from the thumbnail of Figure 31 that also the number of co-channel transmitters have been high with more than four co-channel access points until the Point 5 has been reached. After the Point 5 the number of co-channel access points have been reduced to three simultaneously with the decrease of aggregate interference. The empirically derived values of useful signal power, aggregate interference and SIR have been presented in Table 14.

Table 14. The piecewise study of the Route 2 at the 2.4 GHz band

Studied distance between the points x_k and x_{k+m}	ID of the accessed AP	$P_r(x_k)$ [dBm]	$\Sigma P_i(x_k)$ [dBm]	SIR(x_k) [dB]	$P_r(x_{k+m})$ [dBm]	$\Sigma P_i(x_{k+m})$ [dBm]	SIR(x_{k+m}) [dB]	ΔP_r [dB]	$\Delta(\Sigma P_i)$ [dB]	ΔSIR [dB]
1 - 2	AP_3	-49	-63	14	-52	-67	15	3	-4	1
2 - 3	AP_3	-52	-67	15	-65	-65	0	-13	2	-15
3 - 4	AP_2	-65	-65	0	-57	-65	8	8	0	8
4 - 5	AP_2	-57	-65	8	-48	-65	17	9	0	9
5 - 7	AP_2	-48	-65	17	-76	-69	-7	-28	-4	-24

From Table 14 it may be seen that SIR variations have primarily been caused by the variations of the changes of useful power. The remarkable attenuation of the accessed signal between the Points 2 and 3 has occurred. This has resulted in an almost equal decrease in SIR. Within the given logarithmical distance of 6.3 m in the Point 3 the LOS propagated signal has attenuated 13 dB which has resulted in the slightly negative SIR of -0.3 dB. It may be seen that if the path loss of 14 dB were compared to the modelled path loss between the reference distance and the measured distance of 6.3 m it would approximately equal to the modelled value of 16 dB. So, there has not been any exceptional attenuation effect between the measured distance, but the value of SIR has decreased under 0 dB because the aggregated interference has already been at a high level in the beginning of the route (Table 14).

The measured averages of the aggregate power of interference have been presented in Table 15 for Route 2 to show the high level of aggregate interference within the whole route.

Table 15. The measured power of aggregated interference within the Route 2

Distance from AP3, [m]	2.0	4.3	5.9	6.3	8.7	10.2	15.8	17.8	19.5
Aggregate interference, [dBm]	-63.3	-64.4	-64.1	-64.7	-64.3	-64.7	-66.1	-69.1	-68.9

Because the aggregate power interference has been high within the whole Route 2 at the 2.4 GHz band the variation of SIR has easily been affected by the local variation of the useful signal.

The study of SIR variations within the Route 2 at the 5 GHz frequency region has been presented in Figure 32 and Table 16. SIR has dropped dramatically after the location five. Decrease of 37 dB has occurred primarily because of the strong attenuation of the useful signal. As it has been discussed earlier, the aggregated interference has stayed on a high level within the whole Route 2 and because of a rapid attenuation that has occurred at the end of the route SIR has fallen, respectively. The strong attenuation of the useful signal that has occurred in the end of Route 2 which has also been indicated in the propagation model (Figure 30).

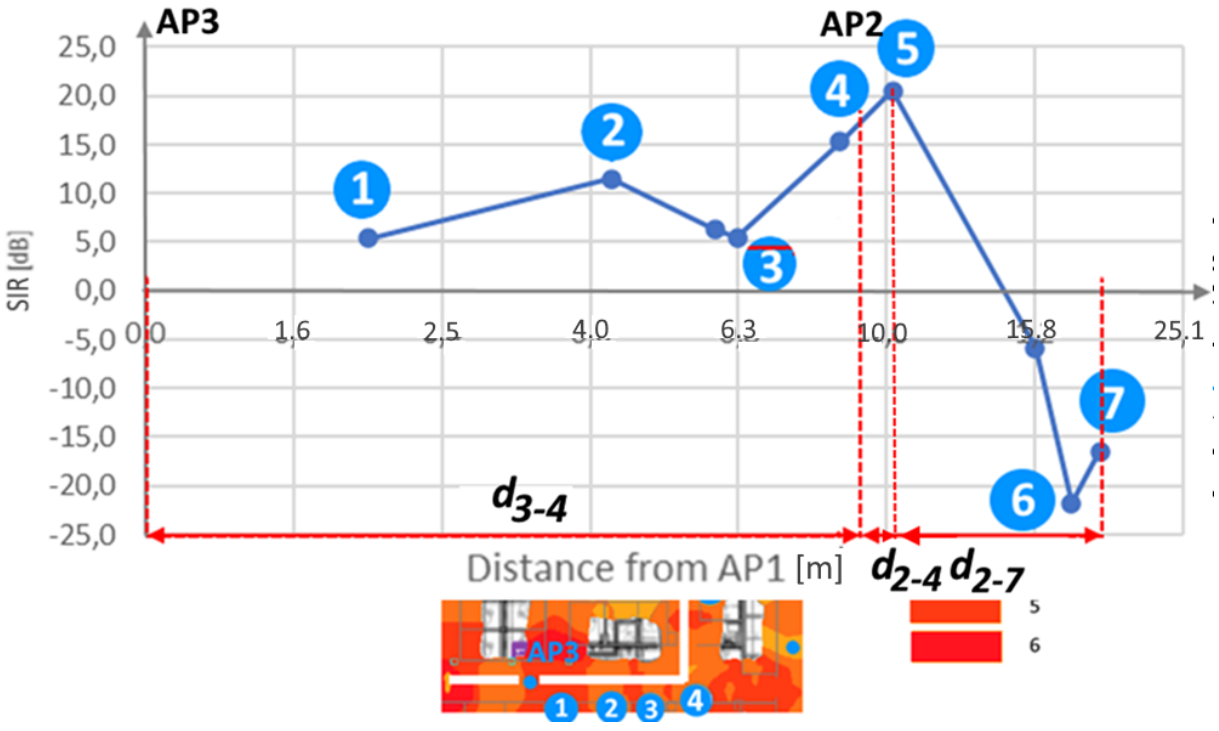

Figure 32. The SIR variations within Route 2 at the 5 GHz band.

Table 16. The piecewise study of Route 2 at the 5 GHz band

Studied distance between the points x_k and x_{k+m}	ID of the accessed AP	$P_r(x_k)$ [dBm]	$\Sigma P_i(x_k)$ [dBm]	SIR(x_k) [dB]	$P_r(x_{k+m})$ [dBm]	$\Sigma P_i(x_{k+m})$ [dBm]	SIR(x_{k+m}) [dB]	ΔP_r [dB]	$\Delta(\Sigma P_i)$ [dB]	ΔSIR [dB]
1 - 2	AP_3	-39	-44	5	-40	-52	12	-1	-8	7
2 - 3	AP_3	-40	-52	12	-43	-48	5	-3	4	-7
3 - 4	AP_2	-43	-48	5	-32	-47	15	11	1	10
4 - 5	AP_2	-32	-47	15	-30	-51	21	2	-4	6
5 - 7	AP_2	-30	-51	21	-56	-39	-17	-26	12	-38

6.4.2 Comparison of the local reasons for SIR variation

The local reasons that have contributed the SIR variations within both routes will be discussed here. It has been based on the piecewise analysis of SIR variations that have been presented in Tables 12, 13, 14 and 16. The cumulative effect of the respective metrics have been calculated by calculating the sum of $\Delta\Sigma P_I$, ΔP_R and ΔSIR that have been measured between the local minimums and maximums. The cumulative effect of the local change of the respective metrics have been presented in Figure 33 for both routes at both frequency bands.

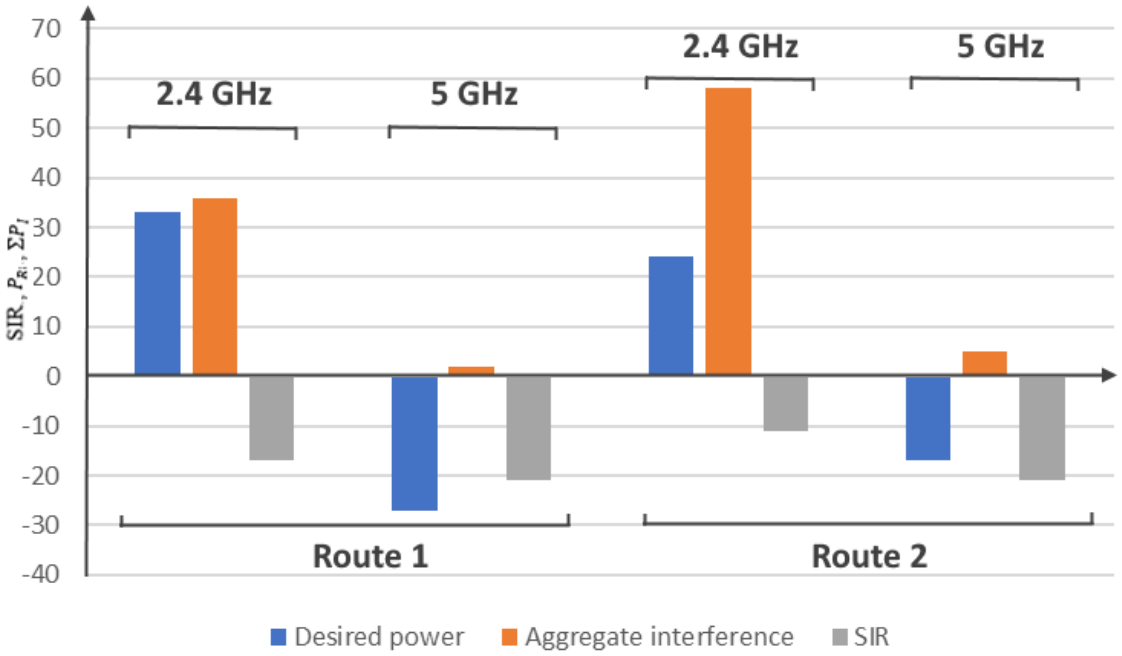

Figure 33. The cumulative effect of the measured local changes over the respective route at both frequency bands.

Based on the figure above, it may be seen that the useful power has been variated less than aggregate power of interference within the Route 1 at both frequency bands. It may also be seen that it has been vice versa within Route 2 where only minor changes of aggregate interference have occurred. Within route 2 there have only been minor changes of aggregate interference which has been in line with the previous discussion based on Table 15. The proportion of the aggregate interference has been remarkably higher within Route 1 compared to Route 2. This may be seen at both frequency bands

and has been caused by different reasons. The higher proportion of aggregate interference has been caused by the access points of the building E at the 2.4 GHz band while it has been contributed by higher signal strength in general at the 5 GHz band.

The analysis of SIR variations within both routes have shown remarkable changes that have been caused by changes of useful power and interference. All local changes within both routes and frequency bands that have led to local maximums and minimums of SIR have been analysed in Figures 29-32 and Tables 12-16 to figure out whether the primary reason for a local SIR variation has been contributed by the change of useful power or aggregate interference between the respective distance within the measured routes.

The measured SIR variations between the consequent maximums and minimums within each route have been studied to figure out whether the reason for variation has been change of signal strength of the useful signal or change of the aggregate power of interference. When the results have been compared between the 2.4 GHz and 5 GHz band, the clear difference may be seen. In two thirds of the studied distances the signal variation of the useful signal has been the primary reason for SIR variation. At the 5 GHz band the primary reason for SIR variation has been the change of aggregated power of interference in the 62% of the studied distances (Figure 34). These findings are in line with the observation that the signal strength has been lower at the 2.4 GHz band than 5 GHz resulting also the higher proportional level of aggregated interference at the 5 GHz band compared to the 2.4 GHz band.

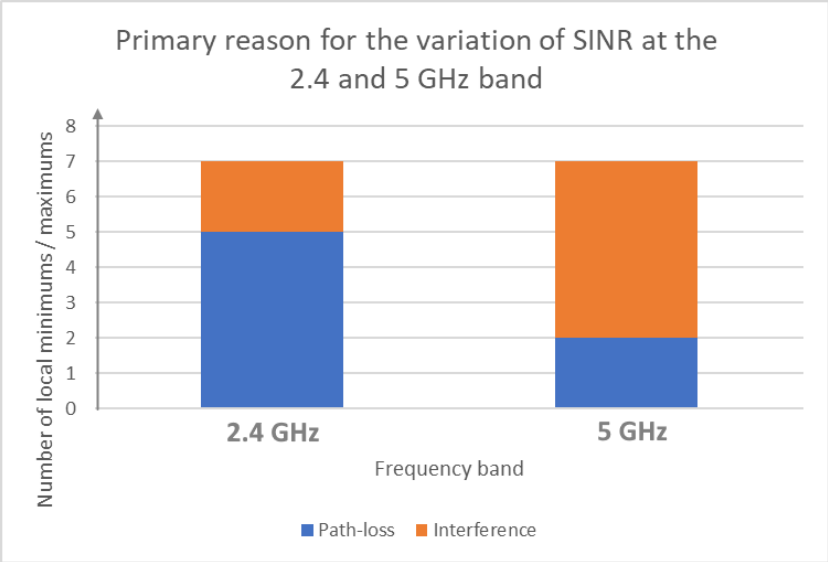

Figure 34. The primary reason for SIR variation at the 2.4 and 5 GHz frequency region in the single locations.

It may be seen that the variations of SIR have been larger on Route 2 than Route 1. They have primarily been caused by the variation of aggregated interference whereas the variations of the path loss have clearly dominated on Route 1.

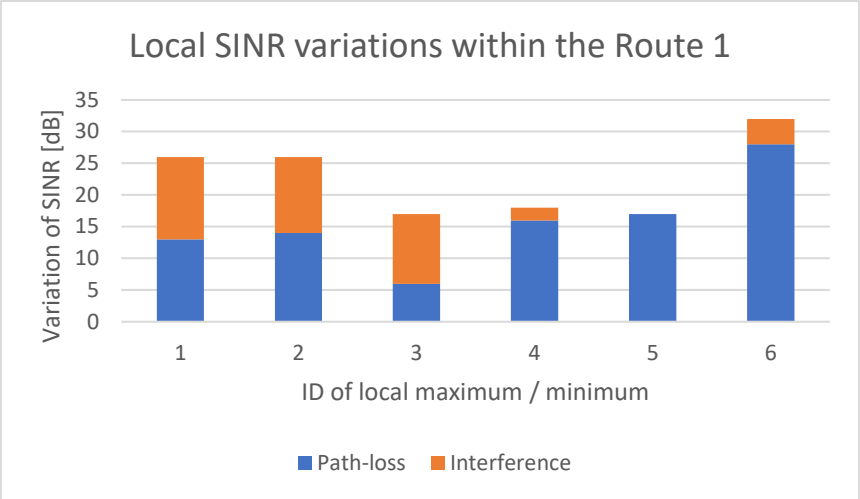

Figure 35. The local variations of SIR within Route 1.

The number of measured ups and downs of SIR variations have been equalled at both frequency regions. Obviously, the portion of the secondary reason for the variation has been the same for both bands because only two metrics have been studied.

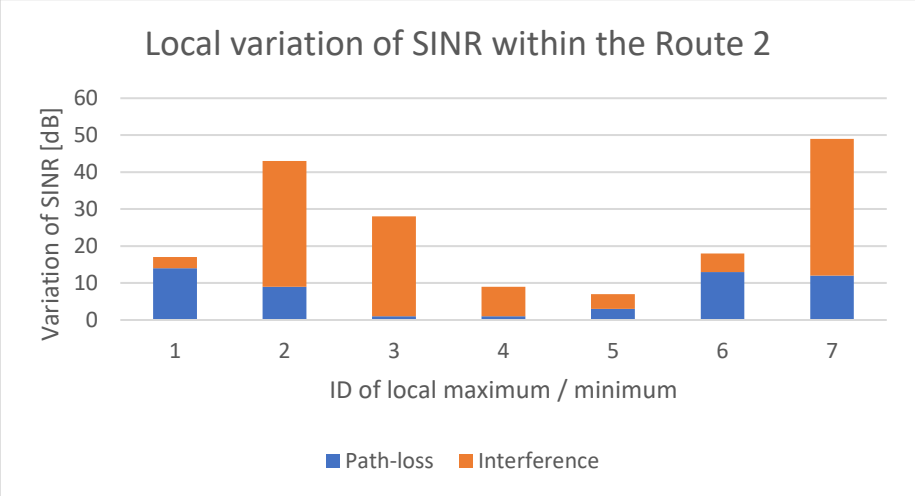

Figure 36. The local variations of SIR within Route 2.

The co-channel interferences in the control ward

The short description of the co-channel interferences that have been presented based on the same measurement campaigns as the earlier discussed interferences during the autumn 2020 has been presented in Figures 37 and 38. The RSSI readings have been measured in the predefined measurement locations within both routes at both frequency regions. The measured values of the respective campaigns have been averaged and the aggregate power of interference has been calculated in any of the measurement locations of both routes. The power of the useful signal has been measured and the averaged results of the measurement campaigns have been used to calculate the SIR as it has been previously discussed. The SIR where only CCI has been included is referred by SIR_{CCI}. The earlier defined noise floor of -97 dBm has been used. The results of the empirically defined SIR_{CCI} at the 2.4 GHz band have been presented in Figures 37 and 38 for Route1 and Route 2, respectively.

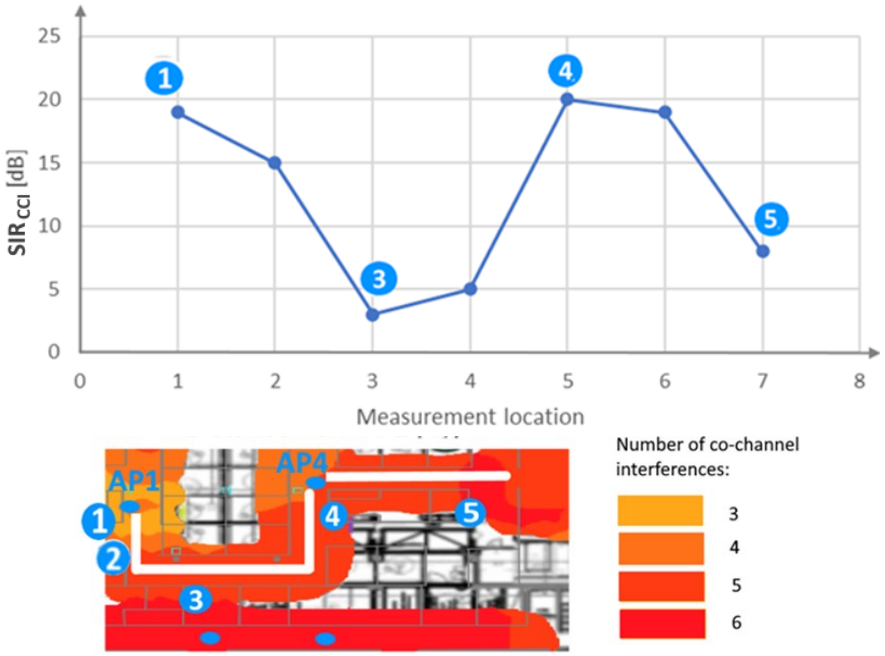

Figure 37 . The measured aggregate interference from the co-channel access points and the number of interfering co-channel access points within the measured route 1.

When the SIR_{CCI} curves of Figures 31 and 32 have been compared to the earlier derived SIR where all received aggregate interference that may be measured by the device that has been used in this work, it may be seen that the shape of the curves has the same symmetry with respect to the accessed AP1, AP2, AP3 and AP4. SIR_{CCI} decreases with increasing distance measured from the accessed access point. The level of the SIR curves has been shifted upwards when only the co-channel interferences have been studied. This has resulted in only one location where the SIR has been under 0 dB (Figures 37 and 38).

It may be seen from Figures 37 and 38 that the number of co-channel interferences that have been presented in the screenshots of the Ekahau channel interference heatmaps indicates coarsely the proportional variation of the measured aggregate interference power that has been measured within the routes. However, the clear correlation between the Channel Interference heatmap of Ekahau and the measured values of co-channel interference may not be seen (Figures 37 and 38).

The aggregate power of the co-channel interference has been measured also at the 5 GHz region. Within Route 1 there have not been indicated other co-channel interferences than the aggregate power of -82 dBm that have been measured in the measurement locations two and three of the Route 1 from the access point on the ground floor. Within Route 2 the aggregate power of the co-channel interferences has not been indicated at the 5 GHz region.

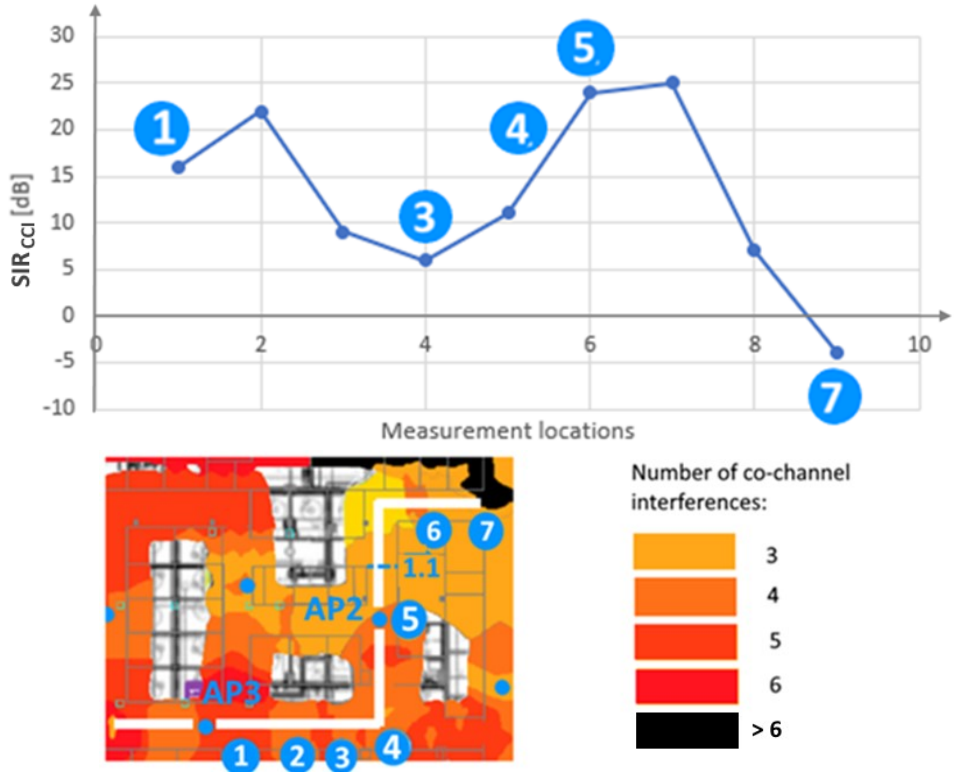

Figure 38. The measured aggregate interference from the co-channel access points and the number of interfering co-channel access points within Route 2.

6.4.3 Effects of the local SIR variations on the data rate

Ekahau measures data rate based on the beacon information of the accessed access point. Data rate in the control ward has been measured simultaneously with the RSSI in the six campaigns during the autumn in the ELI 350 network. It has been measured in the same locations where the aggregate interference has been measured within Route 1 and Route 2. Additionally, similarly with the RSSI measurements the measurement device has measured the data rate continuously also between the measurement locations where the averaged values of data rate have been measured. Because of the strong variation the averaged values of the measured data rates have been calculated based on the lowest value that has been measured in the respective location to figure out the worst-case conditions. The results of the measurements have been presented in Figure 39 and 40.

The standard deviation has been calculated based on the squared error of the measured values in proportion to the averaged values. The standard deviation in the respective location has been variated from 6 to 42 between the locations of the respective route. The strong temporal variation has been indicated. Also, the location-dependent variation has been noticeable so that even if the data rates of 165 Mbps have been measured in the predefined locations of the route the data rates of 50 Mbps may have been indicated within the distance under 1 metre. The results of the measurements have also indicated a strong variation of data rates between the measured values of the respective measurement campaigns. The high temporal variation may be caused by the variation of the network load and should be verified by a different measurement arrangement. There have also been remarkable differences between the measured values of data rates between the locations of the respective routes. Additionally, the averaged data rate has been higher within Route 2 compared to Route 1 where it has also indicated more variation between the respective locations.

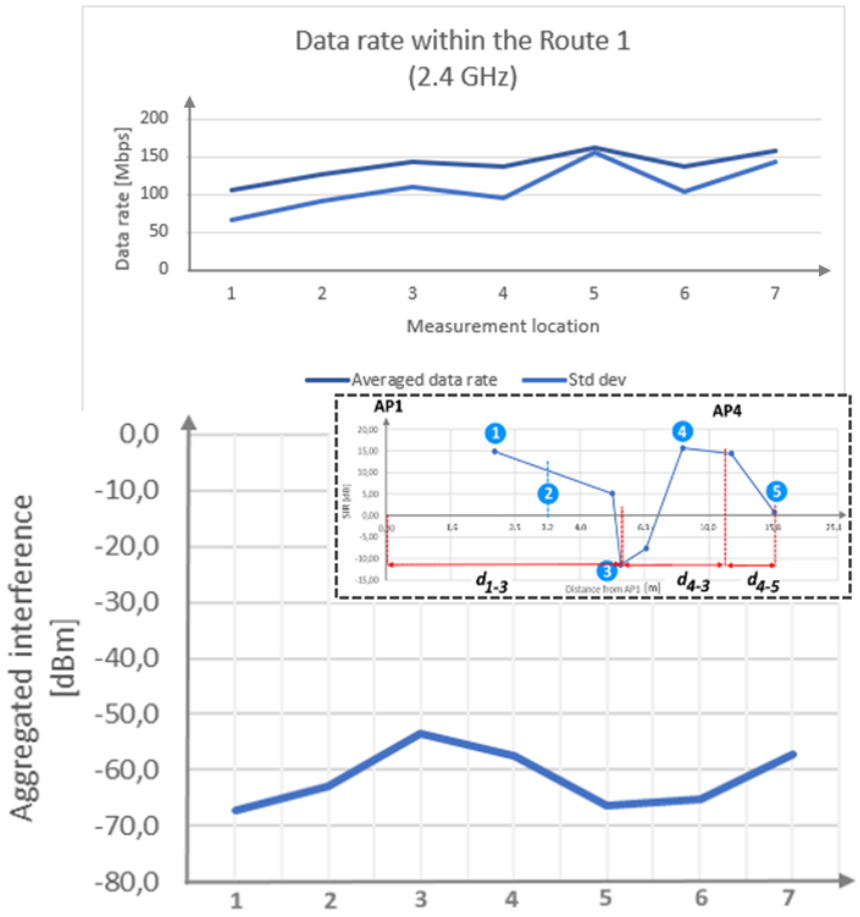

Figure 39. The measured data rates with calculated standard deviation (upper) and the variation of the aggregate power of interference (lower) within Route 1.

Based on the results in Figure 39, the mean value of the measured data rate within Route 1 has been increased with a slightly positive slope from the value of 106 to the value of 162 Mbps. The data rate within Route 2 may be approximated as 165 Mbps with minor deviation of mean value in the beginning and the end of the route. The standard deviation curves of Figures 39 and 40 show clearly that the variation of data rate has been increased with the mean value of measured data rate. It indicates that uncertainty of measured data rate is higher when the measured values are higher. If standard deviation of Route 1 is compared to the measured aggregate interference, it may be seen that uncertainty of results increases with increasing aggregate interference (lower part of Figure 39). Within Route 2 the same has not been indicated. It may be explained by the signal outage that has occurred in the location 7 (Figure 23) which has also resulted in the collapse of SIR regardless of decreased aggregate interference (Figure 31).

The SIR curves of Figures 29 and 31 have been added to Figures 39 and 40 to make it easier to compare measured data rates to SIR curves of the respective routes. The ID of the measurement location that has been shown on the x-axis of both figures corresponds to the respective point of the SIR curves, not the numbered blue circles that refer to Tables 12, 13, 14 and 16. The value of SIR has been dropped in the locations 2, 3, 4 and 7 of Route 1 and in the locations 3, 8 and 9 of Route 2. However, it has not resulted in the decrease of data rate correspondingly which obviously leads to the conclusion that there has not been a clear correlation between measured data rate and variation of SIR (Figures 39 and 40).

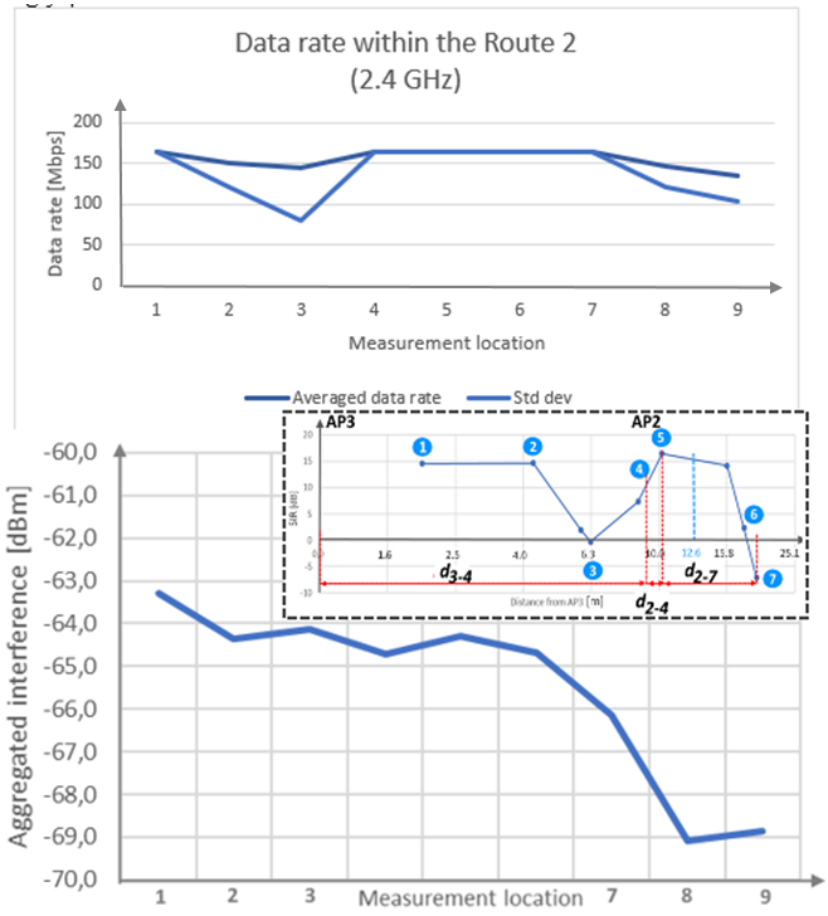

Figure 40. The measured data rates with calculated standard deviation (upper) and the variation of the aggregate power of interference (lower) within Route 2.

When all curves of Figures 39 and 40 have been compared, it may be seen that within the Route 1 SIR and aggregate interference correlates but there cannot be seen any dependence between SIR and data rate. However, within Route 2 the weak correlation between the variation of data rate and SIR can be seen. As it has also been presented in Table 15, the high level of aggregate interference has been maintained until the location 7 which may be seen in Figure 40 too. As it has been discussed above, the signal outage has occurred after the location 7 and it has resulted in the collapse of SIR below 0 dB at the end of the Route 2 although the aggregate interference has simultaneously dropped (Figure 40). There has been a slight decrease in data rate both in location three and after location seven with simultaneous decrease of standard deviation which indicates the weak correlation between variation of data rate and SIR. However, it should be verified by the appropriate measurement arrangement because of uncertainty of data rate measurement and the restrictions of interference measurement of this study.

6.5 Estimating the effects of the SNR variations on the network performance

In Figure 41, the SNR, SINR and SIR_{CCI} that have been measured in the numbered locations of the respective route have been presented along the decibel axis. SNR values have been shown by blue circles. The measured values of SIR have been presented as red circles and SIR_{CCI} have been presented as red squares. The required SNR of the respective MCS has been marked by the yellow vertical lines. The calculated link margins have been added to the MCS thresholds and have been

shown by the blue arrows. The measured values have been compared to the required ones to estimate whether the measured quantity limits the use of the respective MCS (Appendix 2).

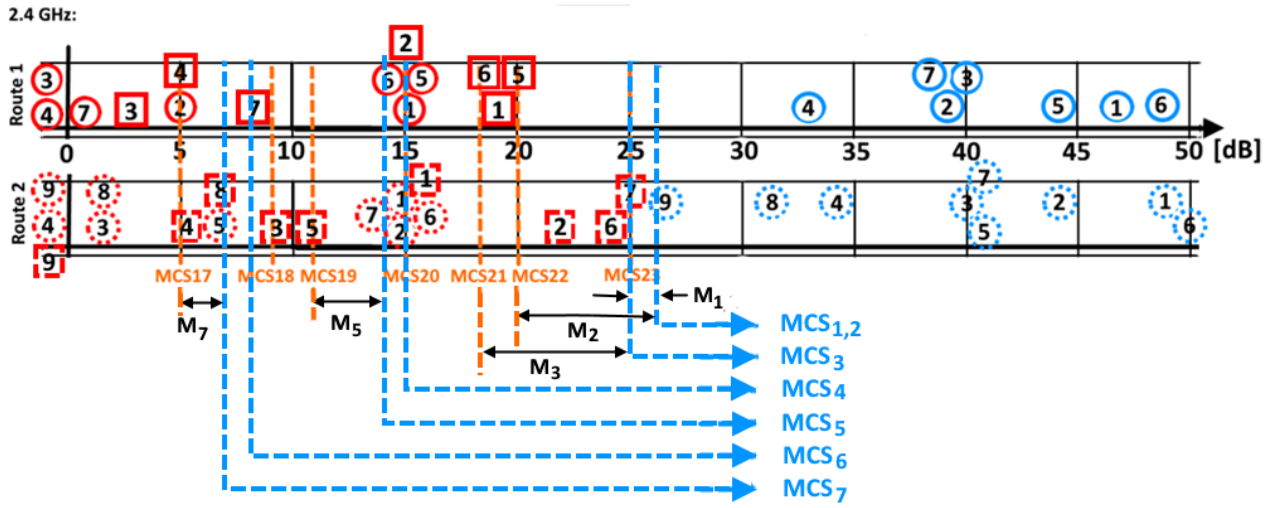

Figure 41. The comparison of the measured values of SIR, SIR_{CCI} and SNR with the SNR_{MCSj} required by the respective MCS_j.

As it was seen from Figure 35, the measured values of SNR have exceeded the SNR requirement of the fastest MCS within both routes which means that the use of fastest MCS has not been limited by the measured values of SNR on either route. However, based on the figure above, it may be seen that none of the measured values of SIR or SIR_{CCI} has exceeded the threshold of SNR that has been required by the fastest MCS. Furthermore, it may be seen that all measured values of SIR and SIR_{CCI} have been spread along the studied SNR axis which may lead to the conclusion that if the measurement criteria of the previously described approach have been appropriate the results indicate that the MCS16 has been the only possible scheme that may have been used resulting the maximum data rate of 21.7 Mbps (Figure 41 and Appendix 2). However, this has not been the case. If the results were compared with the previously discussed measured data rates it may be seen in Figure 39 and Figure 40 that the mean value of data rate has been over 100 Mbps even in the locations where the SIR has been under 0 dB. Specially, on Route 2 there has although been a remarkable variation of data rate although the data rate has been indicated only minor variation within Route 2. So, the indicated weak correlation between the data rate and SIR that has been previously discussed, may obviously not be used as criteria for estimating the effects of the SNR variation on the performance.

If the values of SIR_{CCI} have been compared to the previously discussed values of SIR, the former has indicated 5 dB higher values on average within Route 1 and 5 to 10 dB higher values within the Route 2 (Figure 35). The comparison between the routes may obviously lead to the two findings. First, because SIR_{CCI} has given higher values in proportion to the SIR of the total aggregate power within both routes, the received power except the useful power has dominated the aggregated power that has been expressed by SIR. Secondly, because of previously mentioned differences between the two SIR values, it may be concluded that the contribution of CCI has been higher within Route 2 than Route 1. This has also been indicated earlier when the SIR curves have been derived for both routes (Figure 27-30). However, there has been an exception in the locations three and four of Route 1 where the difference between them has been in the order of 15 dB. This may be explained by the remarkably high received power from the access points in the neighbouring building that locates at the closest to the mentioned locations of Route 1. Consequently, the difference between them two has still remained although the CCI has fallen to the sixth of the value in the locations three compared to the values that have been measured in the previous consecutive location.

When comparing the locations where the equal values have been measured within both routes, it may be seen that in the tolerance of the previously discussed difference of 5 dB on Route 1 and of 5 to 10 dB on Route 2, the equal values have been measured mostly in the same locations within both routes. This refers to the similar shape of the SIR_{CCI} and SIR that may also be seen when the curves Figures 27-30 and Figures 31-32 have been compared.

The co-channel interferences at the 5 GHz band (Figure 36) have only been received from one access point of the ground floor in two locations of Route 1. At the 5 GHz band, the variation of SIR that has been based on all received power except the useful power has been indicated lower variation between the locations of Route 1. The measured values in respective locations of both routes have although indicated even more variation than the values that have been measured at the 2.4 GHz band (Figure 35).

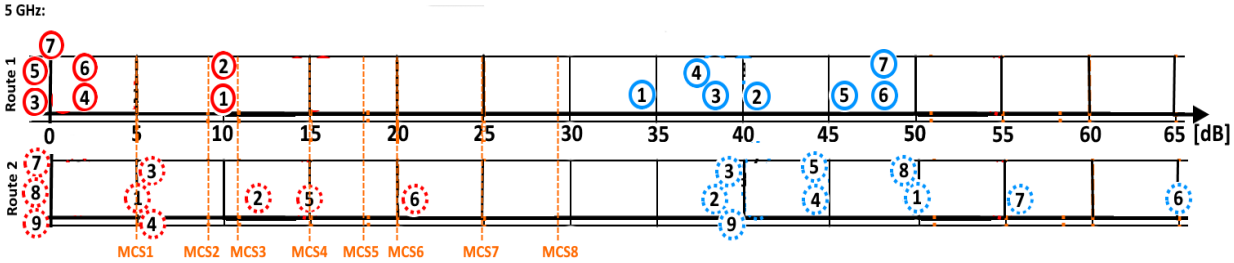

Figure 42. The measured values of SINR and SNR within Route 1 and Route 2 at the 5 GHz frequency band.

None of the measured values of SINR or SIR_{CCI} have exceeded the required SNR of the fastest MCS at either routes or frequency regions. The measured values of SIR have been spread in a way that makes the comparison between them and the required SNR of the respective MCS impossible. The determination of β has neither been possible because the resulting values of SIR have been spread widely.

6.5.1 Calculated link margins

As it may be seen in Figure 41, the link margins U_j have been added to the required SNR threshold of the respective MCS_j. The calculated link margins have been shown in the figure by the blue dashed arrows.

The chosen P_b and the defined shadowing have been considered by the calculated link margins. The link margins have been summed with the required SNR and RSSI that have been defined for each MCS in Appendix 2. The link margins have been calculated in proportion to the required P_b and SNR_{MCSj} yielding the sum of the SNR_{MCSj} and link margin U_j that has been referred as $SNR_{(reqd)j}$ (Figure 43).

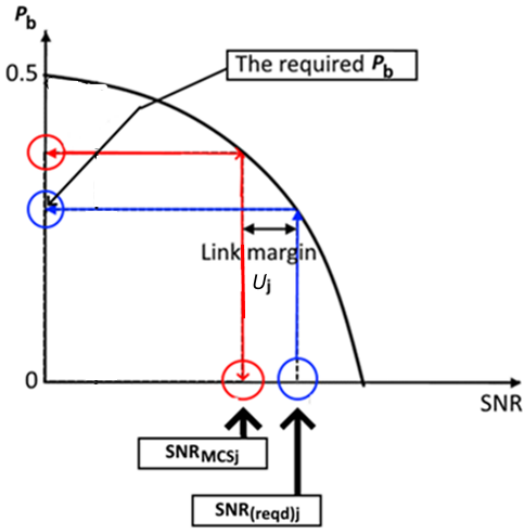

Figure 43. Link margin U_j in respect to the $P_{b(reqd)}$ and SNR_{MCSj}.

The measured values of SNR have been converted to the form of E_b/N_0 using eq. (12) with the given bandwidth of 20 MHz and the maximum data rate $R_{b(MCS)}$ of the respective MCS_j where j = 1 for the highest order of modulation and where j increases with descending order of modulation. So, the MCS of the highest order, MCS_1, of the IEEE 802.11n is MCS23 and for the IEEE 802.11ac it is MCS8 (Tables 16 and 17). The P_b of $1x10^{-2}$ has been chosen as a design requirement and the corresponding $SNR_{(reqd)j}$ has been calculated by iterating eq. (34) using eq. (35-37). The calculated values for IEEE 802.11n have been presented in Table 16 and for IEEE 802.11ac in Table 17.

Table 16. The calculated requirements for the respective MCS of IEEE 802.11n for B = 20 MHz and $P_{b(reqd)} = 1x10^{-2}$

IEEE 802.11n	MCS	$(E_b/N_0)_{MCS}$ [dB]	$R_{b(MCS)}$ [Mbps]	$RSSI_{MCS}$ [dBm]	P_b $1x10^{-2}$	U_j [dB]	$(E_b/N_0)_{(reqd)j}$ [dB]
MCS_1	MCS23	15	217	-64	0.988	0.6	15.6
MCS_2	MCS22	10	195	-65	0.915	6.1	16.1
MCS_3	MCS21	9	173.3	-66	0.988	6.6	15.6
MCS_4	MCS20	7	130	-70	0.949	-0.1	6.9
MCS_5	MCS19	5	86.7	-74	0.390	2.6	7.6
MCS_6	MCS18	3	65	-77	0.816	-0.1	2.9
MCS_7	MCS17	2	43.3	-79	0.346	1.6	3.6
MCS_8	MCS16	2	21.7	-82	0.346	1.6	3.6

The IEEE 802.11n has been used at the 2.4 GHz band with three spatial streams in the control ward. The IEEE 802.11ac has been used in the control ward with 4 spatial streams and the same bandwidth of 20 MHz. The short guard interval has been used in both cases. The required $(E_b/N_0)_{(reqd)j}$ has previously been defined for 802.11n based on the required $(E_b/N_0)_{MCSj}$ and $P_{b(reqd)}$. It has been calculated for the IEEE 802.11ac, respectively. The results of the calculations have been presented in Table 17.

Table 17. The calculated requirements for the respective MCS of IEEE 802.11ac for B = 20 MHz and $P_{b(reqd)} = 1x10^{-2}$

IEEE 802.11ac	MCS	$(E_b/N_0)_{MCSj}$ [dB]	$R_{b(MCS),}$ [Mbps]	$RSSI_{MCSj}$ [dBm]	$P_{b(Mj)}$ $1x10^{-2}$	U_j [dB]	$(E_b/N_0)_{(reqd)j}$ [dB]
MCS_1	MCS8	17	346.7	-59	0.978	26.6	43.6
MCS_2	MCS7	13	288.9	-64	0.871	3.4	16.4
MCS_3	MCS6	9	260	-65	0.953	6.9	15.9
MCS_4	MCS5	5	231.1	-66	0.876	11.4	16.4
MCS_5	MCS4	4	173.3	-70	0.791	0.6	4.6
MCS_6	MCS3	2	115.6	-74	0.884	4.4	6.4
MCS_7	MCS2	2	86.7	-77	0.364	1.6	3.6
MCS_8	MCS1	1	57.8	-79	0.455	2.4	3.4

Because the $P_{b(reqd)}$ has been given as design parameter of the system and the required $(E_b/N_0)_{(reqd)j}$ has additionally been dictated by the $(E_b/N_0)_{MCSj}$, the needed link margin should be added to the yielded value of $(E_b/N_0)_{(reqd)j}$. Based on the earlier discussion and the empirically defined shadowing of the generated path loss models, the typical approximation of indoor shadowing of 10 dB may be used. It may be seen from Figure 42 that if the safety margin of 10 dB were added to the $(E_b/N_0)_{(reqd)j}$ the measured values of SNR would have exceeded the required SNR with the margin but none of the measured values of SINR where the interference has been considered.

6.5.2 Comparison of SIR variation to the defined thresholds

The SIR has been expressed in proportion to the threshold β in eq. (22). As it has been discussed earlier, the threshold β must be exceeded to meet the requirements of the link 1. Based on the calculated link margins of Table 16 and Table 17 the threshold β has been defined as $(E_b/N_0)_{(reqd)j}$ for the respective MCS_j of the used technology (Table 18.) The index j = 1 refers to the fastest MCS_j in a similar way as it has been discussed earlier. The values of SIR that have been defined in the measurement locations have been compared to the values of β (Table 18) and if the threshold has been exceeded, the modulation of respective MCS_j can be used in the location.

Table 18. The threshold β [dB] for respective MCS_j of the used technology

	j = 1	j = 2	j = 3	j = 4	j = 5	j = 6	j = 7	j = 8
IEEE 802.11n	16	16	16	7	8	3	4	4
IEEE 802.11ac	44	16	16	16	5	6	4	4

The results of the comparison between the measured SIR and β have been presented in Figure 44. The index j of the attainable MCS_j has been presented at both frequency bands. The minus sign indicates the situation where β of MCS_8 has not exceeded (Figure 44).

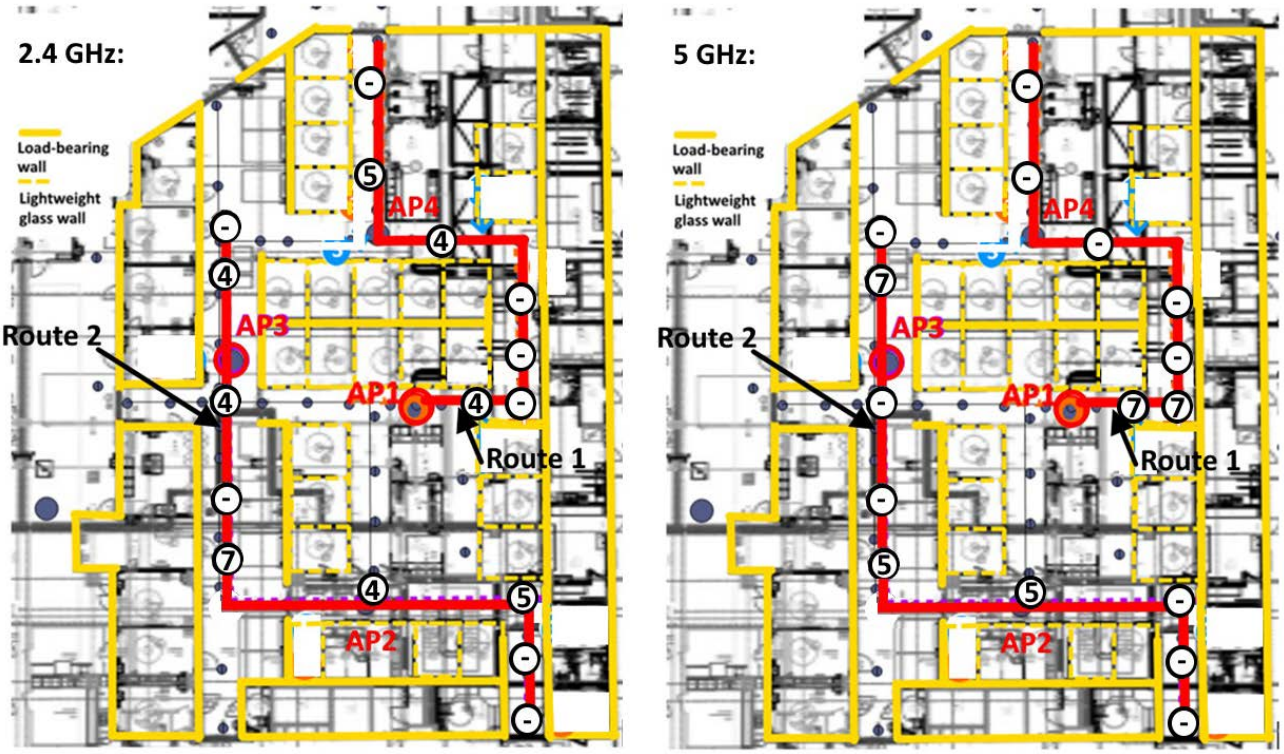

Figure 44. The attainable MCS_j based on the comparison with measured values of SIR described as index j.

The variance of the measured SIR within the respective routes at both frequency bands have been calculated using eq. (13) where β has been replaced by the link margins $(E_b/N_0)_{(reqd)j}$ of Tables 16 - 17. The measured values of SIR have been converted to the form of E_b/N_0 by eq. (25). The standard deviation of the SIR variation in proportion to the β, that has been defined in Table 18, have been presented for the maximum data rates of the MCS_3, MCS_4, MCS_5 and MCS_6 in Figure 45 for 2.4 GHz band and in Figure 39 for the 5 GHz band.

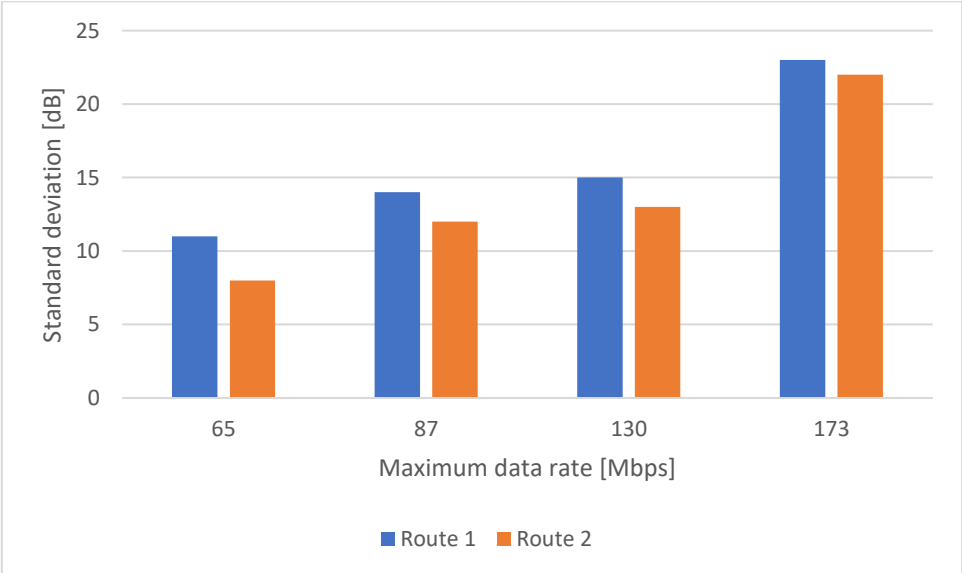

Figure 45. The variation of SIR in proportion to the defined β for the maximum data rate of the respective MCS at the 2.4 GHz frequency band.

It may be seen that SIR has variated more in proportion to the defined β in the lower data rates which has been as assumed. At the 2.4 GHz band, the variation has strongly increased between 130 Mbps and 173 Mbps which may be seen caused by the remarkable increase of $(E_b/N_0)_{(reqd)j}$ (Tables 16). The increase may not be seen at the 5 GHz band because there may neither have been seen the corresponding increase of $(E_b/N_0)_{(reqd)j}$ at the 5 GHz band between the respective MCS. More variation of SIR has been indicated on the Route 1 than the Route 2 at 2.4 frequency band whereas at the 5 GHz band the indicated variation has been higher on the Route 2. However, the difference of variation between the respective routes has been lower at the 5 GHz band.

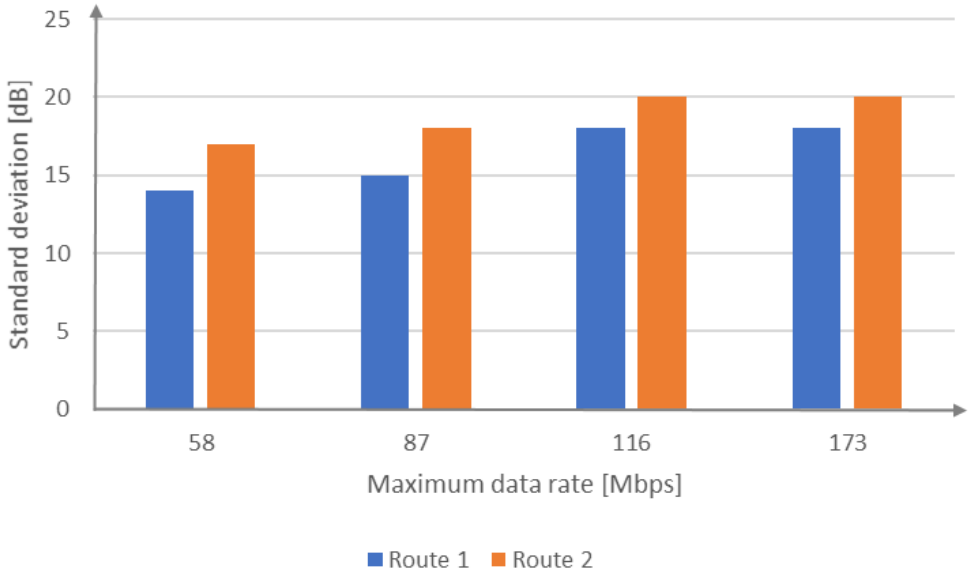

Figure 46. The variation of SIR in proportion to the defined β for the maximum data rate of the respective MCS at the 5 GHz frequency band.

6.5.3 RSSI requirement of the MCS

The shadowing has been used as link margin when the threshold $RSSI_{MCSj}$ of the MCS_j has been considered. The desired signal must exceed the sum of $RSSI_{MCSj}$ and $X_{\sigma k}$ with k = 1 for Route 1 and k = 2 for Route 2 to use the respective MCS_j. The averaged values of desired signal have been described in Figure 47 in respect to the threshold with link margin. As it has been discussed earlier, the shadowing has typically been approximated in the office environment as 10 dB [7]. Based on the measurements that have been discussed in Table 9, the higher values of X_σ must be used outside the measured routes because the fading has been considered as the averaged value of the cumulative shadowing in all directions from the access point AP1. So, the required useful power must be approximately 9 to 14 dB higher than the required threshold in the Control ward (Table 9). The results may not be extended outside the studied room without first measuring the shadowing effect in the studied room.

When the measured useful power has been studied based on Figure 47, the difference in signal strength at the 2.4 GHz (IEEE 802.11n) and 5 GHz (IEEE 802.11ac) that has been discussed earlier, may clearly be seen. The signal strength of the useful signal has been on average -57 dBm within Route 1 and -58 dBm within Route 2 at the 2.4 GHz and at the 5 GHz band -45 dBm and -42 dBm, respectively. The variation of the signal strength that has been measured from the accessed access point has been in the order of 15 dB within Route 1 and 25 dB within Route 2 at both frequency bands. This has also been indicated by the earlier generated propagation models.

The measured values of P_r have exceeded the required minimum $RSSI_{MCS1}$ of the fastest MCS_1 within Route 1 at the 2.4 GHz band except the locations three and four. When the shadowing $X_{\sigma 1}$ of 6.3 dB (Table 10) for the Route 1 has been considered, the threshold of $RSSI_{MCS1}$ has barely

exceeded in the locations two and seven. So, the threshold has been safely exceeded only in the locations one, five and six of the Route 1 at the 2.4 GHz band. When the same analysis has been carried out for Route 2 of the same frequency band, it may be seen that the threshold of the fastest MCS_1 has been safely exceeded in the locations one, two, six and seven which refers to the locations in the proximity of the accessed access points as it has been in the respective locations of Route 1 too. The thresholds of the MCS_2, MCS_3 and MCS_4 are within the fade margin from the locations three and four of both routes, which means that MCS might have been fallen even to the level of MCS_5 in the locations three and four resulting the maximum data speed of 86.7 Mbps in these locations. As it has been discussed earlier, there has been a major variation in the data rates in these locations with the minimum of 43 Mbps which is in line with the previously discussed finding.

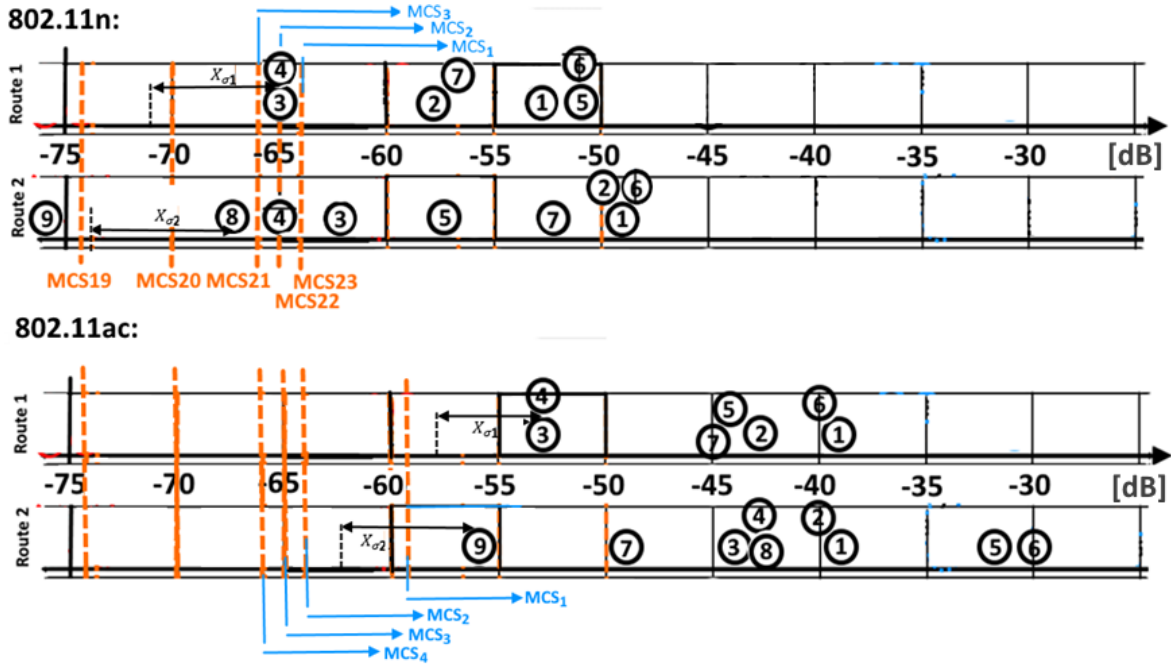

Figure 47. The signal strength of useful signal with shadowing in the measurement locations of Route 1 and Route 2 in respect to the required signal strength $RSSI_{MCS}$ of the respective technology.

The averaged useful signal has been 14 dB stronger at the 5 GHz band than the 2.4 GHz band, as it has been discussed earlier. This may also be seen in Figure 47. The threshold of MCS20 has not been exceeded only in the location nine of Route 2 with the shadowing $X_{\sigma 2}$ of 5.8 dB (Figure 47).

6.6 Coexistence study by frequency spectrum and spectrogram

The coexistence has been studied by the frequency spectrums that have been measured in the chosen locations within the routes and outside them. The locations within the routes have been chosen if SINR has been under 0 dB in the location. These locations have been chosen because the worst-case scenario of the coexistence has been tried to figure out. Secondly, the locations outside the routes have been chosen if there have been detected an exceptional amount of energy from the sources outside the network in the given location. The spectrogram of Ekahau Pro has been used for finding out the locations because the degree of the channel utilization may roughly be estimated by it.

The frequency spectrum has been measured in two campaigns that have been carried out in September and November. These campaigns have been part of the six campaigns that have been described earlier when the arrangements of interference measurement have been described. The frequency spectrum has been measured on Friday that has been assumed to be the busiest weekday in the emergency department and thus in the control ward too. The Covid-19 pandemic has affected

the operation of the hospital and in a way that the number of patients has been lower compared to the normal conditions, as it has been discussed earlier. This has obviously resulted in lower utilization of the network too. Although, in these circumstances the airtime utilization and the channel occupancy have not been measured the channel utilization has been considered by searching for the interferences with the help of spectrogram as it has been described earlier. On the other hand, the measurement device of this work cannot be used for the measurement of the channel power which causes some limitations. The frequency spectrum and spectrogram that have been measured in one of the studied locations will be presented as an example of how the locations have been determined and the frequency spectrum together with spectrogram has been used in the study of the interferences.

Ekahau Pro shows the frequency spectrum with span of the whole frequency spectrum of the respective frequency band. Because only the channel ID has been shown on the x-axis the frequency scale has been added to the screenshots of the spectrum (Figure 48).

Figure 48. The graphic determination of the frequency.

The given values in GHz below the axis refer to the centre frequencies of the respective channels 1, 6 and 11. The scale above the axis has been expressed in MHz and it has been divided every 5 MHz because the bandwidth of the channel is 20 MHz and the difference between the consecutive orthogonal channel bandwidths is 5 MHz. The bandwidth of received WLAN signal has been marked by the rectangles of different colours so that each colour represents the specific access point. The channels 1 and 11 have been used by the access points of building J2 and the channel 6 has been used by the network of the neighbouring building. In the location where spectrum above has been measured, WLAN channels 1, 6, 11 and the WLAN signal of the same bandwidth on the channel 10 have been received. The centre frequencies of the channels, 2.412 GHz, 2.437 GHz and 2.462 GHz may be read from the GHz-scale of x-axis. As an example, the lower and upper frequencies of channel bandwidth of channel six have been determined using the GHz- and MHz-scale of x-axis (Figure 48). The lower frequency of 20 MHz bandwidth may be determined by summing up the centre frequency of WLAN channel below the f_L and the value of MHz scale in the point where f_L exists. So, the lower frequency, f_L = 2.412 GHz + 15 MHz. The upper frequency f_U may be determined correspondingly by adding the centre frequency of 2.437 GHz and 10 MHz span on MHz-axis. The resulted lower and upper frequencies of the channel 6 are f_L = 2427 MHz and f_U = 2447 MHz, respectively. The frequencies of other signals have been determined in a similar way (Figure 48).

In Ekahau Pro the duration of the time window where the spectrum has been displayed may be chosen between the minimum of 1 s and maximum of 120 s. This means that the spectrum has been

displayed before the time spot and after it by the half of the chosen value of duration. So, if the value of 120 has been chosen the displayed signals has been received 60 s before the time spot and 60 s after it have been displayed.

The chosen time window has also been shown by dashed horizontal lines in the spectrogram that has been presented in Figure 49. The numbers of respective channels have been presented on the x-axis and the time spot when the displayed frequency spectrum has been measured may be read on the y-axis where the blue horizontal line is located. The colours (red, yellow, green) in the diagram describes the utilization of the frequency in descending order. The spectrogram shows roughly the channel, and the frequency of the signal must be determined in a way that have been described above.

The screenshot of Figure 49 describes the received signals in the same location where the frequency spectrum of the figure above has been measured at the same moment. The short red line in the channel four refers to the received signal that has been described as the first of two narrow band power peaks in the frequency spectrum above. The time spot of the measurement has been shown by the blue horizontal line in the screenshot of spectrogram (Figure 49). The measurement has been begun in the location at 17:04:30, and the spectrum of Figure 48 has been measured at the time spot of 1:30 from the time of beginning. It may be seen from the spectrogram that the measured amount of traffic has been remarkably higher on the frequency of 2426 MHz compared to the other frequencies of the band although the same signal in the frequency spectrum has appeared green. This has been caused by the variation of the channel utilization that happens to be low at the time spot of the measurement. This may be seen from the spectrogram where the blue line shows the time spot of the displayed frequency spectrum. The short green line may be seen on channel four at the moment that has been shown by the blue line (Figure 49).

As it may be seen in Figure 48, two narrow band power peaks have been received and their frequencies have been determined by the scale of the figure above as of 2426 MHz and 2439 MHz, respectively. The former of the peaks have been received everywhere on the first floor of J2. The power level of the peak has been varied between -40 and -50 dBm. The peak appears on the frequency of 2426 MHz that is the pilot frequency of Bluetooth [43]. Another power peak has been detected in the frequency of 2439 MHz as it may be seen in Figure 48. It will be discussed later because the corresponding power peak is shown in Figure 50 too.

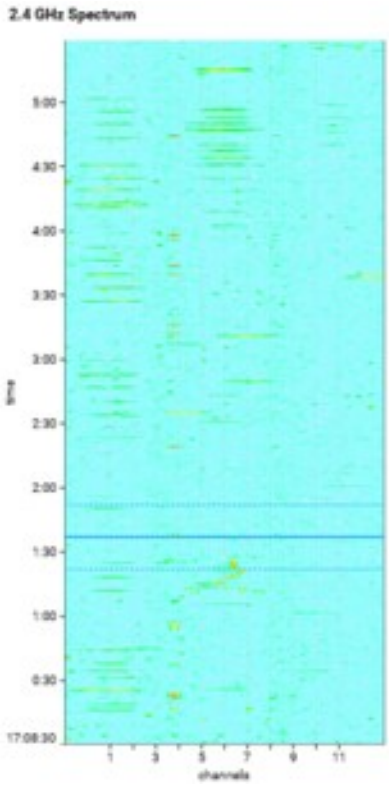

Figure 49. The screenshot of the spectrogram.

The wireless devices that use the same ISM frequencies than IEEE 802.11 may use other wireless technologies like IEEE 802.15.1 and IEEE 802.15.4 or they operate independently using the same IEEE 802.11 technology that is used by the network (Hotspots). There are also other possible sources of interference that use the same ISM frequencies as microwave ovens or wireless phones. In this work the coexistence has been studied only to figure out the examples of interferers that have been received in the control ward and that potentially may be harmful because they operate at the same frequency band.

6.6.1 Frequency spectrum in the locations with low SIR

Two measurement locations have been chosen in the control ward because of low values of measured SIR. The SIR under 0 dB have been measured in the chosen locations in the control ward. The screenshots of the frequency spectrum in the location 2 of Route 2 have been presented in Figure 50. As it has been discussed earlier, SIR in the locations has been -7 dB. The upper screenshot has been taken from the frequency spectrum that has been measured in September and the spectrum below it has been measured in November in the same location.

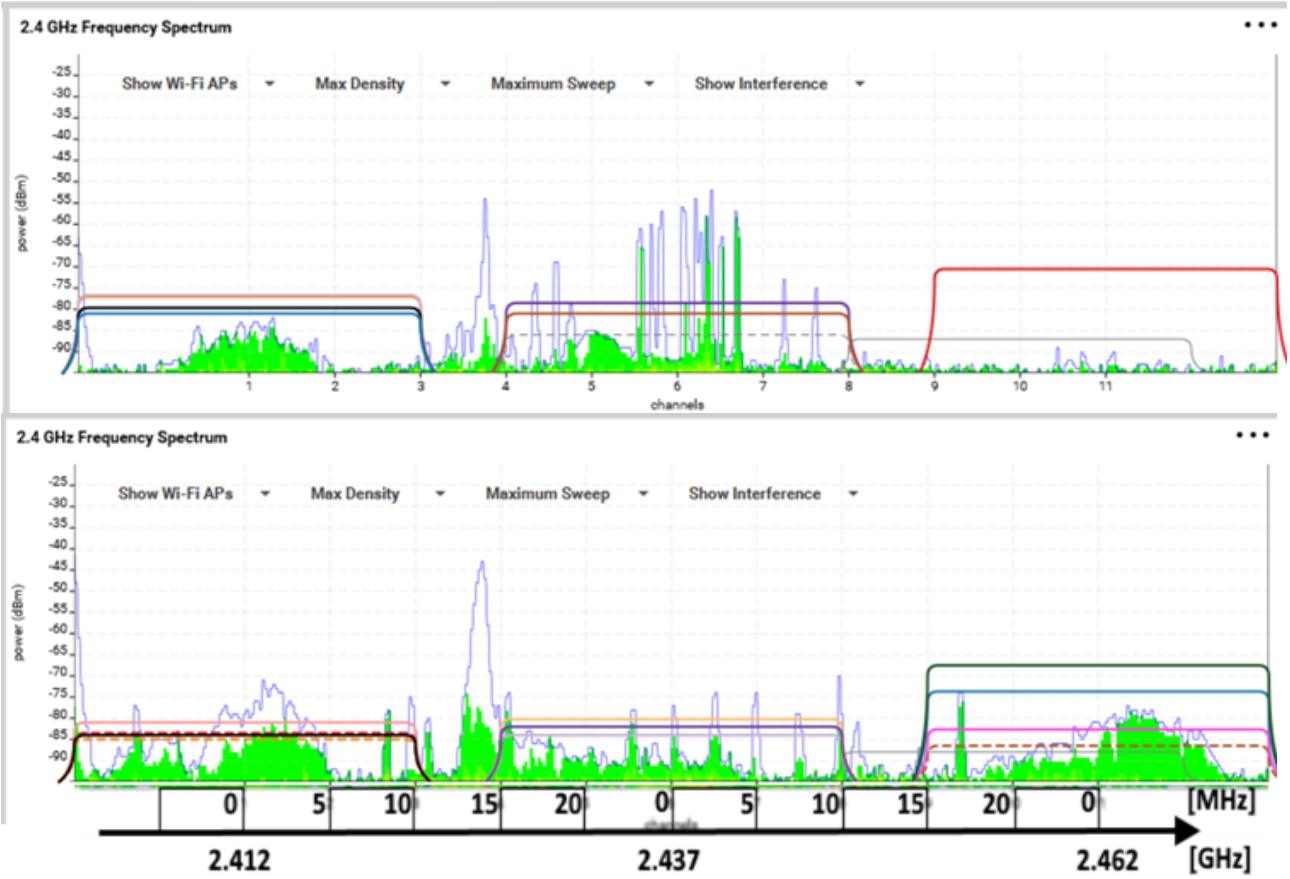

Figure 50. The frequency spectrums in location 2 that have been measured in September (upper) and November (lower).

As it may be seen from Figure 50, the channels 1, 6 and 11 have been used. The number of received co-channel access points has been increased from Sept. to Nov. on channel 11 but the signal strength of the strongest access point has not been changed on the respective channel.

The Figure 48, where the determination of the frequency has been described presents the measured frequency spectrum in the same location 2 that has been presented in the figure above, but the duration of time window has been 60 s while it has been 120 s in Figure 50. The comparison between these two leads to the notice that the power peak in 2426 MHz has remained but the second peak has been changed to a series of peaks that have been superimposed onto the second peak of Figure 48 forming a triangular envelope of the peaks. If the frequency spectrums of Figure 50 are compared with each other, it may be seen that the second peak has disappeared in the lower spectrum that has been measured in November and the flat sequence of power peaks of -75 dBm has appeared instead. Because the series of power peaks indicates the frequency-hopping signal, the frequencies appear on the range of 2400 to 2480 MHz and the bandwidth of the power peaks may roughly be estimated as 1 MHz, the signal obviously has come from a Bluetooth source. Furthermore, because the signal has already been received in September and has been detected in November as well, but the power level of the peaks has been higher in September the Bluetooth transmitter obviously has been in the neighbourhood of the measurement location 2 but has moved farther.

The second power peak that has been received in the same location and has also been shown in Figure 48 has been received on the frequency of 2439 MHz as it has been discussed earlier. The Zigbee uses the frequency of 2440 and the shape of the signal in Figure 48 resembles the mountain-shape of the Zigbee signal with bandwidth of 2 MHz. This may indicate the signal of the Zigbee device. The signal has not been received in the measurement that has been carried out in November.

It may be seen from Figure 50 that there has been a frequency-hopping signal that has been summed with other signals between the frequencies of 2427 and 2457 MHz. The Bluetooth technology uses the frequency range of 2400 to 2480 MHz and the technology is widely used in medical devices. The lower frequency spectrum of Figure 51 has been measured in the same location in November with the same time duration setting as the upper frequency spectrum that has been measured in September. From the figure below it may be seen that there has been a frequency-hopping signal in the same frequency range that has been described above. The 20 dB-bandwidth has been determined from the lower spectrum of Figure 51 as 1 MHz that is the bandwidth of Bluetooth technology [44].

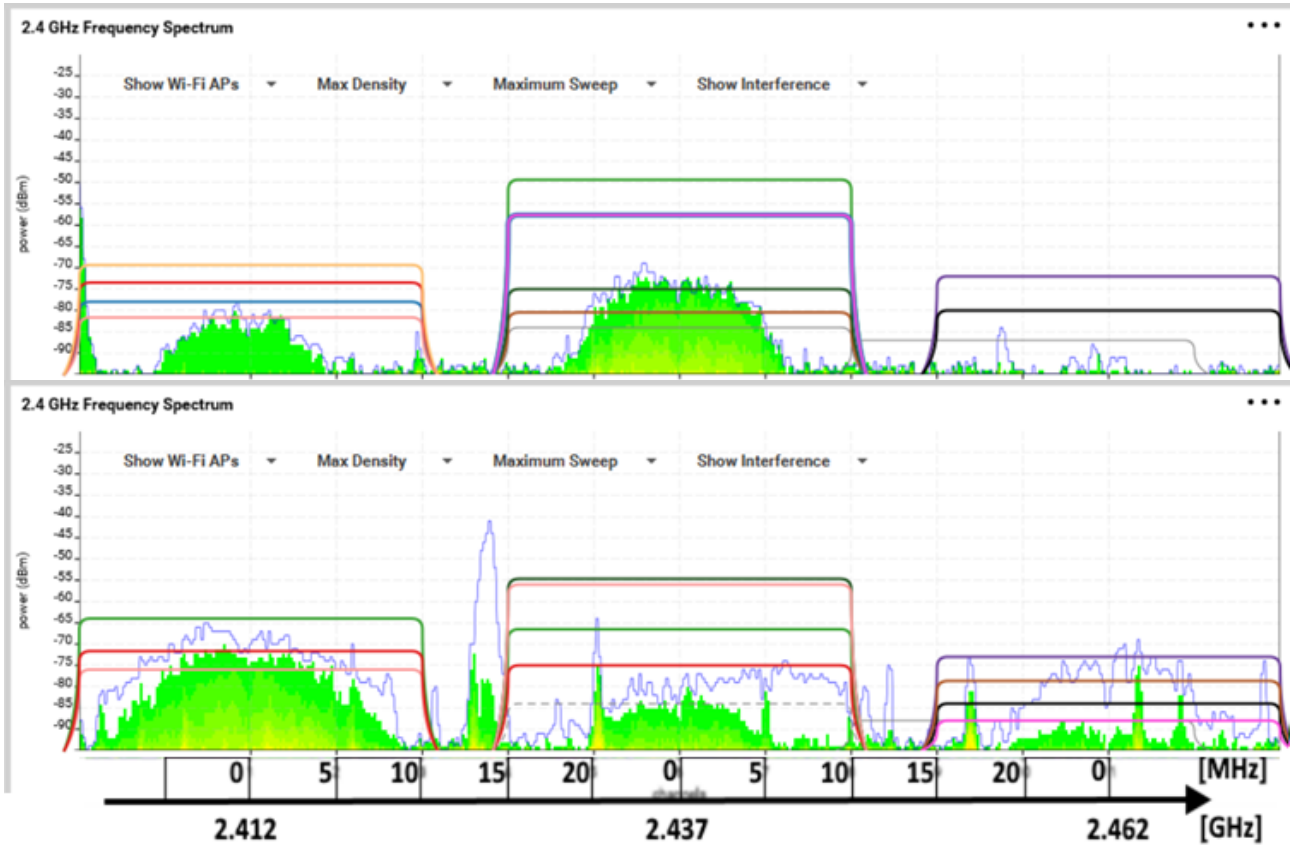

Figure 51. The frequency spectrum in the location 13.

The hotspots have also been received in the control ward. In the location 8 there has been a signal from the IEEE 802.11 source on the channel 7 as it may be seen from Figure 52. The signal has a typical shape of OFDM that has been used in the IEEE 802.11g/n/ac technologies. The location 8 is close to the medical examination rooms along the side of the control ward where hotspots have been received during the campaigns. The frequency of 2402 MHz is another pilot frequency of Bluetooth[43]. The pilot signal may be seen partly overlapped with the bandwidth of channel 1 in the upper frequency spectrum.

The shape of the waveform and side lobes have clearly been detected because at that moment there have not been other signals at the same frequency (Figure 52). The received power of the signal has been -78 dBm and the bandwidth has been about 20 MHz with a centre frequency of 2.442 GHz.

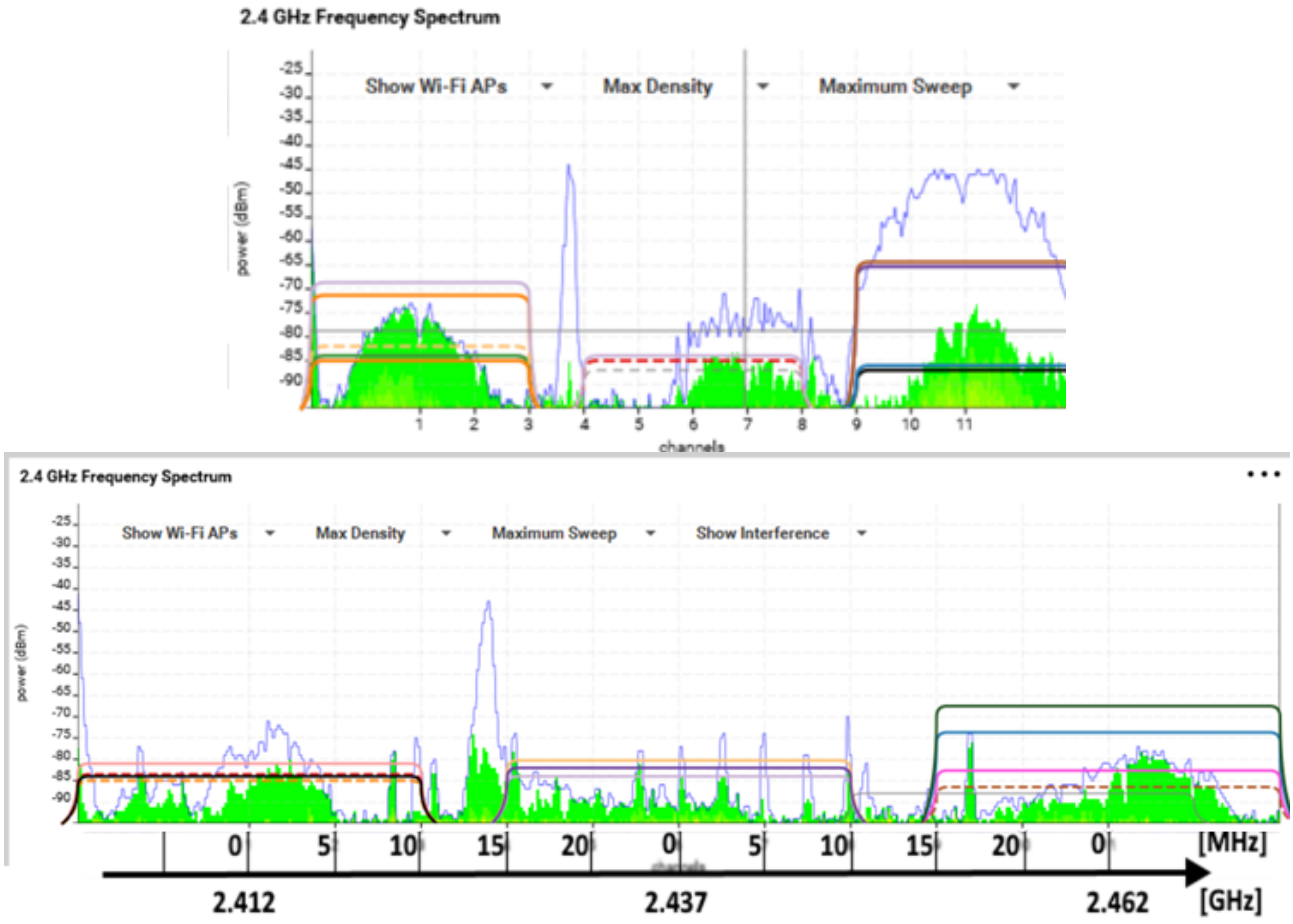

Figure 52. The frequency spectrum in the location 8.

As it has been discussed earlier, only orthogonal channels have been used by the channel allocation automatics of the WLAN of J2. This may be seen from Figure 53 where the screenshot of spectrum view has been presented for 5 GHz. However, the power from access points in the channel 6 has been widely received at the 2.4 GHz band from the Meru network that has been used in the neighbouring building E. The channel allocation of the Cisco system of the building J2 at 2.4 GHz band uses only the orthogonal channels 1 and 11.

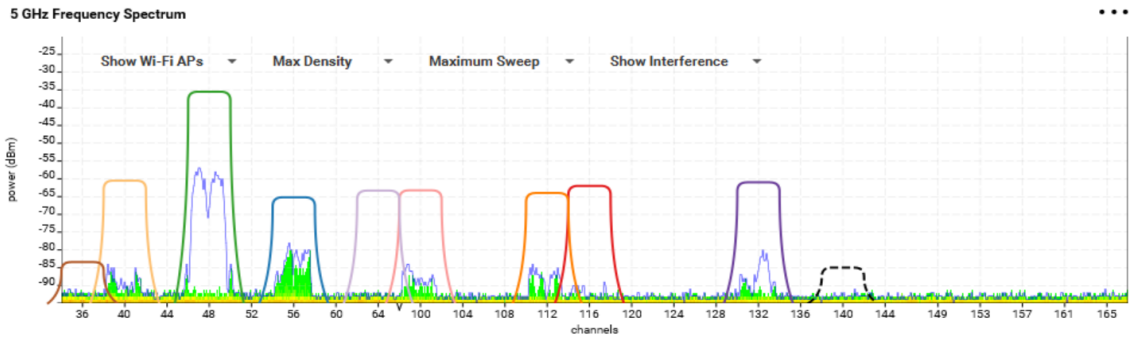

Figure 53. The spectrum of the 5 GHz band in the control ward.

There have been remarkably fewer interfering transmitters at the 5 GHz frequency region compared to the 2.4 GHz region which may also be seen in Figure 53. The use of various wireless technologies causes 2.4 GHz band the most susceptible to interferences, especially in the hospital environment [6].

6.7 Study of rapid SNR variations

Based on the measurement campaigns in September, October, November, and February the indications of rapid variations of SNR in the order of 30 to 40 dB have been measured on all three floors. The rapid variation of SNR has been defined as a 20 dB change of measured SNR between the locations within the maximum distance of 2 metres. The measurement has been carried out as two single site-survey in the department of the abdominal diseases on the ground floor, as a few site-surveys in the emergency department on the first floor and as two site-surveys in the Children's ward on the third floor. The survey has been done by walking slowly without stops. Other ways the measurement arrangement has been the same that has been described earlier. Additionally, the rapid changes of SNR have been indicated in the control ward in three locations where they have been studied based on the six measurement campaigns that have been discussed earlier. Because there has been some variation between the results of the measurement campaigns, only the locations where changes have been indicated in all the studied campaigns have been chosen to analyse. It is also worth mentioning that because the results from the ground floor and the third floor have been based on only two campaigns the accuracy of the results is not as high as it is in the case of the Control ward.

The changes have been studied firstly by Ekahau SNR heatmap and heatmap that presents the borders of the area where the respective access point has been associated (Figure 54). The Figure below describes the changes of SNR and roaming lines in the part of the Children's ward on the third floor near the measurement locations 1 to 4 of Table 19c.

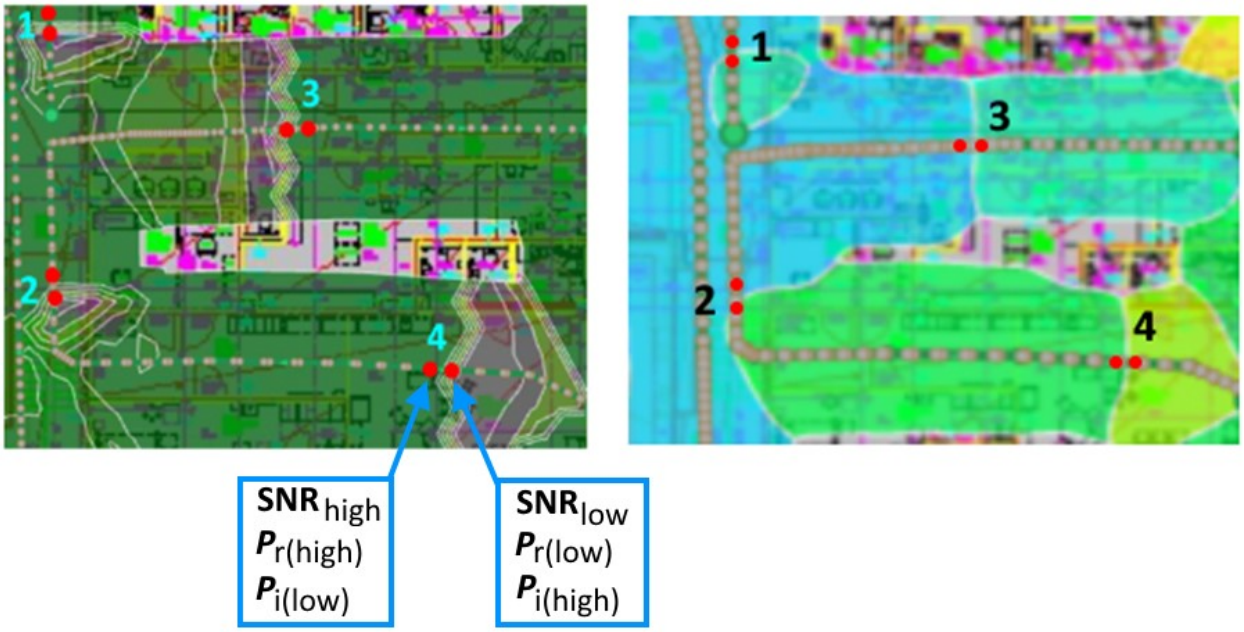

Figure 54. Measured rapid fall of SNR (left) and roaming lines (right) in the measurement locations 1 to 4 on the third floor and the measured metrics.

As it may be seen, the roaming has been occurred between the two points in pairs where one represents the minimum of the measured SNR and the other maximum. They have been referred as SNR_{low} and SNR_{high}, respectively. The walking direction has been towards the sharper edge of the low-SNR area. Based on Figure 54, it may be seen that SNR has gradually been decreased in the direction of walking from the value that has been slightly variated in the different parts of the measured areal but may be kept almost constant over the distances up to 5 metres on averaged. The SNR has gradually been reached the local minimum in the red point as it has previously been discussed. After the minimum, the roaming has been occurred and SNR has increased rapidly to the

measured maximum in the other red point. In this study, only the locations where the distance between the minimum and maximum has been under 2 metres have been studied.

Secondly, the maximums and minimums of SNR have been measured in all locations where the SNR has been decreased 20 dB or more within the distance under 2 metres and the results have been presented in Table 19a-c. The results have been sorted by the floor and ID of the measurement location that has been shown on the first row of Tables 19a – 19c.

Table 19a. The rapid changes of SNR on the Ground floor, [dB]

Location ID:	1	2	3	4	5	6	7	Average
SNR_{high}	57	53	42	36	52	73	55	53
SNR_{low}	25	28	22	14	30	18	19	22
Difference	32	25	20	22	22	55	36	30

Table 19b. The rapid changes of SNR on the first floor, [dB]

Location ID:	1	2	3	4	5	6	7	8	9	10	Average
SNR_{high}	61	54	45	48	46	59	52	71	57	47	54
SNR_{low}	25	18	21	16	17	25	23	25	25	23	22
Difference	36	36	24	32	29	34	29	46	32	24	32

Table 19c. The rapid changes of SNR on the third floor, [dB]

Location ID:	1	2	3	4	5	6	7	8	9	10	11	12	Average
SNR_{high}	44	50	64	52	53	49	42	40	43	59	52	56	50
SNR_{low}	21	30	18	17	17	19	22	12	18	17	16	21	19
Difference	23	20	46	37	35	36	20	28	25	46	36	34	32

As it may be seen from the tables above, there has not been remarkable variation in the averaged maximums and minimums between the floors. The number of SNR drops per floor have slightly variated, partly because the areal of the measured area has been variated between the floors. This in mind, it may although be concluded that there have been more SNR drops on the third floor than on the other floors.

6.7.1 Rapid SNR falls in the Children's ward

The fallen SNR has been analysed in the numbered locations of Figure 55. The accessed signal has been defined as the useful signal, P_r. P_r has been measured in the location where the minimum and maximum of SNR has been measured and the values of P_r have been referred as $P_{r(high)}$ and $P_{r(low)}$, respectively. The received noise power has been measured in all locations and it has been averaged as -91 dBm that has been defined as a value of noise floor.

The changes of P_r and P_i have been studied over the measured difference of SNR to figure out the primary reason for the change of SNR. If only the quantity of the change has been considered, it may be seen that the sum of the variation of P_r and variation of P_i have been equalled to the variation of SIR except in the location two. Because there has been a remarkable increase of SNR in the mentioned direction, the SIR should also have been increased which it has been done except the location two. The exception may be explained by the potential measurement error. So, the variation of useful power and the aggregate interference should have resulted the positive change also in SIR of the respective location. The difference between the $P_{r(high)}$ and $P_{r(low)}$ that has been referred by the variation of P_r in Table 20 has approximately been equalled to the difference between the SNR_{high} and SNR_{low}. The

slight difference between the values may have been resulted from the inaccuracy of the measurements because the results have been based only on the two site-surveys. The minor inaccuracy may also have been explained by the local change of noise power that may have been occurred in the two locations.

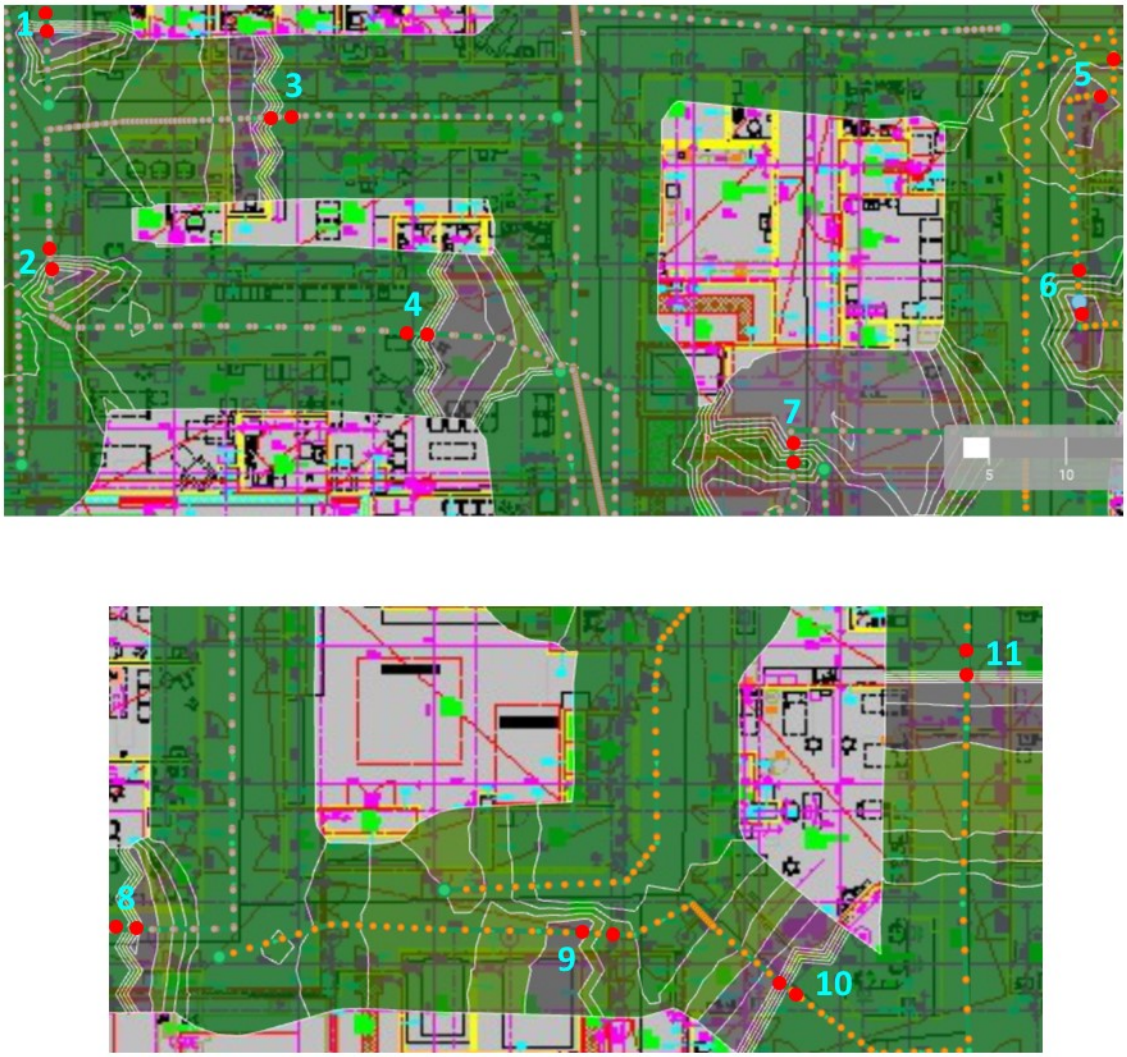

Figure 55. SNR variation in the Children's department of the third floor.

The results of the measured pairs of the values that have been presented in Figure 55 have been presented in Table 20. The average of the discussed SNR changes has been 34 dB and the change of the desired signal power has been 34 dBm on average. Additionally, based on the results of Table 20, it may be concluded that the averaged SIR variation of 38 dB has almost been equalled to the averaged variation of SNR.

Table 20. The results of the measurements in the Children's ward

Location ID	SNR_{high} [dB]	SNR_{low} [dB]	Change of SNR	$P_{r(high)}$ [dBm]	$P_{r(low)}$ [dBm]	Change of P_r [dBm	Change of P_i [dBm]	Change of SIR [dB]
1	62	18	44	-29	-73	44	-20	64
2	51	15	36	-40	-76	36	-14	-22
3	53	17	36	-38	-74	36	-9	-27
4	47	20	27	-44	-71	27	-20	47
6	42	23	20	-49	-68	19	-8	27
7	36	12	28	-55	-79	24	-9	33
8	56	21	35	-38	-71	33	-2	35
10	52	16	36	-41	-76	36	-9	-27
11	59	17	42	-28	-77	49	-22	71
Average:	**51**	**18**	**34**	**-40**	**-74**	**34**	**-13**	**22**

After all, it may be seen based on Table 20 that the major contribution to the positive change of SIR in the direction of the positive SNR change has primarily been caused by the increase of P_r. The decrease of aggregate power of interference has had only the minor effect on the change of SIR in any locations. Furthermore, averaged change of P_r has been 34 dBm that is over hundredfold compared to the change of aggregate interference (Table 20).

6.7.2 Rapid SNR falls in the Control ward

As it has been discussed earlier, the SNR and SIR have been determined in the predefined locations within the two routes in the Control ward. The rapid changes that have also been indicated in the Control ward are to be studied next.

All SNR variations that have been indicated in the six measurement campaigns where they have been exceeded the minimum of 20 dB within the distance below 1.5 metres have been studied regardless of whether they have been located within the routes or not. The distance of 1.5 m has been chosen because of the findings that have been done in the previously discussed case of the Children's ward where the minimums and maximums of the SNR variations have typically been detected within the distance of 1 to 1.5 m.

The results of the measurements have been presented in Table 21. There have been only three locations where the SNR variation have met the previously discussed criteria. Additionally, there have been single indications of rapid SNR variations that exceed the threshold of 20 dB but because they have occurred only one of the six measurement campaigns they have been ignored. The measured values of SNR have been in line with the corresponding values in the Children's ward. There has been a little bit more variation in the SNR values between the locations in the Children's ward than it has been in the Control ward whereas the variation of aggregate power of interference between the measured pairs and the SIR variations between the locations have been larger in the Children's ward than they have been in the Control ward.

Table 21. The measured values of SNR, P_i, P_r and calculated change of SIR between the measurement points of the locations where the rapid SNR changes have been measured

Location ID	SNR_{low} [dB]	SNR_{high} [dB]	Change of SNR [dB]	$P_{i(high)}$ [dBm]	$P_{i(low)}$ [dBm]	Change of P_r [dBm]	Change of P_i [dBm]	Change of SIR [dB]
1	24.8	70.5	45.7	-24.2	-54.6	42.2	-30.4	72.6
2	24.5	57.3	32.8	-31.7	-47.7	33.5	-16.0	49.5
3	22.5	47.0	24.5	-41.0	-44.7	24.5	-3.7	28.2
Average:	23.9	58.3	34.3	-32.3	-49.0	33.4	-16.7	50.1

All rapid SNR changes that have been measured in the Control ward have been occurred over the roaming limit. So, the remarkable rise of the power of useful signal has been caused by roaming as it has been in most cases in the Children's ward too. The signal strength of the useful signal before the roaming has been occurred, $RSSI_{low}$, has been on averaged -67.6 dBm in all three locations with extremely low variation over the results of the six campaigns. The averaged value of $RSSI_{low}$ is based on the measured values that have been presented in Table 23.

6.7.3 Evaluated effects of the rapidly fallen SNRs on the performance

The decreases of SNR that have been occurred before the roaming has been evaluated from the performance point of view. The corresponding study of the link margins for respective MCS index have earlier been done in the case of IEEE 802.11n. As it has been discussed, the MCS index of the respective modulation and coding scheme defines the required SNR and RSSI. In this work these thresholds have been used to evaluate the effects of the degraded SNR readings with the link margin that have been calculated earlier based on the given $P_{b(reqd)}$ of $1x10^{-2}$. The same link margins for IEEE 802.11ac have been used in the evaluation of rapid SNR changes of the Control ward (Table 17).

The measured minimums of SNR in the Control ward have been converted to the form of E_b/N_0 using eq. (12) with maximum data rate $R_{b(MCS)}$ of the respective MCS. The results have been presented in Table 22.

Table 22. The calculated values of E_b/N_0 corresponding the measured values of SNR_{low} in each location compared to the $(E_b/N_0)_{MCS}$ of the respective MCS index

Location ID	SNR_{low},[dB]	MCS8	MCS7	MCS6	MCS5	MCS4	MCS3	MCS2	MCS1
1	24.8	12.4	13.2	13.7	14.2	15.4	16.9	18.4	20.2
2	24.5	12.1	12.9	13.4	13.9	15.1	16.9	18.1	19.9
3	22.5	10.1	10.9	11.4	11.9	13.1	14.9	16.1	17.9

When the measured values of SNR_{low} are compared to the SNR requirement of the respective MCS, it may be seen that MCS4 may be achieved in all locations as the fastest MCS index. Because the maximum data rate $R_{b(MCS)}$ of MCS4 is 173.3 Mbps it may be estimated that the decrease of performance in the location of SNR_{low} has been in the order of 50% from the previously discussed $R_{b(MCS)}$ point of view.

The RSSI requirement of the respective MCS, $RSSI_{MCS,}$ has also been considered. P_r has been measured before roaming when the SNR has reached its minimum and it has been referred as $RSSI_{low}$. The sum of the shadowing and $RSSI_{MCS}$ has been referred as $RSSI_{min}$ that has been compared to the measured minimum, $RSSI_{low}$. $RSSI_{min}$ has been calculated for each MCS index and measurement location and the results have been presented in Table 23. The shadowing for the locations one and two have been given as 5.8 dB and for the location three as 4.8 dB in Table 8.

Table 23. The measured RSSI readings and the required thresholds of the respective MCS

IEEE 802.11ac	$RSSI_{low,}$ [dBm]	$RSSI_{min,}$ [dBm]						
		MCS8	MCS7	MCS6	MCS5	MCS4	MCS3	MCS2
Location 1	-67.2	-53	-58	-59	-60	-64	-68	-71
Location 2	-67.7	-53	-58	-59	-60	-64	-68	-71
Location 3	-68.0	-54	-59	-60	-61	-65	-69	-72

When the measured values of $RSSI_{low}$ have been compared with the calculated values of $RSSI_{min}$, it may be seen that MCS3 has been the fastest MCS index that may be reached in each of the three locations. This results the further decrease in the performance of the network which may theoretically be indicated as a decrease of the maximum data rate to the value of 115.6 Mbps as it has been compared to the previous evaluation that has solely been based on the required SNR (Table 22). The resulted decrease of performance is in the order of 67% from the maximum data rate $R_{b(MCS)}$.

6.7.4 Measurements on the ground floor and the third floor

In addition to the previously discussed measurements in the Children's ward on the third floor, some measurements have also been carried out on the ground floor. The department of the abdominal diseases on the ground floor has been studied by two site-surveys. The measurements have been carried out by walking slowly through the corridors and the chosen rooms of the department. The site-surveys have been carried out in February and March 2021. A few preliminary indications of coexistence issues and the SNR drops that have also been discussed in other floors have been detected. However, it must be emphasized that the findings may only be viewed as guidelines for general evaluation of the wireless system not for the accurate analysis of the RF system.

The department of the abdominal diseases locates on the ground floor of the newly opened J2 building. The connectivity issues of the Ascom Myco mobile devices that has been used for the alarms and communication by the personnel of hospital have been reported. The device is served by the Myco virtual network that operates at the 5 GHz band. Based on the information from the hospital personnel there have not been used other mobile devices on the ground floor. Laptops have been used only in the LAN network.

The geometry of the ground floor is extremely challenging from the RF point of view. The most walls are load-bearing walls with heavy construction. The corridors are narrow and there are plenty of corners and pillars around the ground floor.

The site-surveys have been carried out by walking slowly in one direction in February and March 2021. They have shown moderate signal strength at the most of the areal of the floor. Only some areas with lower access point density, the signal strength at the 5 GHz band has been in the order of -60 dBm while it has been mostly exceeded the level of -40 dBm (Figure 56). The signal strength at the 2.4 GHz has indicated signal outages in a few places and should be studied more in detail. However, because the 5 GHz has been used by Myco, the 5 GHz band has been focused on this short description.

Figure 56. The signal strength of the 5 GHz band on the ground floor.

The spectrum channel power (SCP) parameter of Ekahau shows the received power that has been measured in the location averaged over the time that has been spent in the location. The heatmap of the SCP that has been presented in Figure 57 covers the centre of Figure 56.

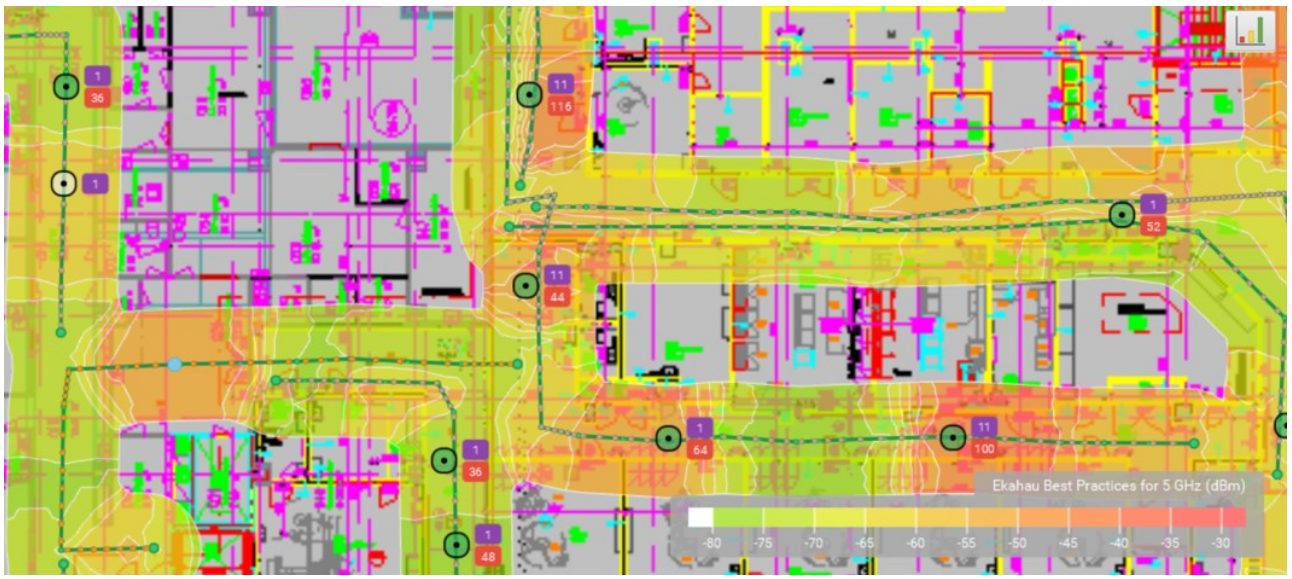

Figure 57. The SCP heatmap of the department of the abdominal diseases (5 GHz).

It may be seen in Figure 57 that the higher received channel power has typically been measured close to the access points (dark orange). However, there are areas where the increased power has been measured without being near the access point. An example may be seen in the location of Figure 57 that has been marked by a light blue point. The averaged power that has been measured in this point has been -55, -56 and -60 dBm for the channels 42, 44, and 46, respectively. The channels use the frequencies of 5150 to 5250 GHz with the bandwidth of 40 or 80 MHz. The bound channels have obviously not been used by the access points of the own network, so the power must have been received from the transmitter outside the own network.

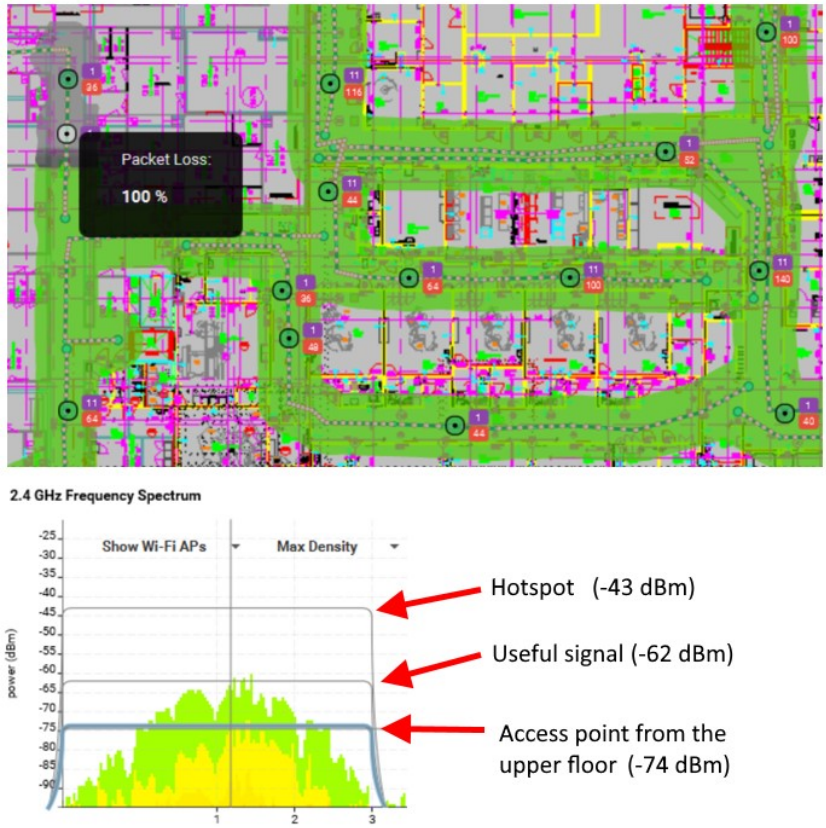

Figure 58. The coexistence finding in the department of the abdominal diseases.

The potential coexistence issue has been detected also near the entrance of the magnetic resonance imaging (MRI) room. In Figure 58, the packet loss of 100% has been shown at the 2.4 GHz band. The screenshot of the spectrum view from the location where the packet loss has occurred shows that in the channel one there has been three co-channel signals within the margin of 30 dBm. The useful signal has the second highest power of -62 dBm while the strongest signal comes from the mobile hotspot. The channel utilization has been remarkably high at the moment of the measurement.

The rapid falls of SNR have been indicated also on the ground floor at the 5 GHz band both in ELI350 and Myco networks. They have been defined in a similar way as on the upper floors as drops of SNR over 20 dB within the distance of 2 metres. Eight rapid falls of SNR have been detected in ELI350 network and 11 falls in the Myco network (Figure 59). Both networks have been served by all access points of the floor.

The SNR variation may be seen in the upper screenshot of Figure 59 for ELI350 network and the heatmap for Myco network has been presented in the lower screenshot. Both heatmaps have been based on the measurements at the 5 GHz frequency band. The different shades of grey-coloured areas show the lowest values of SNR with the lightest shade of grey indicating the SNR under 15 dB. The darkest grey indicates the SNR from 15 to 25 dB. There may be seen some variation between the heatmaps of Figure 59 that may partly be caused by the temporal variations of the results between two measurement series. Because of this, the measurement should be carried out over the longer time periods with enough repeated measurement series.

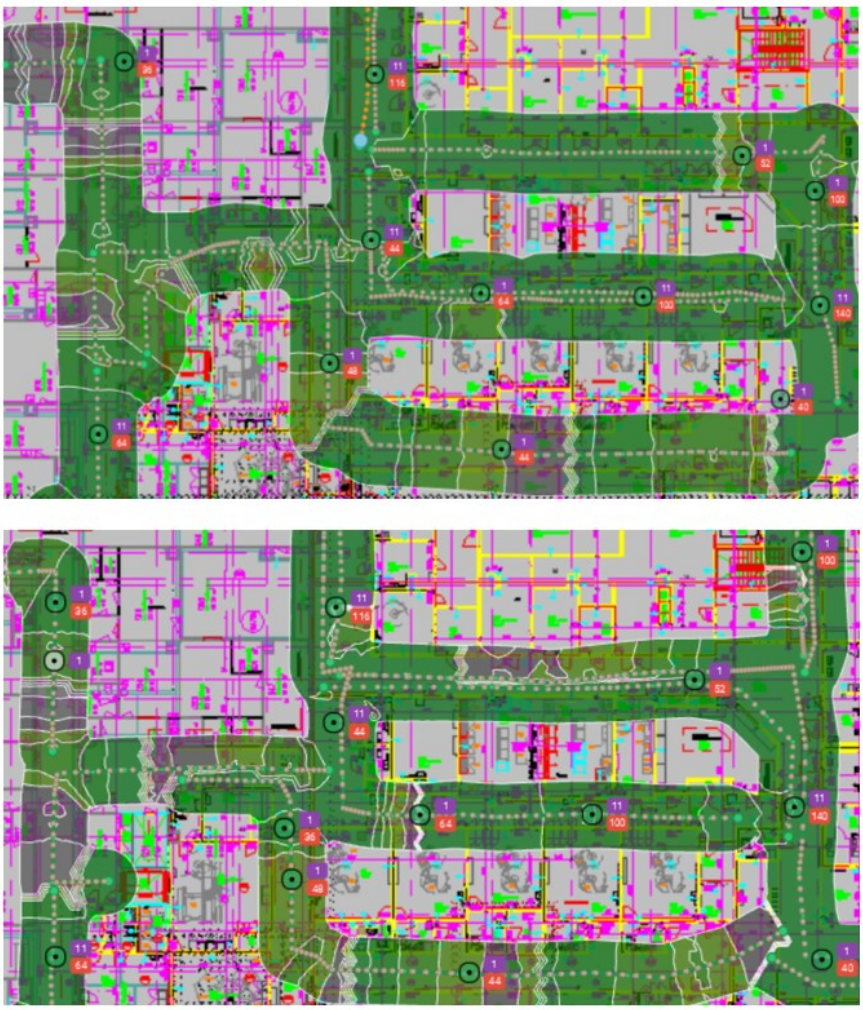

Figure 59. The measured SNR in the ELI350 (upper) and Myco (lower) networks of the ground floor.

In most cases the falls of SNR have occurred before roaming as it has been discussed earlier when the phenomenon has been discussed on the other floors. The walking direction has been towards the sharp edge of the area with low SNR that describes the rapid increase of the measured SNR in the walking direction. When the area of low SNR has been approached the SNR has typically been decreased gradually within the variated distance of a few metres. Two potential reasons for the rapid change of SNR will be discussed next.

6.7.5 Possible reasons for the rapid changes of SNR

As it has been discussed earlier, roaming has been occurred between the values of SNR_{high} and SNR_{low} in every location. In IEEE 802.11 WLAN the client is responsible of roaming. Although the roaming issues have not been in the scope of this study and the different mechanisms of roaming have not been discussed, it may be noted that the roaming may be based on threshold of SNR or RSSI when the client makes the roaming decision. The other criteria may involve the number of clients on the access point, transmit and receive bandwidth that has been used by the AP and RF channel information that has been transmitted by the access point. Although the client is ultimately responsible for the roaming decision, the settings of WLAN controller may limit the choices. In some controllers the default settings of the controller might have been overridden by custom settings resulting the changed thresholds of RF parameters 1.

Based on the earlier discussion, also multipath may explain the rapid attenuation of signal. The measured SNR changes have clearly been contributed by the attenuation of the received signal and the fall of SNR have only been indicated at the 5 GHz frequency band. Because T_c can be expressed as 1

$$T_c \approx \frac{1}{2\pi f_m} \quad , \tag{37}$$

where f_m may be expressed by the ratio of receiver's velocity and wavelength of the signal, the T_c at the given velocity v may be calculated as

$$T_c \approx \frac{\lambda}{2\pi v}. \tag{38}$$

If the velocity of the receiver has assumed to be 1 m/s, the $T_c \approx 8.0$ ms at the 5 GHz band and $T_c \approx 16.6$ ms at the 2.4 GHz band. Based on eq. 36, the T_s may be calculated for both frequency bands assuming that the highest order of modulation has been used as $T_s = 434$ ns for the 5 GHz band and $T_s = 240$ ns for the 2.4 GHz band. Because $T_c >> T_s$, fast fading has not been resulted in distortion and only the slow fading might have been occurred. In practise, the velocity has been lower than the estimated maximum velocity of 1 m/s resulting in the increased T_c compared to the above calculated value of T_c.

7 CONCLUSIONS

The wireless system of NKCH has been studied in the building J2 of the hospital from the RF point of view. The 2.4 GHz and 5 GHz ISM bands have been studied and based on the RSSI measurements the path loss models with shadowing have been generated. The signal outage has been studied within the predefined routes in the Control ward and the generated path loss models have been compared with the path loss models from the publications. The SIR has been determined based on the measured values of desired signal power and aggregate power of interference. The changes of SIR have been analysed and the threshold has been determined based on the given probability of bit error to figure out the attainable maximum data rate. The SNR has been measured and the results have been compared to the determined threshold to figure out if the theoretical deterioration of the performance has been caused by the changes of signal strength or changes of aggregate interference. Additionally, based on the SNR measurements at the 5 GHz band, the indicated rapid changes of SNR have been studied in the whole building J2 and their effect on the performance of the studied system has been evaluated.

7.1 Difference between the signal strength at the 2.4 GHz and 5 GHz band

The measured RSSI readings of all six measurement campaigns have proved that the signal strength of the received signal is lower at the 2.4 GHz band than at the 5 GHz band. The reference path losses have been determined separately for each path loss model. At the given reference distance, the reference path losses should follow the free-space attenuation law. When the values of empirically derived $L_p(d_0)$ have been compared to the calculated values of $L_{p(free)}(d_0)$ it may be seen that $L_p(d_0)$ has been 20 dB and 24 dB higher for respective access points at the 2.4 GHz band while it has been exactly 4 dB at the 5 GHz band for both access points. It is obvious that the propagation results do not follow the free-space attenuation law at the 2.4 GHz region whereas they are close to the free-space propagation at the 5 GHz in the vicinity of both access points. However, because signal has LOS propagated within reference distance, the differences between the measured and calculated path losses at the 2.4 GHz band cannot be explained by the attenuation effect of obstacles. As a result, it can be concluded that the EIRP has not been in line with the presumption of the transmission power. The EIRP has been calculated based on the available information on the settings of the WLAN controller and the specifications of the Cisco 1852 access point (Appendix 4). Because transmitted power depends not only on the frequency band but also the frequency of the used channel, the EIRP has been calculated for all four frequencies that have been used in the Control ward (Tables A and B of Appendix 4).

The lower EIRP of the 2.4 GHz band may also be indicated in the generated propagation models (Figures 18 and 19). The difference of 10 dB in the path losses of the 2.4 GHz and 5 GHz signals has been slightly decreased in proportion to the distance as it has been assumed to do because the signal of higher frequency attenuates more rapidly which is in line with the previous discussion.

Based on the discussion above, it may be concluded that the signal strength at the 2.4 GHz band has been weaker than it should have been when the transmission power has been adjusted to the maximum. It may also be concluded that the signal outages and lower signal strength in general that have been indicated at the 2.4 GHz band in the locations where the signal at the 5 GHz has been strong has been caused by the lower transmission power.

The lower signal strength may probably have been resulted because the access points have reduced the transmission power to mitigate the interference. This assumption may be motivated by the high level of interfering power that has been measured in the network. However, the discussion is out of the scope of this study and should be studied separately.

7.2 Signal propagation in the Control ward

The signal propagation has been modelled for two routes at the 2.4 GHz and 5 GHz bands. The room geometry and the varying wall structures that have been studied by CAD drawings have strongly affected the signal attenuation within both routes. The path loss coefficient has risen on both routes at the location where there has been the load-bearing wall on the signal path side by side with the measured route. This has occurred within both routes when the transversal corridor has been entered behind the corner of the heavy wall, though within Route 1 the change of slope occurred a little bit earlier when the doorway to the corridor has been entered. The path loss may have been approximated as free-space path loss until the second slope of the multi-slope curve has been reached.

Route 2 differs from Route 1 mainly because there has been a long corridor where the LOS has been maintained until the turning point of 12.6 m where the slope has been changed. The path loss coefficient has been approximately two within conditions of LOS which has been as assumed. The second slope that has begun in the corner of the corridors has been $n = 6.3$ for the 2.4 GHz and $n = 8.4$ for the 5 GHz signal. However, the signal can be measured until the distance of 29 m at the 5 GHz and 20 m at the 2.4 GHz band. So, regardless of the stronger attenuation of the 5 GHz signal within the second slope the earlier discussed difference between the signal power of the 2.4 and 5 GHz band have obviously caused the larger coverage at the 5 GHz compared to the 2.4 GHz band. The threshold of Ekahau has been adjusted to -85 dBm which means that the received power that exceeds the threshold will be displayed in Ekahau Pro.

The shadowing has been calculated for both routes and both frequency bands (Table 8). The results show that X_σ has been lower at the 5 GHz band compared to the 2.4 GHz band. Route 2 has resulted in higher values of X_σ at both frequency band. When the difference is studied at the 5 GHz band, it may be seen that the larger coverage of the 5 GHz signal may explain the difference because the cumulative effect of the obstacles along the measured route is higher in that case. The comparison with other researches indicates that the measured values of this study have been quite low which indicates low variation of the signal power accordingly. However, the typical measurement arrangement is based on the spectrum analyser with an automated sampling process yielding a larger quantity of the results. This may obviously increase the variation of the measured signal power, especially with campaigns of longer time periods providing also more reliable measurement results. The measured values of this study are although quite near the general approximation of 10 dB that has been used in the literature, as it has been discussed earlier.

The probability of signal outage has been calculated for both routes at the 2.4 GHz band because of the earlier discussed findings of the signal strength at the band. The calculated curves (Figures 22 and 23) show that the probability of 50% has been attained in the distance of 36 m on Route 1 whereas it has been attained in the distance of 23 m at Route 2. The design requirement of 1 % has been exceeded in the distance of 20 m on Route 1 and 17 m on Route 2. If the modelled propagation may be extended to cover the other measured areas in the building J2, it may be estimated that under the similar propagation conditions the access point density has been sufficient on average, but the locations of the access points have not been optimal in some cases from the coverage point of view.

The shadowing has also been studied as an average on the measurements that have been carried out in the fixed distance of 12 and 15 m from the AP1. The shadowing has been 13.5 dB for 2.4 GHz and 8.8 dB for 5 GHz band and the averaged values of RSSI in the same distances have been -70 dBm and -62 dBm, respectively. When the results are compared to the probabilities of signal outage that have been calculated on the measured route in the same distance, it may be seen that the threshold of -85 dBm is remarkably close to the sum of the signal strength of -70 dBm and the shadowing of 13.5 dB. This leads to the observation that when the shadowing has been studied around the Control ward in the fixed distance from the same access point, the probability of the signal outage has been increased in the given distance compared to the corresponding value on the route. As a result, it may be concluded that if the generated propagation models are used for modelling the signal attenuation

outside the measured routes, the shadowing must be measured over the studied room. The similarity of the propagation models of each route indicates that they may give a relevant approximation of the propagation conditions when they have been used outside the defined routes if the shadowing effect had been considered in the studied environment.

The comparison between the generated models and ITU-R Model Recommendation and IEEE 802.15.2-2003 have been done at the 2.4 GHz band. It may be concluded based on Table 11 that the results that have been yielded based on the generated models of this work describe the propagation conditions of the Control ward more accurately than the other models that have been discussed. The models of this study have yielded about 20 dB higher path losses than the compared models. Because the difference equals to the previously discussed difference between the signal strength at the 2.4 GHz and 5 GHz band, it is obvious that the difference between the models have been caused by the incorrect transmission power. If the indicated and previously discussed difference of transmission power between the 2.4 GHz and 5 GHz band has been considered, the models of this study yield the path losses that fall between the values of compared models.

7.3 Coexistence in the Control ward

7.3.1 Local changes of SIR within the measured routes

There have been remarkable decreases of SIR within both routes. As it has been previously discussed, the change of path loss coefficient has occurred in all generated path loss models approximately in the same distance. Furthermore, the minimum of the SIR has been reached almost in the same distance in all four cases. The turning point of the path loss slopes have occurred in both cases before the minimum of SIR has been indicated at the respective frequencies. Based on these notices, it may be deduced that after turning point of the slopes the strongly decreased desired signal has obviously contributed to the fall of SIR (Table 12 and 13). This may also be seen when the measured decrease of the desired signal before the minimum of SIR has been studied. Based on the respective path loss models and Tables 12 and 13 it may be seen that the minimum of SIR has been caused by the decrease of desired signal power at both frequency bands.

The comparison of the local reasons for the decrease of SIR indicates that at the 5 GHz the major contribution to the decrease has been the change of the useful power and at the 2.4 GHz the changes of useful power and aggregate interference equally. It may further be noticed that the fall of SIR has occurred after roaming to the AP4 in the location where the access points of the neighbouring building have affected the SIR of 2.4 GHz band. Because the access points close to the Control ward have operated only at the 2.4 GHz band, they have not contributed the fall of SIR at the 5 GHz and the SIR has been fallen dramatically by 30 dB only after the corridor when the aggregate power from the access points of the Control ward and the surrounding access points of J2 have caused it. Hence, it may be concluded that the fall of SIR has primarily been caused by the aggregate interference from the access points of the Control ward and the surrounding access points of the J2. This is also in line with the difference of the measured signal strength between the 2.4 GHz and 5 GHz band that have previously been discussed.

7.3.2 SIR variations between the routes

Based on Figure 40 it may be seen that the aggregate power of interference has contributed less to the variations of SIR within Route 2 than Route 1. However, the power of aggregate interference has been constantly at a higher level compared to Route 1 where it has varied more. Even at the 2.4 GHz band where the signal strength generally has been at the lower level, the aggregate power of interference has been at remarkably high.

The variation of the useful signal has proportionally been the primary reason for the SIR variations within the route 2 which has been caused by the LOS propagation within the long distance from the beginning of the route and the part of the route after the turning point of the corridors where path loss coefficient has been changed and the signal has been strongly attenuated. The turning point changes the conditions of propagation in a similar way that has been discussed in the corresponding location of Route1.

7.3.3 Indicated coexistence issues by Spectrum analysis

From Figures 48 - 52 it may be seen that the medical devices that use Bluetooth and Zigbee technologies have been indicated in the spectrum. The lower signal strength compared to the signal strength of the WLAN leads to the conclusion that they probably do not interfere the WLAN traffic. However, because of the remarkably higher transmission power of the WLAN access points, they may be interfered by the access points, especially when they are close to them. The risk for interference should be considered because Bluetooth and Zigbee nodes typically may be used in various patient monitoring applications and may be moved close to the access points. This leads to the conclusion based on the findings, that the use of medical devices in the same wireless environment with WLAN should be surveyed. The sensitivities of the used devices should be studied to consider the threat of coexistence issues between them and WLAN for the designing processes of the wireless environment in the future.

The use of hotspots has also been indicated in the spectrum on all measured floors. They may be a source of interference because the signal strength may typically be in the order of the EIRP of access points. Depending on the location where the hotspot has been used, they may promote the threat for the WLAN as it has been indicated on the ground floor (Figure 58).

7.3.4 Overview of the SIR variations in the Control ward

The Control ward represents the typical hospital environment where the corridors and half-open patient rooms form the changing environment for the signal propagation. Based on the method where the local changes have been estimated by the SIR expression regardless of the route, whether they have primarily been caused by the change of useful power or aggregate interference, it may be concluded that at the 2.4 GHz band the primary reason for SIR variations in the Control ward has been the variation of the desired signal and at the 5 GHz band the aggregate power of interference (Figure 34). This has been in line with the earlier discussed difference of the signal strength between the two bands.

When the previously discussed variations of SIR have been compared to the measured averages of the data rate between both routes, it may be concluded that there has not been a clear correlation between the measured SIR and data rate. However, the standard deviation of the data rate has been in its minimum when the SIR has reached the maximum (Figure 39). It may although be caused by the strong desired signal without any correlation to the aggregate interference. There has also been some difference between the routes so that, on the one hand, when the low standard deviation has been calculated with high values of SIR (Figure 39) within Route 1, on the other hand, the high standard deviation has been calculated with high SIR values within Route 2 (Figure 40). Furthermore, when Figures 29 – 32 are compared to Figure 44, it may be seen that low values of SIR have been measured in the same locations where the maximum attainable data rate has been in its minimum. This has more clearly been seen at the 2.4 GHz band (Figure 44) where the signal strength of desired signal has been lower. The variation of desired signal power has primarily contributed to the changes of SIR at the 2.4 GHz band (Figure 34) while at the 5 GHz band the changes of SIR has primarily been contributed by the variation of aggregate power. Based on this, it may be concluded that the theoretical decrease of maximum attainable data rate within both routes may primarily be caused by the decrease of the desired signal power. This should be verified by the further performance measurements. The

fluctuation of the standard deviation should also be verified by measuring the data rates in longer time periods that include conditions of changing network load.

The performance of the network has been evaluated from the attainable MCS point of view as it has been described earlier. Based on eq. (22) and Tables 16 and 17 the β has been defined for the respective MCS. Based on the measured data rate, the maximum attainable data rate has been assumed to be in the order of 170 Mbps. The standard deviation of the measured SIR has been calculated in proportion to the MCS_5 that allows a maximum data rate of 173 Mbps (Table 17) with the given specifications that have been described earlier. The results of the calculations for IEEE 802.11n and IEEE 802.11ac (Figures 38 and 39) show that more variation has been occurred within Route 1 than Route 2 at the 2.4 GHz whereas the variation within Route 2 has indicated to be higher at the 5 GHz compared to the 2.4 GHz band. The variation has although been within the link margin of 10 dB, so it may be concluded that the variation of the SIR in proportion to the β has not differed between the measured routes at either band. Hence, the difference between the local changes of the respective route has not caused the variation of SIR over the whole measured route that may be seen to affect the attained maximum data rate of the respective route. The cumulative effect of the piecewise defined changes of SIR (Figure 40) have neither affected the variation of the attainable maximum data rate because it has been varied between the routes and the difference between the previously discussed data rate variations of the respective routes may not be indicated. As it has been discussed earlier, the linearity of the dependence between the SIR variation and the maximum attainable data rate, as it has been defined in this study, may be seen at the 5 GHz band but not at the 2.4 GHz band. This has been caused by the calculated $E_b/N_{0(reqd)j}$ that has been defined for the respective MCS using the chosen value of P_b, in a way that has been discussed earlier. The required SNR has been proportionally higher for the fastest MCS_5 of the Figures 38 and 39 because of the higher order of modulation that has been used. The only outcome from the discussion above that may obviously be presented as a conclusion is that the attainable data rate has been dependent on the SIR. On the other hand, it may not be concluded that the estimation of the local contributions to the SIR may not be used in estimating the primary reasons for the local changes that contribute to the SIR of the whole route. After all, when the used method has been concerned, it may be used to evaluate the primary reasons for the variations along the route but the evaluation of the performance, when it is considered from the SNR point of view is solely based on the SNR. In the context of the measured route, it results that the threshold β should be exceeded in any location of the studied route in Figures 38 – 40 to meet the required $E_b/N_{0(reqd)j}$ as it has been stated in eq. (22).

The earlier discussed difference between the signal strength at the 2.4 and 5 GHz band have been indicated in the propagation models. Based on Tables 12, 13, 14 and 16 the lower signal strength of the useful signal at the 2.4 GHz band may be seen clearly. When the SIR has been compared between the frequency bands it may be seen based on the previously referred tables, that although the signal strength has been lower at the 2.4 GHz band the higher aggregate interference at the 5 GHz compensates the difference of SIR between the two bands. The higher aggregate interference at the 5 GHz in turn has been caused by the mentioned difference between the signal strength that is higher for the 5 GHz. This has resulted that the difference may not be indicated between the SIR of the respective frequency bands.

7.4 Rapid SNR variations

The rapid changes of the measured values of SNR have been measured on all three floors where the measurements have been carried out. The rapid SNR variations have been measured only at the 5 GHz band. Because the results of the measurement of the rapid SNR changes have been based only on the two site-surveys on the third floor and the ground floor, the study of the SNR drops have been carried out in the Control ward where the results have been based on the six measurement campaigns that have been described earlier. However, the indications of the rapid changes of SNR on the third

floor and the ground floor may be used as guidelines in estimating the phenomenon because they have been exactly in line with the results that have been obtained in the Control ward (Tables 18a, 18b, 18c).

The desired power and the aggregate power of interference have been measured and the SIR has been calculated using eq. (12). The change of desired power and aggregate power of interference have been calculated over the respective points in each location. In all cases the reason for change of SIR has been evaluated based on the results of Tables 19 a – c and Table 20. The primary reason for the decreased SIR has been the fall of desired signal power. The same has been indicated also in the two single measurement series that have been carried out in the Children's ward. So, although high values of the aggregate power of interference have been measured before the roaming has occurred, the primary reason for the changes of SIR has been the changed signal strength of the desired power, not the aggregate power of the interference (Table 19).

It has been indicated that the roaming has occurred in all measured locations of the three floors between the points where the SNR_{low} and SNR_{high} have been measured. Based on the measurements, the roaming criterion of RSSI for the measurement device has been approximately -68 dBm (Table 19) which may be kept in line with the roaming criteria of other devices that are used in the network. So, they may be assumed to roam based approximately on the same threshold.

Based on the results of the data rate measurements that have been presented in Figures 39 and 40, the mean values of standard deviation of 165 Mbps and 150 Mbps have been measured in the locations one and two, respectively. However, as it has been discussed earlier, the data rate depends strongly on the network load and should be measured over a longer period to obtain a more accurate estimation of the data rate which has not been possible by the device of this study as it has been discussed earlier. It must be emphasized that the conclusion is only a theoretical estimation of the resulting decrease of the performance and should be verified by throughput measurements.

Based on the previous discussion it may be concluded that because the SNR has been decreased in the three locations of the Control ward before the roaming has occurred the potential decrease of the network performance may have been resulted. As a result, the potential degradation of 67% in the maximum attainable data rate can be caused. However, because the performance may not be defined only by the maximum data rate, this conclusion may only be seen as a theoretical limit from the data rate point of view.

Because of the averaged decrease of 34.3 dB in SNR values before the roaming has occurred, the potential effect on the performance of the network has been evaluated by comparing the yielded SNR readings with the SNR that have been required by the respective MCS. The comparison between the results of Tables 17 and 21 yields the conclusion that the network performance may potentially be degraded in each of the locations 1, 2 and 3 so that because of the SNR requirement of the respective MCS, the fastest MCSs may not be used resulting the decrease of the maximum data rate to the value of 173.3 Mbps in each of the measured locations with the given requirement of P_b.

The respective MCS index has also the RSSI requirement that must be exceeded. Based on the results of Table 23, it may be concluded that also the decrease of the signal strength has contributed the potential deterioration of the performance before roaming has occurred. The MCS index that may be achieved because of the decreased signal strength has been MCS3 in all of three locations. This results in theory the fall of maximum data rate to the value of 115.6 Mbps (Tables 17 and 23).

As it has been discussed, the rapidly fallen SNRs have been widely detected also in the Children's ward and the department of abdominal diseases. Because of this the potential consequences should be studied by the throughput study by iPerf especially on the third floor and the ground floor where the findings have been more than in the Control ward. The multipath has obviously not resulted in attenuation of the signal because it is a randomly appeared phenomenon and the fall of SNR has been occurred only close to the roaming line. The roaming-related parameters of the WLAN controller should be checked to figure out if the settings limit the client to maintain the SNR before roaming [45]1.

7.5 Study of coexistence by Ekahau

Ekahau Channel Interference parameter presents appropriate tool to figure out the areas with the potential interference from the co-channel access points. In this work it has been used as a preliminary tool to search for the areas with increased CCI or ACI risk. Because it shows the number of interferers, not the power margin between the desired signal and the interference, it has been used with signal strength parameter in this study. The power margin may be calculated manually between the signals that have exceeded the threshold that may be adjusted in the given range.

The signal strength parameter may be used to measure all received power from the WLAN sources that exceed the chosen threshold, and the received signals may simultaneously be studied in the spectrum analysis window where also the sources outside the IEEE 802.11 network may be detected.

The SCP parameter has also been used in this work to find out the sources of interference outside the WLAN. Although it measures the channel power of the chosen channel, the result that has been displayed is an averaged power over the time that has been stayed in the measurement location. It may be used in searching for the interferers with long duty-cycle and a stable power level.

The frequency spectrum view may be used with Ekahau Sidekick to figure out all received signals. The frequency span may not be adjusted because only the whole chosen frequency band of 2.4 GHz or 5 GHz may be displayed. The use of spectrum view is laborious when the frequency of the received signal needs to be defined because it shows only the channel number of the respective WLAN channel in the centre frequency of the channel bandwidth. In this work the frequencies of the received signals have been defined graphically in a way that has been described earlier. Although the scale is linear so that the frequencies may be defined by calculating them from the centre frequencies of the channel it is not a fully accurate and practical method of determining the frequency of the interference.

The interferences that occur near the other signals may be stayed hidden because of the sidelobes of the signal. The occasional signals may not be seen because they would require the longer measurement periods and although Ekahau has a parameter called duration that may be adjusted between 1 s and 120 s, the signals may be difficult to distinguish from each other.

The described user experiences have primarily been based on the device as an instrument of interference measurement. Although it has limitations that have been discussed shortly, it may be used as a maintenance tool in IEEE 802.11 WLAN. The compact device that presents the results visually in heatmaps and shows the access point IDs simplifies the process where the potential network issues are to be detected and analysed. The spectrum view offers a tool to figure out the interferences of the ISM bands of 2.4 GHz and 5 GHz also from the sources outside the WLAN. So, it may be used in interference hunting though it has shown the mentioned limitations in scientific use.

8 DISCUSSION

The used technologies and devices of the studied environment must be surveyed prior to the coexistence study. All available information on the use of shared frequency spectrum as well as the sensitivities of the connected devices need to be gathered as a part of a preliminary study. The detailed information of the systems, technologies and devices has typically spread wide among the specialists of large organizations, such as hospitals. This may be challenging from the coexistence point of view. So, the importance of coordinated maintenance of the connected systems and devices may not be overemphasized.

The maintenance and the reliability of medical devices are on the responsibility of the commercial companies and because of this, the organizations typically are not involved in the compatibility issues of coexisting systems. The research work has been done in Europe, e.g., by ETSI to find out the standardized methods of measuring the coexistence. They will be needed especially in the hospital environments where the quality requirements of wireless communication are high. The coexistence of the various technologies must be considered in a situation where the mobile applications of the coexisting wireless technologies will be increased.

The hospital of the future will probably not be purely wireless. The limitations of wireless communication have been dictated by the spectrum that has been and will be shared. The channel is imperfect mostly because of the noise from the continuously increasing number of interferers.

9 SUMMARY

In this work, the propagation has been modelled by the path loss model with shadowing. The SNR has been used to figure out the conditions of the propagation and to evaluate the required performance of the network.

The measurements have primarily been carried out in the Control ward of the Emergency Care department to model the typical hospital environment with the number of coexisting technologies. In the framework of the possibilities of Ekahau Sidekick and Ekahau Pro the SIR has also been modelled in the Control ward. Some measurements have also been carried out on the entire floor as well as on the ground floor and the third floor.

The noise floor has been determined based on the averaged noise power measurements as -97 dBm. The signal strength variation of the useful signal and the aggregate power of interference have been measured firstly in the whole Control ward and then within the predefined routes that have been defined based on the earlier measurements. The measurements have been carried out at the 2.4 GHz and 5 GHz frequency region. The walls and building constructions have been considered when the routes have been defined to make it possible to compare the results of the two routes. The generated models may be implemented in evaluation of the other parts of the hospital if the given limits have been considered.

The dependency of the network performance on the local changes of SIR has been studied. The comparison has been made between the required SNR of the respective MCS with the calculated link margin where the chosen bit error probability has been considered. Because of some limitations of the measuring device the data rate has been measured to figure out the variations without considering the temporal dimension and the possible effects of the varying network load over the longer period.

The signal strength at the 2.4 GHz band was found to be lower than at the 5 GHz band. The path loss models of this study have been based on the incorrect information about the transmission power and it has resulted the error of 20 dB in path losses at the 2.4 GHz band. The error has also been indicated when the path loss models of other publications have been compared to the models of this study. Due to reduced transmission power at the 2.4 GHz band, low values of SNR and SIR have locally been measured. It can be indicated in the generated propagation models but not very clearly in the comparison of the SIR measurements.

The outcome of the study may be summarized based on the results of the propagation models and the piecewise analysis of SNR variations that ultimately may be discussed together. The strong variation of signal strength that has been indicated by the generated path loss models and that may mostly be explained by the obstacles and room geometry, may be seen as the primary reason for the variation of SIR in the Control ward. Additionally, the indicated rapid falls of SNR on the three floors of J2 have been indicated to cause by the decrease of desired signal before the roaming has occurred. The effect of the SNR and SIR variations has also been evaluated from the attainable MCS index point of view. The maximum data rate has been calculated and it has given a theoretical approximation of the decreased performance in the measured locations.

10 REFERENCES

[1] Sklar B., (2017) Digital Communications, Fundamentals and Applications, Second ed., Prentice Hall PTR, 1011 p.

[2] Raymond R., Hampton R. (2011) Design and Deployment of Wireless Healthcare IT Networks, Biomedical instrumentation & Technology, Volume 45, Issue S2, AAMI, https://meridian.allenpress.com/bit/article/45/s2/53/142213/Design-and-Deployment-Of-Wireless-Healthcare-IT, (read: 19th April, 2021) 2011.

[3] IEEE 802.11n-2009 – IEEE Standard for Information technology – Local and metropolitan area networks. https://standards.ieee.org/standard/802_11n-2009.html. (read: 11th April, 2021), IEEE Standards Association

[4] Garg V. K. (2007) Wireless Communications and Networking, Elsevier Inc., San Francisco, 821 p.

[5] Amzucu D.M., Li H., Fledderus E., (2014) Indoor Radio Propagation and Interference in 2.4 GHz Wireless Sensor Networks: Measurement and analysis. Wireless Personal Communication, 76:245-269, Springer Science+Business Media, New York, 2014.

[6] Karvonen H., Mikhaylov K., Hämäläinen M., Iinatti J. (2017) Interference of Wireless Technologies on BLE Based WBANs in Hospital Scenarios. 13th EAI International Conference on Body Area Networks, IEEE, pp. 147-156.

[7] Goldsmith A. (2005) Wireless Communications, Cambridge University Press, 561 p.

[8] Sandoval R.M., Garcia-Sanchez A.J., Garcia-Haro J. (2018) Improving RSSI-Based Path-Loss Models Accuracy for Critical Infrastructures: A Smart Grid Substation Case-Study, IEEE Transactions on Industrial Informatics, Vol. 14. 14, No. 5, May 2018, p. 2230 – 2240.

[9] Tuta J., Juric M.B. A Self-Adaptive Model-Based Wi-Fi Indoor Localization Method. Sensors 16 (2016), 2074, MDPI Publishing 2016, p. 1-22.

[10] Chrysikos T., Georgopoulos G., Kotsopoulos S. (2009) Empirical Calculation of Shadowing Deviation for Complex Indoor Propagation Topologies at 2.4 GHz, IEEE Explore, 2009

[11] Bellekens B., Penne R., Weyn M. (2018) Realistic Indoor Radio Propagation for Sub-GHz Communication. Sensors 18 (2018), 1788, MDPI Publishing 2018, p. 1-33.

[12] LaSorte N.J., Barnes W.J., Refai H. (2009) Characterization of the Electromagnetic Environment in a Hospital and Propagation Study. IEEE Xplore, 2009, p. 135-140.

[13] Dobkin D. M. (2011) RF Engineering for Wireless Networks: Hardware, Antennas, and Propagation. Elsevier Science, 447 p.

[14] Santi P., Maheshwari R., Resta G. (2009) Wireless Link Scheduling under a Graded SINR Interference Model. FOWANC'09, May 18, 2009, ACM, New Orleans.

[15] Chandra P. et al. (2007) Wireless networking: Know it all. Newnes, Elsevier Science, 2007, Oxford. 572 p.

[16] Lopez-Aguilera1 E., Garcia-Villegas E., Casademont J. (2017) Evaluation of IEEE 802.11 coexistence in WLAN deployments. Wireless Network, 2019, 25:87-104, Springer Science, 2017.

[17] Petäjäjärvi J., Mikhaylov K., Vuohtoniemi R., Karvonen H. and Iinatti J. (2016) On the human body communications: wake-up receiver design and channel characterization. EURASIP Journal on Wireless Communications and Networking, 2016:179, Springer Open, 2016.

[18] Omomule T., Olarinde D., Ugwu C., Falana T. (2019) QoS Performance Metrics for Analyzing Wireless Network Usability. IRE Journals, Volume 3, Issue 6, Dec 2019.

[19] Hasan et al. (2019) A comprehensive review of wireless body area network. Journal of Network and Computer Applications 143 (2019), Elsevier, p. 178-198.

[20] Ravindranath N.S. et al (2017) Study of Performance of Transmit Beamforming and MU-MIMO Mechanisms in IEEE 802.11ac WLANs. International Conference on Inventive Communication and Computational Technologies, IEEE, 2017.

[21] Börjesson P.O., Sundberg C.-E. (1979) Simple Approximations of the Error Function Q(x) for Communications Applications, https://ieeexplore-ieee-org.pc124152.oulu.fi:9443/stamp/stamp.jsp?tp=&arnumber=1094433, (read: 2nd Mai, 2021), IEEE Transactions on Communications, Vol. COM-27, No. 3, March 1979.

[22] Wireless LAN Professionals, https://wlanprofessionals.com/mcs-snr-rssi-chart/ (read: 28th March, 2021), 2020.

[23] Gimenez-Guzman J.M., Marsa-Maestre M., Orden D., de la Hoz E., Ito T. (2018) On the Goodness of Using Orthogonal Channels in WLAN IEEE 802.11 in Realistic Scenarios Wireless Communications and Mobile Computing, Hindawi, Wiley, Vol. 2018.

[24] Kong D., Mellios E., Hilton G., Doufexi A., Nix A. (2015) The Impact of Regulatory Transmit Power Constraints on the Relative Performances of Wi-Fi Beamforming and Antenna Selection, IEEE 81st Vehicular Technology Conference (VTC Spring), 2015.

[25] Karvonen H. et al. (2017) Interference of Wireless Technologies on BLE Based WBANs in Hospital Scenarios. 13th EAI International Conference on Body Area Networks, pp. 147-156

[26] Alwarafy A., Sulyman A.I., Alsanie A., Alshebeili S., Behairy H. (2015) Receiver Spatial Diversity Propagation Path-Loss Model for an Indoor Environment at 2.4 GHz, 6th International Conference on the Network of the Future, In: IEEE Xplore, 23 November, 2015.

[27] Ni L., Zheng P., Peterson L., Davie B., Garg V. (2014) Wireless networking complete. Elsevier, Morgan Kaufman, Burlington, 859 p.

[28] Bluetooth, https://en.wikipedia.org/wiki/Bluetooth, (read: 22nd April, 2021)

[29] Bluetooth Low Energy, https://en.wikipedia.org/wiki/Bluetooth_Low_Energy , (read: 22nd April, 2021)

[30] Nallanathan A., Feng W., Garg H.K. (2006) Coexistence of wireless LANs and Bluetooth networks in mutual interference environment: An integrated analysis. Computer Communications 30 (2006) 192.201, Elsevier, 2006.

[31] Aqsa Malik A., Junaid Qadir J., Basharat Ahmad B., Kok-Lim Alvin Yau KL., Ubaid Ullah U. (2014) QoS in IEEE 802.11-based Wireless Networks: A Contemporary Survey. 11 Nov 2014.

[32] Gislason D. (2008) Zigbee Wireless Networking. Newnes, Elsevier Inc., Burlington, 2008.

[33] Mucchi L., Vuohtoniemi R., Virk H., Conti A., Hämäläinen M., Iinatti J., Win M.Z. (2020) Spectrum Occupancy and Interference Model based on Network Experimentation in Hospital. IEEE Transactions on Wireless Communications, Vol. 19, No. 9, pp. 5666-5675.

[34] Berger H.S. (2016) The challenge of wireless reliability and coexistence, Approaches to Wireless Technology on Healthcare. Horizons Fall, AAMI, 2016.

[35] Hayajneh T., Almashaqbeh G., Ullah S., V. Vasilakos A.V. (2014) A survey of wireless technologies coexistence in WBAN: analysis and open research issues, Wireless Network, 20:2165-2199, 2014.

[36] Blough D.M., Resta G., P. Santi P. (2010) Approximation Algorithms for Wireless Link Scheduling With SINR-Based Interference. IEEE Transactions on Networking, Vol. 18, No. 6, IEEE, 2010.

[37] Virk M.H., Vuohtoniemi R, Hämäläinen M., Iinatti M. and Mäkelä J.-P. (2015) Stochastic Spectral Occupancy Modeling: A Body Area Network Perspective in ISM Band. 9th

International Symposium on Medical Information and Communication Technology (ISMICT), In: IEEE Xplore, 2015.

[38] Ekahau Sidekick Datasheet, https://www.ekahau.com/wp-content/uploads/2020/05/Ekahau-Sidekick-Data-Sheet-2.pdf (read: 26th March, 2021) Ekahau Inc., 2020.

[39] Ekahau Pro Datasheet, https://www.ekahau.com/wp-content/uploads/2020/05/Ekahau-Pro-Datasheet-052020.pdf (read: 18th February, 2021)Ekahau Inc., 2020.

[40] Intel Wireless-AC 9560 (Jefferson Peak 2), Revision 1.7, External Product Specification (EPS), Intel Corporation, January, 2018.

[41] Cisco Aironet 1850 Access Point, Data sheet. (2020) Cisco Systems, Inc, San Jose, 2020.

[42] Basic Service Set, https://www.sciencedirect.com/topics/computer-science/basic-service-set (read: 20th April, 2021), Science Direct, Elsevier B.V., 2021.

[43] Bluetooth Low Energy Channels, Microchip Developer Help, https://microchipdeveloper.com/wireless:ble-link-layer-channels , (read: 22nd April, 2021), Microchip Technology, Inc. 2021.

[44] Bluetooth Specifications, https://www.bluetooth.com/specifications/specs/, (read: 22nd April, 2021)Bluetooth SIG, Inc., 2021

[45] Voice over Wireless LAN 4.0, Design guide. https://www.cisco.com/c/en/us/td/docs/solutions/Enterprise/Mobility/vowlan/41dg/vowlan41dg-book/vowlan_ch5.html, (read: 26the March, 2021), Cisco Systems Inc., San Jose.

11 APPENDICES

Appendix 1. The MCS index, SNR and RSSI values for 802.11ac

Table A.

802.11ac - VHT MCS, SNR and RSSI

VHT MCS	Modulation	Coding	Data Rate 800ns	Data Rate 400ns	Min. SNR	RSSI	Data Rate 800ns	Data Rate 400ns	Min. SNR	RSSI	Data Rate 800ns	Data Rate 400ns	Min. SNR	RSSI
			1 Spatial Stream				2 Spatial Streams				3 Spatial Streams			
0	BPSK	1/2	6.5	7.2	2	-82	13.5	15	5	-79	29.3	32.5	8	-76
1	QPSK	1/2	13	14.4	5	-79	27	30	8	-76	58.5	65	11	-73
2	QPSK	3/4	19.5	21.7	9	-77	40.5	45	12	-74	87.8	97.5	15	-71
3	16-QAM	1/2	26	28.9	11	-74	54	60	14	-71	117	130	17	-68
4	16-QAM	3/4	39	43.3	15	-70	81	90	18	-67	175.5	195	21	-64
5	64-QAM	2/3	52	57.8	18	-66	108	120	21	-63	234	260	24	-60
6	64-QAM	3/4	58.5	65	20	-65	121.5	135	23	-62	263.3	292.5	26	-59
7	64-QAM	5/6	65	72.2	25	-64	135	150	28	-61	292.5	325	31	-58
8	256-QAM	3/4	78	86.7	29	-59	162	180	32	-56	351	390	35	-53
9	256-QAM	5/6			31	-57	180	200	34	-54	390	433.3	37	-51
0	BPSK	1/2	13	14.4	2	-82	27	30	5	-79	58.5	65	8	-76
1	QPSK	1/2	26	28.9	5	-79	54	60	8	-76	117	130	11	-73
2	QPSK	3/4	39	43.3	9	-77	81	90	12	-74	175.5	195	15	-71
3	16-QAM	1/2	52	57.8	11	-74	108	120	14	-71	234	260	17	-68
4	16-QAM	3/4	78	86.7	15	-70	162	180	18	-67	351	390	21	-64
5	64-QAM	2/3	104	115.6	18	-66	216	240	21	-63	468	520	24	-60
6	64-QAM	3/4	117	130.3	20	-65	243	270	23	-62	526.5	585	26	-59
7	64-QAM	5/6	130	144.4	25	-64	270	300	28	-61	585	650	31	-58
8	256-QAM	3/4	156	173.3	29	-59	324	360	32	-56	702	780	35	-53
9	256-QAM	5/6			31	-57	360	400	34	-54	780	866.7	37	-51
0	BPSK	1/2	19.5	21.7	2	-82	40.5	45	5	-79	87.8	97.5	8	-76
1	QPSK	1/2	39	43.3	5	-79	81	90	8	-76	175.5	195	11	-73
2	QPSK	3/4	58.5	65	9	-77	121.5	135	12	-74	263.3	292.5	15	-71
3	16-QAM	1/2	78	86.7	11	-74	162	180	14	-71	351	390	17	-68
4	16-QAM	3/4	117	130	15	-70	243	270	18	-67	526.5	585	21	-64
5	64-QAM	2/3	156	173.3	18	-66	324	360	21	-63	702	780	24	-60
6	64-QAM	3/4	175.5	195	20	-65	364.5	405	23	-62			26	-59
7	64-QAM	5/6	195	216.7	25	-64	405	450	28	-61	877.5	975	31	-58
8	256-QAM	3/4	234	260	29	-59	486	540	32	-56	1053	1170	35	-53
9	256-QAM	5/6	260	288.9	31	-57	540	600	34	-54	1170	1300	37	-51

VHT MCS	Data Rate 800ns	Data Rate 400ns	Min. SNR	RSSI
0	58.5	65	11	-73
1	117	130	14	-70
2	175.5	195	18	-68
3	234	260	20	-65
4	351	390	24	-61
5	468	520	27	-57
6	526.5	585	29	-56
7	585	650	34	-55
8	702	780	38	-50
9	780	866.7	40	-48
0	117	130	11	-73
1	234	260	14	-70
2	351	390	18	-68
3	468	520	20	-65
4	702	780	24	-61
5	936	1040	27	-57
6	1053	1170	29	-56
7	1170	1300	34	-55
8	1404	1560	38	-50
9	1560	1733.3	40	-48
0	175.5	195	11	-73
1	351	390	14	-70
2	526.5	585	18	-68
3	702	780	20	-65
4	1053	1170	24	-61
5	1404	1560	27	-57
6	1579.5	1755	29	-56
7	1755	1950	34	-55
8	2106	2340	38	-50
9			40	-48

Source: Wireless LAN Professionals, 2020, https://wlanprofessionals.com/mcs-snr-rssi-chart/.

Table B. The MCS table for 802.11n/ac

MCS Index - 802.11n and 802.11ac

802.11n 802.11ac

HT MCS	VHT MCS	SS	Modulation	Coding	20MHz No SGI	20MHz SGI	40MHz No SGI	40MHz SGI	80MHz No SGI	80MHz SGI	160MHz No SGI	160MHz SGI
0	0	1	BPSK	1/2	6.5	7.2	13.5	15	29.3	32.5	58.5	65
1	1	1	QPSK	1/2	13	14.4	27	30	58.5	65	117	130
2	2	1	QPSK	3/4	19.5	21.7	40.5	45	87.8	97.5	175.5	195
3	3	1	16-QAM	1/2	26	28.9	54	60	117	130	234	260
4	4	1	16-QAM	3/4	39	43.3	81	90	175.5	195	351	390
5	5	1	64-QAM	5/6	52	57.8	108	120	234	260	468	520
6	6	1	64-QAM	3/4	58.5	65	121.5	135	263.3	292.5	526.5	585
7	7	1	64-QAM	5/6	65	72.2	135	150	292.5	325	585	650
	8	1	256-QAM	3/4	78	86.7	162	180	351	390	702	780
	9	1	256-QAM	5/6	n/a	n/a	180	200	390	433.3	780	866.7
8	0	2	BPSK	1/2	13	14.4	27	30	58.5	65	117	130
9	1	2	QPSK	1/2	26	28.9	54	60	117	130	234	260
10	2	2	QPSK	3/4	39	43.3	81	90	175.5	195	351	390
11	3	2	16-QAM	1/2	52	57.8	108	120	234	260	468	520
12	4	2	16-QAM	3/4	78	86.7	162	180	351	390	702	780
13	5	2	64-QAM	5/6	104	115.6	216	240	468	520	936	1040
14	6	2	64-QAM	3/4	117	130.3	243	270	526.5	585	1053	1170
15	7	2	64-QAM	5/6	130	144.4	270	300	585	650	1170	1300
	8	2	256-QAM	3/4	156	173.3	324	360	702	780	1404	1560
	9	2	256-QAM	5/6	n/a	n/a	360	400	780	866.7	1560	1733.3
16	0	3	BPSK	1/2	19.5	21.7	40.5	45	87.8	97.5	175.5	195
17	1	3	QPSK	1/2	39	43.3	81	90	175.5	195	351	390
18	2	3	QPSK	3/4	58.5	65	121.5	135	263.3	292.5	526.5	585
19	3	3	16-QAM	1/2	78	86.7	162	180	351	390	702	780
20	4	3	16-QAM	3/4	117	130	243	270	526.5	585	1053	1170
21	5	3	64-QAM	5/6	156	173.3	324	360	702	780	1404	1560
22	6	3	64-QAM	3/4	175.5	195	364.5	405	n/a	n/a	1579.5	1755
23	7	3	64-QAM	5/6	195	216.7	405	450	877.5	975	1755	1950
	8	3	256-QAM	3/4	234	260	486	540	1053	1170	2106	2340
	9	3	256-QAM	5/6	260	288.9	540	600	1170	1300	n/a	n/a
24	0	4	BPSK	1/2	26	28.9	54	60	117	130	234	260
25	1	4	QPSK	1/2	52	57.8	108	120	234	260	468	520
26	2	4	QPSK	3/4	78	86.7	162	180	351	390	702	780
27	3	4	16-QAM	1/2	104	115.6	216	240	468	520	936	1040
28	4	4	16-QAM	3/4	156	173.3	324	360	702	780	1404	1560
29	5	4	64-QAM	5/6	208	231.1	432	480	936	1040	1872	2080
30	6	4	64-QAM	3/4	234	260	486	540	1053	1170	2106	2340
31	7	4	64-QAM	5/6	260	288.9	540	600	1170	1300	2340	2600
	8	4	256-QAM	3/4	312	346.7	648	720	1404	1560	2808	3120
	9	4	256-QAM	5/6	n/a	n/a	720	800	1560	1733.3	3120	3466.7

Source: Wireless LAN Professionals, 2020, https://wlanprofessionals.com/mcs-snr-rssi-chart/.

Appendix 2. The Modulation and Coding index and maximum data rates

Table A. MCS and the used values of NSS, R_B, GI, and bandwidth in 802.11ac

Feature	Specifications					GI = 400ns, BW = 20 MHz		
	4	2	78	162	351	86.7	180	390
	5	2	104	216	468	115.6	240	520
	6	2	117	243	526.5	130	270	585
	7	2	130	270	585	144.4	300	650
	8	2	156	324	702	173.3	360	780
	9	2	-	360	780	-	400	866.7
	0	3	19.5	40.5	87.8	21.7	45	97.5
	1	3	39	81	175.5	43.3	90	195
	2	3	58.5	121.5	263.3	65	135	292.5
	3	3	78	162	351	86.7	180	390
	4	3	117	243	526.5	130	270	585
	5	3	156	324	702	173.3	360	780
	6	3	175.5	364.5	-	195	405	-
	7	3	195	405	877.5	216.7	450	975
	8	3	234	486	1053	260	540	1170
	9	3	260	540	1170	288.9	600	1300
	0	4	26	54	117	28.9	60	130
	1	4	52	108	234	57.8	120	260
	2	4	78	162	351	86.7	180	390
	3	4	104	216	468	115.6	240	520
	4	4	156	324	702	173.3	360	780
	5	4	208	432	936	231.1	480	1040
	6	4	234	486	1053	260	540	1170
	7	4	260	540	1170	288.9	600	1300
	8	4	312	648	1404	346.7	720	1560

NSS

MCS

Source:
Cisco Aironet 1850 access point
Data sheet
Cisco Systems International BV Amsterdam

2020

Table B. MCS and the used values of NSS, R_B, GI, and bandwidth in 802.11n

Feature	Specifications				
Data rates supported	MCS Index[3]	GI[4] = 800 ns	GI = 800 ns	GI = 400 ns	GI = 400 ns
		20-MHz Rate (Mbps)	40-MHz Rate (Mbps)	20-MHz Rate (Mbps)	40-MHz Rate (Mbps)
	7	65	135	72.2	150
	8	13	27	14.4	30
	9	26	54	28.9	60
	10	39	81	43.3	90
	11	52	108	57.8	120
	12	78	162	86.7	180
	13	104	216	115.6	240
	14	117	243	130	270
	15	130	270	144.4	300
	16	19.5	40.5	21.7	45
	17	39	81	43.3	90
	18	58.5	121.5	65	135
	19	78	162	86.7	180
	20	117	243	130	270
	21	156	324	173.3	360
	22	175.5	364.5	195	405
	23	195	405	216.7	450
	24	26	54	28.9	60
	25	52	108	57.8	120
	26	78	162	86.7	180
	27	104	216	115.6	240
	28	156	324	173.3	360
	29	208	432	231.1	480
	30	234	486	260	540

Source:
Cisco Aironet 1850 access point
Data sheet
Cisco Systems International BV Amsterdam, 2020

Appendix 3. The frequencies of the WLAN channels at the 5 GHz frequency band

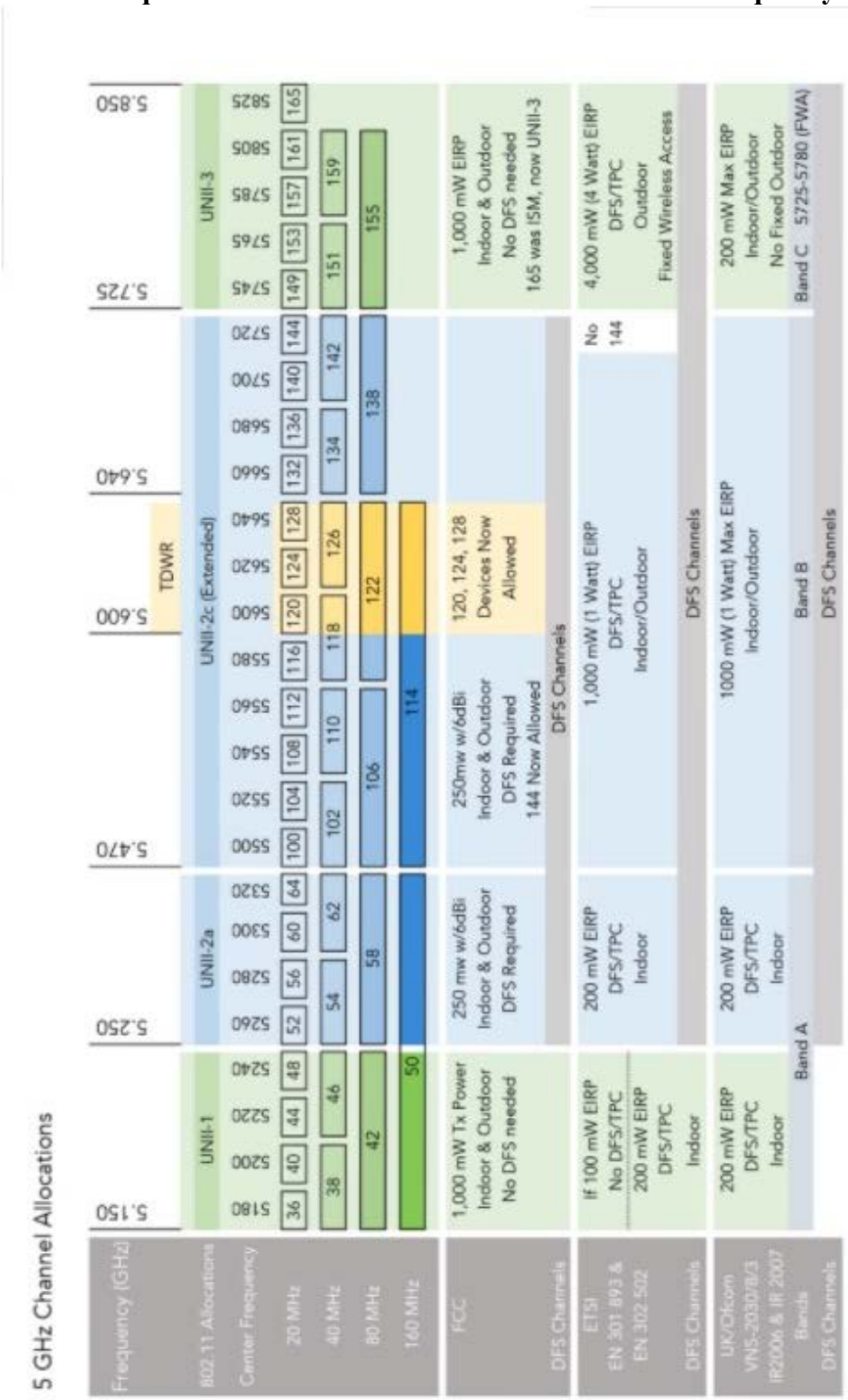

Source: Wireless LAN Professionals, 2020. https://wlanprofessionals.com/5ghz-allocations/

Appendix 4. The transmit power of Cisco 1852 1

Table A. The calculated EIRP-values of Cisco 1852.e on 802.11n (HT/VHT20, Antenna gain: 3 dBi, Dual/triple antennas) [3].

MCS	Ch	Tx-power [dBm]	EIRP [dB]
M0 - M23	1 -11	17	20

Table B. The calculated EIRP-values of Cisco 1852e on 802.11ac (HT/VHT20, Antenna gain: 5dBi) [3]

Non-Beam form:

MCS	Ch	Dual / triple / quad antennas:	
M0 - M23	UNII-1, 2	18	23

Beamform		Dual antennas:		Triple antennas:		Quad antennas:	
MCS	Ch	Tx-power [dBm]	**EIRP [dB]**	Tx-power [dBm]	**EIRP [dB]**	Tx-power [dBm]	**EIRP [dB]**
M0 - M7	UNII-1, 2	15	**20**	13	**18**	12	**17**
	UNII-2 Ext.	20	**25**	19	**24**	18	**23**
M8 - M15	UNII-1, 2	18	**23**	16	**21**	15	**20**
	UNII-2 Ext.	20	**25**	22	**27**	21	**26**
M16 - M23	UNII-1,2			18	**23**	17	**22**
	UNII-2 Ext.			22	**27**	23	**28**
M24 - M31	UNII-1,2					18	**23**
	UNII-2 Ext.					23	**28**